

UC Berkeley

UC Berkeley Electronic Theses and Dissertations

Title

Three Dimensional Sub-diffractive Imaging and Optical Stimulation of Neurons

Permalink

<https://escholarship.org/uc/item/4dc4w41n>

Author

Labno, Anna

Publication Date

2013

Peer reviewed|Thesis/dissertation

**Three Dimensional Sub-diffractive Imaging and Optical Stimulation of
Neurons**

by

Anna Labno

A dissertation submitted in partial satisfaction of the
requirements for the degree of
Doctor of Philosophy

in

Biophysics

in the

Graduate Division

of the

University of California, Berkeley

Committee in charge:

Professor Xiang Zhang, Chair
Professor Carlos Bustamante
Professor Mu-ming Poo
Professor Daniel Fletcher

2013

**Three Dimensional Sub-diffractive Imaging and Optical Stimulation of
Neurons**

Copyright 2013
by
Anna Labno

Abstract

Three Dimensional Sub-diffractive Imaging and Optical Stimulation of Neurons

by

Anna Labno

Doctor of Philosophy in Biophysics

University of California, Berkeley

Professor Xiang Zhang, Chair

Development of new instruments results in new discoveries and opens up new research directions. In particular novel imaging and optogenetics stimulation techniques merging classical photonics with other fields have a great potential to advance medicine, biology, physics, chemistry and engineering.

Here we present the development of two novel, plasmonic-aided imaging techniques (BOM and BEAST) and describe discovery of a new activity driven plastic alteration of dendritic excitability, which was enabled by utilizing a new dynamic light modulation scheme for neural activation.

The first technique, termed Brownian Emitter Adsorption Superresolution Technique (BEAST), is a novel single molecule super-resolution technique, which relies on stochastic adsorption of molecules to measure surface enhancement of an electromagnetic field. We used BEAST to map - for the first time - the electromagnetic field within single hotspots as small as 15nm on a metal surface with a resolution down to 1.2 nm. The hotspots are localized optical modes on the surface of noble metals exhibiting a giant enhancement effect and have attracted a broad interest, from understanding their mechanism to developing practical applications. However, characterizing these hotspots has been difficult, due to the limited resolution of current imaging techniques. BEAST improves the resolution significantly to single nanometer level, which allowed us to image the EM field inside single hotspots for the first time and discovered that the field distribution follows an exponential decay - strong experimental evidence for Anderson localization mechanism of the hotspots, which has been extensively debated over the last decades.

The second imaging technique described here - Brownian Optical Microscopy (BOM) - is the first technique to offer true three-dimensional imaging with nano-resolution. Scanning probe microscopy (SPM), which is commonly used to image 3D topology now, offers nanoscopic resolution but the use of the tip and slow scanning speed limits its throughput and makes it unable to image high aspect ratio or cavities. On the other hand optical tomography is able to image complex three-dimensional shapes but its resolution is limited to the micron range, while electron microscopy offers higher resolution but requires imaging in

vacuum. BOM does not suffer from these limitations. It is an all-optical imaging technique, which relies on Brownian motion of gold nanoparticles to sample the shape of the object, akin to scanning the sample in parallel by millions of small, freely diffusing SPM tips. In BOM an object of an arbitrary shape is placed in a solution of randomly diffusing nanoparticles, which are illuminated with an evanescent field so that the scattering intensity of resonant NPs correlates with their vertical position. We demonstrate that BOM is capable of imaging complex shapes with 30nm resolution in all three dimensions, including overhang samples, which cannot be imaged with any other technique.

Finally we use optogenetics combined with dynamic light modulation to explore plasticity of dendritic excitability. It was long believed that that plasticity, which plays a crucial role in the formation of neural circuits, is based on alteration of synaptic weights. Recent studies indicate that modulations of dendritic excitability may contribute the other part of the engram and critically impact the emergence of complex network behavior. However, a fundamental question remains whether dendritic excitability is controlled by synaptic inputs or arises independently. We used a novel optical system, which offers high spatiotemporal control over neural stimulation to decouple synaptic and non-synaptic activity and observed plasticity of local dendritic excitability which is autonomous from synaptic plasticity and arises only as a result of local activity. This persistent change in dendritic excitability arises as a result of a back propagating action potential interacting with simultaneous dendritic depolarization and triggering MEK-regulated phosphorylation of Kv4.2 by CamKII. This major discovery of activity dependent dendritic plasticity sheds new light on the role of dendrites in plasticity and may profoundly impact our fundamental understanding of neural plasticity as well as a number of neurodegenerative diseases where Kv4.2 channel deregulation is thought to play a crucial role.

To my family

Contents

Contents	ii
List of Figures	iv
1 Introduction - Bio- and Nano- Photonics	1
1.1 Optical Super-resolution Nanoscopy	1
1.2 Non-Optical Super-resolution Nanoscopy	4
1.3 Plasmonics Aided Nanoscopy	5
1.4 Challenges in Super-Resolution Imaging	7
1.5 Optogenetics	8
1.6 Controlling Neural Circuits and Microscopy Aid Study of Structural Plasticity	9
1.7 Organization of the Dissertations	10
2 Brownian Emitter Adsorbtion Superresolution Technique	12
2.1 Background and Motivation	12
2.2 Methods	15
2.3 Results	20
2.4 Discussion	28
2.5 Outlook	30
3 Brownian Optical Imaging	31
3.1 Background and Motivation	31
3.2 Methods	34
3.3 Results	39
3.4 Discussion	42
4 Synaptically Independent Dendritic Plasticity	48
4.1 Background and Motivation	48
4.2 Methods	53
4.3 Results	56
4.4 Discussion	63
5 Conclusions and Outlook	65

Bibliography

List of Figures

- 2.1 The principle of Brownian motion single molecule super-resolution imaging. (A) Hotspots appear on the surface of a thin aluminum film under a total internal reflection (TIRF)-type illumination at 532nm. To map the field distribution inside the hotspots, we use the Brownian motion of fluorescence dye molecules (Chromeo 546). The dye molecules stochastically adsorb to the surface. After a few frames (50 - 100ms per frame), the dye molecules photobleaches, which gives rise to a blinking pattern where each blink corresponds to one adsorption-bleaching event. By controlling the concentration of the dyes, the adsorption rate can be adjusted to ensure that within a diffraction limited spot, only one molecule is adsorbed at a time; therefore the position of the molecule can be determined by a maximum likelihood localization method with accuracy down to 1.2nm. (B) The raw image as viewed in the camera showing two hot spots with molecules adsorbed to them. The hot spot with an arrow pointing to it is the one whose reconstruction is shown in C. (C) By using the adsorption locations as the x and y coordinates and the fluorescence intensity as the z coordinate, we obtain a 3D scatter plot of the fluorescence enhancement profile of the hotspot, with each sphere representing one single molecule event. 16
- 2.2 Gaussian Kernel Rendering Procedure. We start with the simple image where each ball represents one adsorption event with location at the x and y coordinates, and the fluorescence intensity as the z coordinate. Then each pixel X of the rendered image $I(X)$, is a weighted average of the intensity from all of the single molecule events, with molecules closer to X carrying more weight. The window size of the kernel is determined by the accuracy of the single molecule localization. The rendered image reports an averaged profile of the local fluorescence enhancement. A hotspot may have complex structures that are smaller than the size of the kernel; these fine structures are removed in the stochastic rendering process 19

- 2.3 Single molecule localization in BEAST. (A) raw camera image of a hot spot with a fluorescent molecule adsorbed to it. The molecule appears as a round, bright spot that is roughly 10 pixels wide. (B) Cross section of the single molecule fluorescence intensity (black). The shape of the intensity is an Airy function with clearly visible side lobes. The 2D Gaussian that we used to fit the fluorescence profile (red) fits the fluorescence profile very well. (C) Fluorescence trace from a single hot spot over time. The black region indicates a 50ms time period when one molecule is adsorbed to the hot spot. Afterwards the molecule is bleached in a single step demonstrating that it was in fact a single molecule. (D) In order to estimate the localization accuracy we compare localization of a single molecule over time (green - x position estimation and blue - y position estimation). The standard deviation of the localization is less than 3nm. (E) Using Eq. 1.2 we estimated the maximum likelihood estimated variance of 2.59nm (red dash curve). There is a good agreement between the measured variance and the calculated variance. Therefore, Eq.1.2 is sufficient for estimating the single molecule localization accuracy. (E) We plot the centroid position from each frame within this period in the figure above. The error bar corresponds to the variance estimated from Eq. 1.2 The distribution of the data points provides an estimation of the surface diffusion. Most of the data points are located within a circle of 5nm. The standard deviation is only 2.6nm and 3.3nm in x and y direction respectively, which is smaller than the variance of the single molecule localization. Therefore, the effect of the surface diffusion of adsorbed molecule is not detectable. 21
- 2.4 The relationship between molecule's fluorescence and EM field enhancement. (A) We varied the EM field intensity of the excitation light by changing the angle of a halfwave plate sandwiched between two polarizers and measured the fluorescence intensity of single molecules that are randomly adsorbed on the surface of a quartz cover slide. The histograms represent fluorescence counts of the single molecule fluorescence intensity excited with the excitation powers of 6.92mW, 7.97mW, 8.98mW and 10.05mW, respectively (bottom to top). (B) The average fluorescence intensity follows the excitation power in a linear manner. (C) Relationship between the number of the single molecule events and the accuracy of the final averaged result. Events collected at 10.05mW were picked at random and grouped into group of variable size then the average intensity of the groups was plotted against their size. The shaded region corresponds to a 15% level of uncertainty. From the figure, it is clear that about ≈ 10 events are sufficient for an accurate estimation of the final intensity. 23

- 2.5 Imaging the EM field enhancement of a single hot spot. (A) By using the adsorption locations as the x and y coordinates, and the fluorescence intensity as the z coordinate, we obtain a 3D scatter plot of the fluorescence enhancement profile of the hotspot, with each sphere representing one single molecule event. The inset shows a SEM of a Al film from which the hot spots were imaged. (B) As the fluorescence of a single molecule is intrinsically stochastic, we remove this randomness by using a Gaussian kernel method to render the image of the field distribution. The field distribution of an example hot spot after the rendering is shown. Each pixel X of the rendered image corresponds to average intensity from all of the single molecule events, with molecules closer to X carrying more weight. The kernel window size is 2.1 nm; this small window size makes the image appear noisy. (C) Cross section of EM field enhancement of the hot spot. An exponential decay field profile is visible in the two cross-sections of the hotspot along x and y directions through the peak (blue and green curves respectively). The exponential shape is even more evident on a log scale where it clearly shows as a straight line (red solid line). The FWHM of the spot is ≈ 20 nm. (D) The accuracy of the reconstructed field profile, estimated from the variance of the maximum likelihood localization, depends on the number of photons collected from the molecules, with brighter single molecule events showing better accuracy, down to 1.2 nm. (E) The distribution of the single molecule events belonging to this hot-spot provides a direct measure of the size of the hotspot. The width of the hotspot characterized by the standard deviation of the single molecule events is 15.2 nm and 15.4 nm in x and y directions, respectively. (F) Cross-section of the hotspot at $y = 0$ nm. The molecules within $-2\text{nm} < y < 2$ nm are shown. (G) Cross-section of the hotspot at $x = 0$ nm. The envelope appears as an exponential decay with a constant of 9.83 nm (red dashed lines). To avoid crowding, only the single molecule localization variance of a few spheres near the envelope is shown. 25
- 2.6 EM field enhancement statistics across multiple hot spots. (A) All of the hotspots observed are of deep sub-wavelength size, with an average width of 32.3 nm. (B) By plotting the enhancement factor of the hotspots against their width, an inverse relationship between the size and the enhancement factor is visible: tighter confinement leads to stronger enhancement. 26

- 2.7 A hotspot formed on silver nanoparticle clusters appears similar to those formed on the aluminum film. A 644-nm laser is used for excitation, and Chromeo 642 dye (Active Motif) - whose emission centers around 660 nm - is used. The maximum enhancement factor at the center of the peak corresponds to 136x the florescence from the same dye molecules adsorbed on a glass surface. (B) The hotspot exhibits a similar exponential decay profile as those formed on the surface of the aluminum film. Two cross-sections of the hotspot along x (green) and y (blue) directions through the peak are plotted on a logarithmic scale, with the solid red lines as eye-guides for the exponential profile. (C) The widths of the hotspot, estimated from the distribution of the single molecule events on a scatter plot, are 13.2nm and 20.3nm along the two axes. 27
- 2.8 Measuring a 3D profile of a hot spot. (A) Experimental overview. A hot spot on a thin Al film is localized and imaged using standard BEAST technique (left), then BSA is flown and forms a 4-14nm layer. Then the hot spot is imaged again, however this time the intensity obtained is obtained 4-14nm above the surface of the metal. (B) Intensity before applying BSA (left) and after (right). The decrease in EM field enhancement is evident. (C) Cross section of the hot spot before BSA (solid line x -cross section green line and y -cross section blue line) and after (dashed line, x -cross section green line and y -cross section blue line). While the exponential decay is present in both cases there is a 36% drop in the enhancement and a 26% increase in the width were observed after BSA layer has been applied. (D) Statistics of width change across multiple hot spots showing that the increase in width ratio was comparable among them (E) Statistics of width change across multiple hot spots showing that the decrease in enhancement was comparable among them. 29
- 3.1 Summary and comparison of existing three-dimensional imaging techniques. AFM exhibits nanometric resolution and is capable of imaging samples in ambient conditions, however it does not offer true three-dimensional resolution and has a very low throughput due to the nature of tip scanning. Electron microscopies (SEM and TEM) also have great resolution and are capable of imaging some three dimensional objects, however they typically place stringent conditions on sample preparation and imaging conditions. Finally, optical coherence tomography (OCT) allows for wide-field truly three dimensional imaging, however its resolution is limited to the μm range. The technique presented here - Brownian Optical Microscopy (BOM) - allows for true three dimensional imaging in ambient conditions with nanometric resolution. 33

- 3.2 Principle of the BOM technique. A) BOM relies on three-dimensional localization of freely diffusing NPs. An object of arbitrary shape (gray) is placed in solution of randomly diffusing nanoparticles, denoted here by small green spheres, which are illuminated with an evanescent field established by total internal reflection (TIR) at the interface between the substrate and the object. A series of raw images of scattering from those particles is acquired and the NPs are individually localized in three dimensions as they randomly probe the volume around the object by Brownian diffusion. Images taken at different times will record different NPs randomly distributed around the field of view as the particles freely diffuse in the space around the object. The lateral localization is obtained by finding the center of the scattering signal by Gaussian fitting while the height of particle is estimated by measuring the intensity of the scattering signal (the height of the Gaussian). Since the evanescent field decays exponentially with the distance from the interface, the NPs close to the interface will interact with stronger field and hence appear brighter than ones further away from the boundary. Space occupied by the object is inaccessible to the NPs, and the resulting image of the excluded volume corresponds to the shape of the object. B) Once a large number of particle positions are recorded the volume excluded by the object can be estimated. The more particles are collected the finer the space sampling around the object and the better the shape of the object can be reconstructed. C) Experimental Setup. The sample, composed of glass cover slip with a MgF2 or PMMA structure nanofabricated on it enclosed in a flow chamber filled with a low density solution of freely diffusing 50nm NPs. The chamber is illuminated with a laser in such a way that evanescent field originates on the MgF2/glass or PMMA/sapphire interface and penetrates into the sample. The scattering signal is then detected on the other side of the sample using a 100X oil immersion objective. 35
- 3.3 BOM can image three-dimensional topology of complex shapes with 30nm lateral resolution. A) Schematics of the CalNano shape fabricated by E-beam lithography. (B) Two dimensional SEM image (C) Two dimensional optical image, which allows us to resolve only the large features of the shape (D) Three-dimensional BOM image in which the CalNano patterns geometry is clearly resolved. (E) SEM of fabricated lines with progressively decreasing width ranging from 120nm down to 20nm (F) BOM image of the lines including the averaged cross section (yellow) showing that the smallest 30nm line is clearly resolved. (G) Zoom-in highlighting the ability of BOM to resolve 100nm-150nm features in the letters "l" and "n" of the CalNano shape. H) Three-dimensional reconstruction of the line sample. 40

3.4	BOM can achieve 30nm vertical resolution. A) Schematics of a fabricated staircase pattern consisting of three steps with 30nm, 35nm and 40nm height respectively. B) AFM image of the sample. C) BOM image of the same sample showing three distinct steps. D) Averaged cross section of the AFM (black) and BOM images (orange) showing that BOM accurately resolved the heights of the steps with under 30nm resolution.	41
3.5	Imaging the topology of three-dimensional shapes with internal geometry A) Schematics of the fabricated structure consisting of a silicon dioxide layer on a sapphire substrate patterned into a smiley face in the first EBL step, and an overhanging PMMA structure fabricated from PMMA and MMA co-polymer in a second EBL step. B) SEM image of the structure on which a small gap can be seen but the top PMMA layer obscures the underlying smiley face. C-D) BOM images of the sample showing clearly the smiley face structure as well as the overhang roof supported by a thick post	43
3.6	Imaging of topology of biological samples. A) AFM image of <i>E.Coli</i> deposited on sapphire surface B) BOM image of <i>E.Coli</i>	44
3.7	Dependence of accuracy of localization of a single surface on number of particles and standard deviation deviation of their size. For the particles with size deviation of 10%, which is similar to the particles used in experiment, we need to collect ≈ 20 particles to achieve localization of ≈ 20 -25nm.	46
4.1	Experimental setup to achieve decoupling of synaptic and dendritic processes. (A) EYFP-ChR2 expressing hippocampal neuron is stimulated with 28 um light spot (blue circle) applied on the proximal dendrites coupled with somatically induced spike. (C) The stimulation protocol where 2s photostimulation of proximal dendrite is coupled with a spike (C) Schematics of the optical setup. Patterned ChR2 stimulation is achieved by a 470nm LED is collimated by a lens (CL) and directed using a mirror (M) to Digital Micromirror Device (DMD). The light reflected from DMD is collimated and scaled using a lens system (L) and coupled into the microscope via a beam splitter (BS).	54
4.2	Persistent decrease in dendritic excitability following paired stimulation. (A) An example trace for 2s photo depolarization before (black trace) and after (blue trace) the treatment. When no stimulation was applied (top) no change in dendritic excitability is observed, however after paired stimulation (bottom) excitability decreased (B) Dendritic excitability prior to paired stimulation, shows a steady basal level of dendritic excitability as assessed by measuring the peak magnitude of the ChR2-induced photo current. After paired stimulation the current decreases by 13% for 2s report as compared to 0.74% for no stimulation.	57

- 4.3 Persistent decrease in dendritic excitability following paired stimulation. (A) Only stimulation by paired APs and dendritic depolarization causes DED= 12.6% ($p < 0.05$). Controls, where no stimulation takes place or either APs or light alone are delivered show no significant DED ($p > 0.05$ in all cases). (B) There is no change in spike-current relationship between stimulated (blue square) and unstimulated neurons (open circle) or neurons stimulated only with APs (black filled rhombus) indicating no change in intrinsic excitability. 58
- 4.4 DED is spatially localized. (A, B, C and D) Top panels display the dendritic location used for dendritic stimulation (blue circle) and the range of possible report locations (white dotted lines). Bottom panels show example current measurements before (black) and after stimulation (grey or blue) as well normalized current before and after stimulation. Following proximal dendritic stimulation, (A) proximal dendritic current decreases (DED=2.65%, $p < 0.05$) (B) somatic current shows increase in excitability by $6.2\% \pm 2.1\%$. (C) Un-stimulated dendrites don't show DED (DED= $0.28\% \pm 3.4\%$, $p = 0.84$) and (D) Current resulting from whole cell photo-stimulation does not change significantly (increase= $1.6\% \pm 1.9$). 59
- 4.5 Kv4.2 channels are responsible for DED and the process requires Ca²⁺ and MEK. (A-D) Example current measurements before (black) and after stimulation (grey) showing that DED is blocked by HpTx (A) and TTX (B). Moreover DED does not happen in the absence of Ca²⁺ (C) and is blocked by MEK inhibitor U0126 (D). (E) Time trace showing the effect of chelating calcium (by EGTA) and MEK by (U0126) showing that blocking their action clearly abolished DED as compared to its normal magnitude (blue circles). (F) Bar graph summarizing effect of different drugs. When no drugs are applied 10% DED is observed. Application of TTX ($1\mu\text{M}$), TEA (20mM) and Stromatotoxin-II (100nM) reduced the amount of DED to 3% while application of Hptx (100mM) or U0126 ($10\mu\text{M}$) or removal of calcium from external solution completely abolishes DED. 60
- 4.6 Kv4.2 phosphorylation is enhanced along the stimulated dendrite. (A) Immunostaining against Kv4.2 phosphorylated at Ser 438 shows enhanced phosphorylation at the stimulated dendrite as compared with the un-stimulated dendrite of the same cell. The dendrites have comparable amounts of ChR-YFP. Dendrites from two representative cells are shown (top and bottom). (B) Mean immunofluorescence of pKv4.2 along the stimulated dendrite is much higher (mean fluorescence = 36.5 ± 2.84) than along the non-stimulated dendrite (mean fluorescence = 19.8 ± 3.17), $p = 0.01$ 61

4.7	: Kv4.2 channels are responsible for DED. (A) Example time trace showing clusters on unstimulated dendrite moving somatically and ones on stimulated dendrites not moving (B) Summary of cluster movement on stimulated and unstimulated dendrites. Clusters on stimulated dendrites preferentially move distally (33%) or remain in place (61%) with only 5% moving somatically. Clusters on unstimulated dendrites preferentially move somatically (38%) or remain in place (45%) with only 17% moving distally (C) Example images of showing clustering of somatic Kv4.2 channels.	62
4.8	Possible Mechanism behind DED. MEK regulates Kv4.2 phosphorylation by activating CamKII which can then directly phosphorylate Kv4.2. CamKII phosphorylates Kv4.2 at Ser438 which increases the inactivating A-type potassium current and hence decreased dendritic excitability.	63

Acknowledgments

I would like to express my appreciation to my advisor, Prof. Xiang Zhang, for his guidance, patience, contagious enthusiasm and inspiration. He provided me with encouragement and freedom to formulate and develop my own research vision while at the same time taught me how to choose relevant questions that are at the forefront of the field and how to communicate my ideas to the scientific community. He worked relentlessly to make sure that the lab had funding and that I had whatever I needed to pursue my research. I could always count on him to cultivate my career development, help me meet my professional milestones, celebrate my successes and offer moral support in case of failure. His faith in my ability and support over the years made the work presented here possible.

I would also like to thank Prof. Carlos Bustamante, Prof. Mu-ming Poo, and Prof. Dan Fletcher for not only serving on my dissertation committee but also helping me along the way. I truly appreciate the time they have invested in my success and it has been a pleasure to get to know them over the years.

I also wish to thank many gifted researchers that I have been privileged to have as colleagues and mentors, particularly Ajith Warier, Zhaowei Liu, Kevin O'Brian, Hu Cang, Guy Bartal and Jun Rho. They made the lab the unique, creative place it is and frequently served as a catalyst to move forward in my research.

I am forever grateful to my parents, grandmother and sister for providing me an environment in which I was able to grow and explore my love for science, and for believing in me when only a mess was visible. I cannot express how important your presence was for me. It allowed me to take on risks and challenges I would otherwise not have the courage to undertake. I am also very indebted to my husband - Carl Rogers - for his unwavering love and support throughout the good times as well as the trying ones.

Chapter 1

Introduction - Bio- and Nano-Photonics

Bio-photonics, nano-photonics are emerging multidisciplinary fields that draw upon research from physics, materials science, chemistry, electrical engineering, biology and medicine to realize a whole range of novel technologies and apply them to the emergent questions at the frontier of biology, physics and chemistry. Both of those fields evolved from photonics, which derives from the Greek word *photos* meaning light. Photonics is the study of light including its generation, emission, transmission, modulation and detection/imaging [24]. While biophotonics is a fusion of photonics and biology in which photonics technologies are applied to the fields of medicine, biology and biotechnology [293], nanophotonics strives to understand and exploit the behavior of light on the nanometer scale [294]. Basic research and innovation in photonics is very fundamental in science and engineering and required to lay the foundation for new technologies beyond ones that are currently available. This thesis describes advances in two of the most dynamics aspects of biophotonics and nanophotonics - wide field super-resolution imaging and optogenetics.

1.1 Optical Super-resolution Nanoscopy

In 1873, Ernst Abbe [1] and colleagues - Émile Verdet [105] and Lord Rayleigh [298] developed the concept of resolution limit by studying the propagation of light through apertures. They concluded that light of a wavelength λ focused by a classical lens of numerical aperture $n \sin \alpha < 1$ cannot simultaneously discern objects that are closer together than distance $d = \lambda / (2n \sin \alpha)$, because diffraction of visible light wavefronts, as they pass through the circular aperture such as the one at the rear focal plane of the objective, blurs their images into an overlapping image that cannot be distinguished. By the same argument, light cannot be focused more sharply than to a spot of $d \approx 200$ nm in diameter and 400-700 nm in axial length. This corresponds to the resolution limit of basically all glass-based microscopes and since it is governed by a fundamental set of physical laws that cannot be easily overcome by

rational alternations in objective lens or aperture design. These resolution limitations are often referred to as the "diffraction barrier" or "diffraction limit", which restricts the ability of optical instruments to distinguish between two objects separated by a lateral distance less than approximately half the wavelength of imaging light [277].

Despite this limitation light microscopy became workhorse of in many fields of science and engineering including biology, physics, chemistry, material science and engineering as well as medicine. Unfortunately, virtually all nano materials and most cellular systems involved in physiologically important processes are below that limiting threshold of 200 nm. For example, nano photonics and plasmonic devices, carbon nanotubes, surface features, synaptic vesicles, receptor proteins complexes and cellular skeletal assemblies can be as small as 50 nm yet our understanding of their function and structure could be greatly improved if only direct optical recording was possible.

For decades since the rule of diffraction-limited imaging was proposed, researchers believed that the ability to resolve two nearby points was fundamentally limited by the wavelength of light. However recently several novel microscopic techniques took advantage of ingenious ways to overcome this limit and made it possible to map previously inaccessible nano-environments. One of the first ways to break the diffraction limit was proposed by Synge in 1928, who proposed using a sub-wavelength aperture to scan the surface. The concept was however only demonstrated in 1884 [224, 291] and then evolved into a rapidly expanding field, now known as near-field scanning optical microscopy (NSOM) [33]. Since the initial discovery NSOM has been widely used in nanotechnology for example to study carbon nanotubes, material surfaces and nano-devices such as nano lasers [168] and biology where it was instrumental in imaging ion channel clusters [174], human chromosomes [154] and compartmentalization of cell membranes [366] just to name a few. One limitation of NSOM however is that the aperture has to be placed very close (less than one wavelength) to the imaging specimen, limiting NSOM's use to the study of surfaces, and its applicability in biology is limited because the scanning probe can interfere with the sample and due to the difficulty imaging in liquid. Additionally the aperture probe is difficult to make, and the need for feedback to maintain a constant distance from an irregular sample limits the speed of image acquisition.

Research in far field optical techniques initially focused on improving axial resolution and led to development of I5M [145] and 4Pi [25, 161, 315] microscopies which combined the apertures of two opposing lenses to allow imaging with a large improvement in axial resolution down to 100 nm using wide-field and confocal set-ups, respectively. However the lateral resolution in those techniques remained diffraction limited, until the 1990s when we witnessed a whole suite of fundamentally new microscopies which for the first time achieved breaking the lateral resolution diffraction limit in fluorescence microscopy. All of those techniques relay on a key insight - that to overcome the diffraction limit one must spatially and/or temporally modulate the imaging of the fluorophores. This is typically achieved by

controlling the transition between two molecular states of a fluorophore (for example, a dark and a bright state). Some techniques achieve super resolution by tightening the point spread function (PSF) of an ensemble image of many fluorophores. These techniques include stimulated emission depletion (STED)[162], ground-state depletion (GSD)[160], and saturated structured-illumination microscopy (SSIM)[146, 157] and its recent combination with I5M (I5S)[322]. STED is one of the techniques which is widely used today. Here, the sample is illuminated by two laser beams: an excitation laser pulse, which activates fluorophores and a red-shifted pulse (the STED beam), which transfers excited fluorophores back to their non-fluorescent ground state. This nonlinear de-excitation of the fluorescent state by the combined STED illumination effectively narrows the PSF, thus confining the fluorescence emission and increasing imaging resolution. STED microscopy has achieved 20 nm resolution in the focal plane [97] and, recently, 45 nm resolution in all three dimensions [313] and has been extensively used to reveal basis of cellular machinery such as synaptic zone [190, 196, 384, 386], mitochondria [98] and endoplasmic reticulum [156]. Although many applications of STED have been reported, the instrumentation required is still complicated and this is the main limitation to its widespread use [162]. Saturated structured-illumination microscopy is a similar technique but it exploits the saturation of fluorophore transition from the ground state S_0 to the excited singlet state S_1 . This differs from STED in that ultrasharp dark regions of molecules are created with steeply surrounded regions of molecules in the bright state [146, 157].

Other super-resolution imaging techniques detect single molecules and rely on the principle that a single emitter can be localized with high accuracy if sufficient numbers of photons are collected [34]. This requires using photoactivatable fluorescent labels, which allow for a controlled activation of a subset of the fluorescent molecules [395, 28]. Because the number of activated (fluorescing) molecules is small, typically there is only one fluorescent molecule located within a diffraction-limited volume. Therefore, it is possible to image and then localize with high accuracy a subset of well-separated molecules one at a time. The process is then repeated for different groups of fluorescent proteins within the sample. The techniques that rely on photo activation include photoactivated localization microscopy (PALM) [34], fluorescence photoactivation localization microscopy (FPALM) [163] and stochastic optical reconstruction microscopy (STORM) [307]. Those techniques can typically provide lateral resolution of 10-20nm and have been used to image a number of molecular structures such as lysosomes, mitochondria [34], microtubules and clathrin coated pits [29] in fixed cells. The techniques have been recently extended to allow for multicolour [29, 329] and three-dimensional (3D) super-resolution imaging with ≈ 30 -75 nm axial resolution [172, 181] as well as live-cell imaging [248, 328]. Those techniques, although very powerful, require the sample to be labeled with photo switchable fluorophores which limits the use of those techniques to imaging biological structures with known molecular identity and have not been widely applied in nanoscale engineering or material science. Moreover the brightness and stability of current fluorophores limits the S/N ratio [115].

1.2 Non-Optical Super-resolution Nanoscopy

One way to improve the resolution beyond what's available with optical microscopes is to use electrons, which have much shorter wavelength. There are two main families of electron microscopes - the transmission electron microscope (TEM) and the scanning electron microscope (SEM). TEM uses a high voltage electron beam focused by electrostatic and electromagnetic lenses to impact the specimen. The sample modifies the phase and amplitude of the transmitted electrons allowing the TEM to use the electrons that have been transmitted through the sample to form an image. While TEM is capable of achieving atomic level resolution, the highest possible resolution of all methods, the samples need to be very thin (10-100nm), which may be difficult to obtain especially in biology, and the observed section may not be representative of the entire sample. The scanning electron microscopy is more flexible and versatile than TEM. SEM scans a focused beam, typically with energy between ≈ 500 eV and 30 keV, over the surface of a (bulk) sample, collecting backscattered or secondary electrons pixel by pixel. Since SEM relies on the electrons back scattered from the sample it can be used to image thicker objects and uses a more straightforward specimen preparation. The resolution of SEM is limited to a few nm and most instruments in laboratories operate at 30-50nm. Additionally SEM requires samples to scatter strongly which is not true for many dielectric materials including biological tissues [179]. Typically all electron microscopes require vacuum, both to allow operation of the electron source and to minimize scattering other than from the sample. Samples must therefore be stable under vacuum, and so are traditionally prepared in the solid state which may distort the features of the sample. In spite of such limitations, atomic resolution has been attained in some EM studies of biological materials including membranes and molecular complexes [106, 203]. Recent improvements in EM allow for imaging in liquid albeit with lower resolution [86].

Another class of non-optical imaging techniques are scanning probe microscopes in which a proximal probe is exploited for investigating properties of surfaces with subnanometre resolution. They are typically used to image topology only, as it is difficult to functionalize the probe to allow for detection of chemical identity. One of the most popular scanning probe techniques is atomic force microscopy (AFM), where a sharp probe tip attached to a cantilever is used to scan the specimen surface. The position of the cantilever is measured using a laser spot reflected from its top surface [132]. AFM allows high-resolution measurements of native biological samples in physiological conditions [99, 50], avoiding complex sample preparation procedures and artifacts associated with them. AFM can generally achieve nanometric resolution although its top performance is achieved with hard and flat samples, with low aspect ratio. AFM has been extensively used in mapping microstructural properties of superalloys [131], investigating structure of soft polymers [374], DNA interactions, proteins and cell structures [11]. Beyond imaging AFM can also be applied to force spectroscopy, the direct measurement of tip-sample interaction. Forces as small as few piconewtons can now be routinely measured with a vertical distance resolution of better than 0.1 nanometers as function of the gap between the tip and sample [51, 116, 164]. Piezoelectric

elements that facilitate tiny but accurate and precise movements on (electronic) command enable the very precise scanning. In some variations, electric potentials can also be scanned using conducting cantilevers. In more advanced versions, currents can be passed through the tip to probe the electrical conductivity or transport of the underlying surface [216].

1.3 Plasmonics Aided Nanoscopy

An emerging family of super-resolution imaging techniques that will be of special interest are techniques where super-resolution is achieved by engineering plasmonic interactions. Those techniques can be roughly divided into two classes: first, when the plasmonic interactions act as a nano-antenna helping to optically visualize the sample and second, when plasmonic materials (metamaterials) are used to actively shape the dispersion relationship of light to circumvent the diffraction limit.

The first group consist of optical antennas, not unlike the NSOM tip, that have the potential to access the size regime not accessible to classical light microscopy by enhancing optical fields on nanoscale. One of the most common methods of realizing nano-antennas is to fabricate metal nano structures, which are capable of concentrating light such as stripes or bow ties on glass substrates [265, 316, 299]. They have a potential to generate white-light-supercontinuum radiation in the antenna feedgap enhancing the emission from the antennas more than 1,000 times [265]. So far those systems have been widely used in chemical sensing since it improves detection limits, sensitivity, selectivity, and dynamic range [135] but they could be used in the future to investigate molecular reactions on the membrane or monitor diffusion of on the cell membrane. Early results in this direction demonstrated that high-concentration single-molecule spectroscopy was possible using zero-mode waveguides and fluorescence correlation spectroscopy [223] and trajectories of freely diffusing individual proteins were traced as they sequentially pass through, and are enhanced by, multiple gaps in a fabricated nano-antenna array [236]. In order to enable microscopic measurements of the entire structure those nano antennas are attached to a cantilevers or glass tips and scanned around the surface [19, 210, 111]. Recently they have been used to image single calcium channels on erythrocyte plasma membranes with 50nm resolution [167]. Finally antennas attached to the top of a normal NSOM nano-aperture have also been used to improve S/N and have been shown to achieve successful topography and fluorescence measurements down to 10nm-30nm resolution and very low background [353, 121]. Such monopole antennas have been used to enhance Raman and CARS imaging to examine for example single-walled carbon nanotubes (SWNTs), fullerenes (C60), strained silicon and DNA [187] as well as to enhance fluorescence imaging and image single proteins and nanodomains with 30 nm resolution in cell membranes in liquid [367].

The second class of techniques allows for achieving super resolution imaging by using surface plasmon polaritons (SPP) that travel on the surface of metal slower then free space light

with the same frequency constant [239] and allow for design and fabrication of materials with negative permittivity or permeability, or both. A slab of such material would substantially enhance evanescent waves, compensating for the evanescent loss outside the superlens and thus restoring an image not only below the diffraction limit but perfectly. Such a lens was first proposed by Pendry and is commonly referred to as a "perfect lens" or "Pendry's lens" [287]. However there is a phase mismatch between SPP and propagating light at the same frequency and hence the SPP cannot be easily excited by the propagating far field light. They can however be coupled to evanescent light near the surface of a metal resulting in resonant excitation of SPP [239]. Moreover near-field light cannot be transmitted to the far field, so a plasmonic microscope must include a mechanism that can convert the near field into far field - such as surface roughness or periodic corrugation on the metal surface, which can couple SPP out to the far field [239, 297, 43]. The use of SPP for super resolution imaging was demonstrated by Smolyaninov and colleagues who imaged a periodic nanohole array set on the gold film under a glycerin droplet with 70nm resolution ($\lambda/7$). The SPP were excited along the gold film and the small droplet of liquid dielectric on the metal surface, which has high effective refractive index, decreases the resolution limit and also serves as a strong lens for surface plasmons propagating through the droplet from the outside [336]. Immediately afterwards Zhang developed a metamaterial superlens, which consisted of a silver slab separated from an object by a spacer layer, and coated on the opposite side with an imaging material. By designing the thin metal slab so that the surface plasmons match the evanescent waves from the object, the superlens was able to substantially enhance the amplitude of the field and enhance imaging resolution to 65nm. In this case both the object and the image had to be within the near-field of the lens and therefore the image was recorded on photoresist directly on the top of the lens and read it by atomic force microscopy (AFM) [110]. Subsequently a superlens with magnifying function that can be used to couple magnified image to the far field and detect it with a conventional microscope was later proposed by Zhang (hyperlens) [235] as well as several authors independently [337, 330, 188]. Such lenses rely on either a cylindrical geometry [235, 337] of the imaging metamaterial or a tapered arrangement of silver nanorods [330, 188]. The cylindrical imaging schemes have recently been extended to imaging in 2D by replacing cylindrical symmetry with spherical one [301]. Although these proof-of-concept experiments have produced hyperlenses with hyperbolic dispersions working at both ultraviolet [235] and visible wavelengths [301] they have not been extensively used in imaging due to practical difficulties such as obtaining very high structural quality lens surface roughness and protecting the material against oxidization and/or sulphurization. Additionally the loss caused by the imaginary part of the dielectric constant of a metal is not negligible causing loss of information and hence blurring of the image preventing us currently from realizing Pendry's perfect lens.

While plasmonic aided nano imaging techniques are still in infancy they might become key techniques in modern biology by providing tools for studying processes both *in vitro* and *in vivo* at relevant spatial scales and physiological concentrations.

1.4 Challenges in Super-Resolution Imaging

Now, for the first time, direct optical recordings of sub-resolution structures may allow us to address important structural and physiological questions. Answers to these questions will dramatically improve our understanding of the nature of processes involving responses of living cells to stress, damage, proliferation and their interactions as well as physics of nano materials.

1.5 Optogenetics

Optogenetics is a technology that allows targeted control of precisely defined events with high-temporal resolution and cellular precision within intact mammalian neural tissue including culture, slices and live animals. This is achieved by introducing bacterial rhodopsin - Channelrhodopsin2 into neurons. This channelrhodopsin-2 (ChR2) from *Chlamydomonas reinhardtii* are blue-light-activated nonspecific cation channel [271]. In common with other type I opsins, these proteins require retinal as the photon-sensing cofactor to function. In response to light stimulation, the channel shuttles from the dark-adapted state through a number of functional and conformational states to eventually return to the dark-adapted (photo cycle) [31, 26, 345]. ChR2 stimulation results in transient peak photocurrent, evoked at the onset of light stimulation, which then decays slowly (on the order of ms) to a steady-state photocurrent even in the presence of continuous stimulation, owing in part to the desensitization of a certain population of channels. The desensitized population can recover slowly (seconds) in the dark allowing for subsequent stimulation later [271]. Channelrhodopsin was first introduced into hippocampal neurons in 2005 [42] where it was found to confer millisecond-precision control of neuronal spiking. ChR were then subsequently improved by improving expression [138, 405, 139] and photocurrent in mammalian systems [138, 270, 231]. Since then many novel opsins have been engineered including ones that are activated by red-shifted wavelengths [402], exhibit nanoampere-scale currents that exceed those of ChR2 [396] and have inhibitory rather than excitatory effect [403, 137].

The ChR2 is typically delivered via viral delivery system using lenti and adeno-associated (AAV) viral vectors or via transfection in cultured neurons or via the use of transgenic knock-in animals, including mice, *Caenorhabditis elegans*, fly, zebrafish, rats and even primates [114]. In most experiments the ChR2 is employed to initiate precise spiking by exposing the cells to short pulses of blue light [401]. *In vitro*, ChR2 is typically activated with filtered light from mercury arc lamps [32, 42, 144], lasers [57, 81, 205] or light-emitting diodes (LEDs) [7, 377]. To obtain a better spatial resolution and enable multisite stimulation LED arrays [143] or dynamic light modulator [379] can be used. *In vivo*, stimulation of behaving animals has been conducted mostly with laser light delivered to the tissue via optical fibers inserted through chronically implanted cannulas [6, 21, 401] or with fiber-coupled high-power LEDs [378].

Since optogenetics allows millisecond-scale optical control of defined small-scale events occurring in specified cellular populations while these populations remain part of the functioning neural system within freely moving mammals or other intact and complex biological systems it has been used in countless studies. Optogenetics played a crucial role in illuminating aspects of behavior, psychiatric disorders, learning and memory, neuronal circuits and many others [114]. For example it was instrumental in determining specific types of electrical activity that trigger sleep-state transitions [6], and the precise causal role of dopamine neurons in reward learning [365]. Moreover various disease models have also been explored optoge-

netically, including for Parkinsons disease, anxiety, retinal degeneration, respiration, cocaine conditioning, and depression [396].

1.6 Controlling Neural Circuits and Microscopy Aid Study of Structural Plasticity

In 1979 Francis Crick challenged the world of neuroscience to develop a research method that would allow for precise control over particular types of neurons, while leaving the remaining neurons unaffected by a stimulus so that the properties of neural networks can be understood. Currently the optogenetics tools allow us to gain insight into how neural circuits integrate and process information as well as how those processes are stored. Since ChR2 is typically delivered to neurons through viral delivery it is possible to choose an appropriate viral promoter so that the genetic payload expresses more highly in certain cell types than others for example by injecting ChR2 gene in reverse orientation and flanked by Cre-recombinase sites into mouse types that express Cre recombinase in specific cell types [23, 209, 361]. Recently developed anterograde labeling or retrograde labeling of defined projections that enter a target region, or that innervate a target cell type, allows identifying neurons that are monosynaptically connected either to some other cell group or, especially, to a single cell [139, 385, 230, 185]. Over the last couple of years the methods have been further refined to target single cells or even sub-cellular regions [282].

These approaches allowed us to tackle fundamental questions about learning and memory that haven't been addressed before, and in particular attempt to understand what is the physical signature of neural plasticity. Such structural changes that relate to plasticity were discovered first in 1999 when structural synapse modifications paralleling functional synapse modifications were observed. At that time several studies demonstrated that LTP-inducing stimuli also trigger formation of new spines [107, 247, 358], and more recently it was demonstrated that LTP also stabilizes potentiated spines and leads to clustering of new synapses in their vicinity [87]. Moreover, potentiation of single spines by two photon glutamate uncaging induces rapid spine volume increase, which may be a general morphological correlate of enhanced synaptic transmission [251, 152]. On the contrary LTD induction by extracellular stimulation enhances bouton turnover and leads to spine retraction for several hours [272, 27, 30]. Structural reorganization accompanies also other forms of plasticity such as homeostatic plasticity, where ultrastructural studies suggest that prolonged pharmacological modulation of electrical activity can affect pre- and post-synaptic elements. For example, chronic AMPAR blockade induces a correlated increase in active zone area and post synaptic density size, suggesting that pre- and postsynaptic components remain precisely matched during functional homeostatic adaptation [268].

The new developments in high-resolution microscopy combined with novel cell-specific la-

belonging techniques [226, 12] and optogenetics allowed recently for to trace down the memory engram down to single cells within intact neural network. Recent studies indicate that that particular neurons in the lateral amygdala, a brain region important for fear, are specifically involved in particular fear memories [180] and that memory allocation is not random, but rather specific mechanisms regulate where information is stored within a neural circuits [333]. Those findings taken together might indicate a broader trend where defined populations of neurons corresponding to a specific memory trace. This would suggest a cellular correlate of a memory engram. These neurons can be tagged during learning for subsequent identification in a transgenic mouse. In these mice the long-lasting genetic tagging of c-fos-active neurons [300] and CREB engineering allows the competition between the neurons to be traced [150]. Additionally selective ablation or inhibition of such neuronal populations erased the fear memory response [151, 406] indicating that these cells are necessary for fear memory expression. However, to prove that a cell population is the cellular basis of a specific fear memory engram it is necessary to conduct a mimicry experiment to show that direct activation of such a population is sufficient for inducing the associated behavioral output [250, 128]. Those experiments were enabled by ChR2, which was used to label a population of hippocampal dentate gyrus neurons activated during fear learning. In mice optogenetic reactivation of hippocampal neurons activated during fear conditioning was sufficient to induce freezing behavior only upon light stimulation, indicating light-induced fear memory recall. Finally, activation of cells labeled in a context not associated with fear did not evoke freezing in mice that were previously fear conditioned in a different context, suggesting that light-induced fear memory recall is context specific. This indicated that activating a sparse but specific neurons that form the memory engram is in fact sufficient for the recall of that memory [234].

Together, those findings begin to close in on understanding the physical memory engram even within context of the entire neural network and optogenetics and microscopy offer a general method of mapping cellular populations bearing memory engrams. Further development of both imaging and activation methods will without a doubt allow us to illuminate more details about this system. In this thesis microscopy and optogenetics have been applied to understanding plasticity of dendritic excitability.

1.7 Organization of the Dissertations

The work in this dissertation is devoted to development of nano-photonics and bio-photonics approaches to nanoscience and neurobiology of learning and memory. This includes design, implementation and characterization of novel imaging and actuation techniques as well as new understanding of hot spots and dendritic plasticity that was afforded by those techniques. As such, this dissertation is organized in the following manner.

Chapter 1 broadly introduces the concepts in nano photonics and biophotonics and how

the work presented here fits into the broader framework of those novel disciplines. Particular focus is placed on introducing super-resolution imaging techniques including both optical and non-optical techniques including plasmonic aided techniques. Additionally I introduce the optogenetics approaches that are fundamental to biophotonics and extensively used in this thesis as well as how those approaches have been used up to date to illuminate the physical signatures of learning and memory.

Chapter 2 will be devoted to the development of a novel super-resolution imaging technique for imaging electromagnetic field enhancement. This technique termed Brownian Emitter Adsorption Super-resolution Technique (BEAST) relies on freely diffusing emitter molecules that become transiently adsorbed onto the surface to report EM field enhancement at the site of adsorption. BEAST design and implementation will be discussed as well as results of applying this technique to understand EM field profile of hot spots on metallic surfaces.

In chapter 3, another super-resolution technique is presented. This technique called Brownian Optical Microscopy (BOM), is the only technique that allows imaging true 3D shape with nanoscopic resolution. Here we focus on the principle behind BOM and discuss its design in depth. Careful characterization of the technique capabilities - including imaging with 30nm in all three dimensions in ambient conditions is presented.

In Chapter 4 we will venture into bio-photonics and discuss how optogenetics combined with dynamic light modulation was used as a novel system for precise spatiotemporal control of neuronal activity. The new system will be briefly introduced and then we will focus on its application to understanding neural plasticity and in particular to de-coupling of synaptic and dendritic excitability that led to the discovery of activity-driven dendritic excitability decrease and its molecular mechanism.

This dissertation concludes with a brief summary of the major findings arising from this work and an outlook on future directions and perspectives.

Chapter 2

Brownian Emitter Adsorption Superresolution Technique

2.1 Background and Motivation

Hot Spots

When light illuminates a rough metallic surface, hotspots can appear, where the light is concentrated on the nanometre scale, producing an intense electromagnetic field. This phenomenon, called the surface enhancement effect has a broad range of potential applications, such as the detection of weak chemical signals, even single molecules, through Surface Enhanced Raman Spectroscopy [217, 198]. Detecting single molecules with high sensitivity and molecular specificity is crucially important in bioengineering, analytical chemistry, biology, medicine, pharmacology, nanostructure materials, and environmental science [323, 15, 380]. For example in biology SERS has been used extensively for label-free fingerprinting and in conjunction with appropriate Raman active labels for detection and quantification. For example - the detection of proteins and DNA, *in vivo* or *in vitro*, to observe targeting. Some of the most promising applications include rapid DNA sequencing [198] and methylation analysis [169]. Interesting environmental applications include ultrasensitive environmental detection, monitoring and determination of the fate of pollutants in soil, air and water or the structural characterization of environmentally relevant organic phases as well as characterization of macromolecules [15]. SERS also recently found applications outside laboratory primarily for detection of chemical warfare agents [349], art preservation and authentication [278] and in forensic science [175].

Surface-enhanced Raman scattering (SERS) is a useful technique resulting in strongly increased Raman signals from molecules in the vicinity of "hot spots". SERS was first discovered in 1977 when two nearly simultaneous reports were published showing that the rough silver electrode produce a Raman spectrum that is a million fold more intense than what was expected. This enormously strong signal was named surface enhanced Raman scattering

(SERS)[176, 10]. The seminal discovery of single-molecule SERS (SM-SERS) by the groups of Nie [275] and Kneipp [198] opened up a the door for using SERS to many applications requiring this sensitivity. This was then followed by the work of Brus and coworkers [254] who attempted to use scanning probe microscopy (SPM) to image the structural features at the origin of this phenomenon. This provided the first evidence that SM-SERS originated from nanoparticle aggregates. While many fundamental questions about the origin of the effect remained unanswered, the SERS field has dramatically progressed from the originally observed enhancement on roughened silver electrodes to the current fields of sensing and imaging applications.

Since effective SERS requires substrates that would reliably and robustly deliver high field enhancement, substrates design in order to maximize the electromagnetic enhancement has been of a great interest. A major research push in this direction came over the last ten years or so after the development of nanofabrication methods. Since the presence of hot spots is critical for inducing SERS substrates generation of hot spots is one of the key aspects of preparing a SERS substrate. Both top-down and bottom-up nanofabrication strategies are being explored for the generation of hot spots. The fabrication of hot spots can be carried out through a large variety of top-down processes, the simplest of which is thermal evaporation of a thin metal film on a glass (or other appropriate dielectric) surface, which provides random nm-scale roughness. Although this approach is simple and popular it does not offer any control over the location, geometry, and density of hot spots. Similarly other large-scale approaches such as island film deposition [96] and metallic film over nanospheres (MFONs) substrates [52] offer limited ability to control substrate's geometry. The lack of control poses a problem when a small number of molecules is present and some of them adsorb to sites with no enhancement. It can be somewhat mitigated by limit the available molecular adsorption sites to only the electromagnetic hot spots on the substrate using multiphoton-induced exposure of a commercial photoresist to physically restrict the number of available adsorption sites [95]. Bottom-up approaches allow for larger control over the location and number of hot spots but typically are more laborious. They include lithographic techniques, which can also be combined with electrochemical methods for the fine-tuning of the surface features [197]. Another approach that allows for more control of the surface features yet is easily scalable and efficient is assembly of colloids. Here the particles are typically controlled by either chemical processes such as passivation or functionalization [229, 228, 140] or mechanical processes such as convective flow upon solvent evaporation of a nanoparticle solution [170].

EM field of the Hot Spot

Since the discovery of Raman effect the physics behind the extraordinary field enhancement was puzzling. The two original groups that in 1977 discovered the effect each proposed a mechanism for the observed enhancement. Jeanmaire and Van Duyne [176] proposed an electromagnetic effect which hinges on interaction of localized surface plasmons, while Albrecht

and Creighton [10] proposed a chemical theory proposes the formation of charge-transfer complexes. Both groups' optical experiments revealed that the roughness of the surface has a critical role in determining the strength of the enhancement [176, 10, 118]. Further experimental [78] and theoretical [261] studies on the impact of the surface roughness led to the connection between the surface enhancement effect and the surface plasmon, as well as to the hotspots being termed localized surface plasmon polaritons [348, 261, 129, 310]. Each of those theories alone cannot explain the surface effect since the chemical theory only applies for species which have formed a chemical bond with the surface, so it cannot explain the observed signal enhancement in all cases, while the electromagnetic theory can apply even in those cases where the specimen is only physically adsorbed to the surface, but it cannot explain the entire magnitude of the effect. Currently, it is generally thought that SERS is likely to be a combination of those two effects. Hotspots are believed to be associated with localized electromagnetic modes [321, 348] caused by the randomness of the surface texture. The debate whether those electromagnetic modes arise as a result of localized or delocalized plasmons (or both) is still a subject of hot debate. The possibility of Anderson localization of surface plasmons (i.e delocalized mode) would allow for transfer of energy over the entire extent of the system, while localized modes permit concentration of energy in a small part of it [321, 348].

Probing the electromagnetic field of the hotspots would offer much insight towards uncovering the mechanism generating the enhancement; however, it requires a spatial resolution of 12 nm, which has been a long-standing challenge in optics. The resolution of an optical microscope is limited to about half the wavelength of the incident light, approximately 200-300 nm due to diffraction limit. As a result, after more than 30 years since the discovery of the surface enhancement effect [176, 10, 118] how the local field is distributed remains unknown. Although current state-of-the-art techniques, including near-field scanning optical microscopy [33], electron energy-loss spectroscopy [273], cathode luminescence imaging [369] and two-photon photoemission imaging [206] have subwavelength resolution, they either introduce a non-negligible amount of perturbation, complicating interpretation of the data, or operate only in a vacuum. Despite this they have recently, been used to shed light on fluorescence enhancement within hot spots. Recently, near-field intensity statistics in semicontinuous silver films was studied over a wide range of metal concentrations using near-field scanning optical microscopy to reveal that variance of intensity fluctuations and the high-order moments of intensity enhancement exhibit local minima at the percolation. It was postulated that this threshold reduction in local field fluctuations resulted from resonant excitation of delocalized SP modes. By comparing experimental data with numerical results, the authors obtained the effective delocalization index at the percolation threshold, which provided the first experimental evidence for the existence of delocalized SP modes in the strong scattering regime [319]. Subsequently cathodoluminescence imaging of gold nano wires shows that those nanowires behave as plasmon resonators with eigenmodes with distinct spatial profiles and the dispersion relationship of those modes is very close to the dispersion relation for surface plasmons on a gold-vacuum interface [369]. Petek and

coworkers used two-photon photoemission imaging to image the spatio-temporal evolution of plasmon fields and localized and propagating surface plasmons on resonant and nonresonant silver gratings. In this case resonant gratings showed a strong spatially inhomogeneous interaction between the localized and the propagating modes [206]. All those experiments as well as electron energy-loss spectroscopy of silver nano triangles [273], and experiments with a waveguide mode excitation [173] have confirmed that, at these hotspots, the fluorescence enhancement is confined to a region far smaller than the wavelength of light, yet the field of a single hotspot has not been resolved.

While those studies of field and intensity statistics have helped us understand features of hot spots and have deepened our general understanding of mesoscopic transport and localization in disordered systems they have suffered from not having appropriate imaging tool. Here we present a technique that uses Brownian motion of single molecules to probe the local field. It enables two-dimensional imaging of the fluorescence enhancement profile of single hotspots on the surfaces of aluminium thin films and silver nanoparticle clusters, with accuracy down to 1.2 nm.

2.2 Methods

Principle

Briefly, in BEAST the sample made out of rough metallic field deposited on a glass cover slip is submerged in a solution of fluorescent dye. The chamber containing the sample is mounted on a total internal reflection (TIRF) set-up. As the diffusion of the dye molecules is much faster than the image acquisition time the fluorescence from the rapidly diffusing dye molecules contributes to a homogeneous background. However when a dye molecule is adsorbed onto the surface of a hotspot, it appears as a bright spot. By using a maximum likelihood single molecule localization method [260] the molecule can be localized with single-nanometre accuracy [34, 307, 393] and the fluorescence enhancement can be deduced from the intensity of the fluorescence. After the dye molecule is bleached the fluorescence disappears and another adsorbed dye can be imaged.

Setup

To image hot spots formed on the aluminum films a 200mW 532nm laser (Lambda Pro) was passed through a neutral density filters to decrease intensity to 7mW and then by a 532nm/1nm laser line band pass filter (Edmund optics) before impinging on a quartz Pellin-Broca prism (Thorlabs Inc.). The resulting evanescent wave on the surface of the sample excites fluorescent molecules inside a sample chamber. This resulting fluorescence is collected by 60X, NA1.25 objective lens (Zeiss GmbH), passed through a 532nm long pass filter (Semrock) and a 582/80m band pass filter (Chroma Technology) and recorded by EMCCD

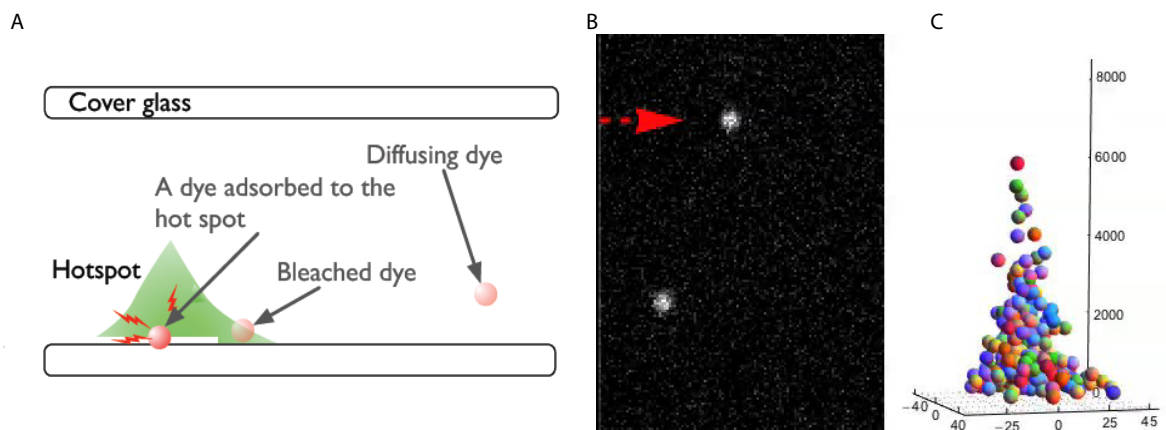


Figure 2.1: The principle of Brownian motion single molecule super-resolution imaging. (A) Hotspots appear on the surface of a thin aluminum film under a total internal reflection (TIRF)-type illumination at 532nm. To map the field distribution inside the hotspots, we use the Brownian motion of fluorescence dye molecules (Chromeo 546). The dye molecules stochastically adsorb to the surface. After a few frames (50 - 100ms per frame), the dye molecules photobleaches, which gives rise to a blinking pattern where each blink corresponds to one adsorption-bleaching event. By controlling the concentration of the dyes, the adsorption rate can be adjusted to ensure that within a diffraction limited spot, only one molecule is adsorbed at a time; therefore the position of the molecule can be determined by a maximum likelihood localization method with accuracy down to 1.2nm. (B) The raw image as viewed in the camera showing two hot spots with molecules adsorbed to them. The hot spot with an arrow pointing to it is the one whose reconstruction is shown in C. (C) By using the adsorption locations as the x and y coordinates and the fluorescence intensity as the z coordinate, we obtain a 3D scatter plot of the fluorescence enhancement profile of the hot spot, with each sphere representing one single molecule event.

(Cascade 512 from Photometric Inc.). 4X magnifier (Nikon Inc.) was placed right in front of the EMCCD, resulting in a final pixel size of 72nm. The typical acquisition time is 80ms.

To image silver NPs clusters an objective-side TIRF set-up built on the top of inverted Nikon microscope with a TIRF objective (N.A. 1.49 100X) was used. The excitation beam from a 40mW 644nm laser (Coherent Inc. Cube) was reflected by a 650DCLP (Chroma Inc.) into the objective lens. After the reflection the power at the objective lens is ≈ 4 mW. The fluorescence from the dye is collected by the same objective and passed through dichroic and then through a 710/130m (Chroma Inc.) emission filter placed before an EMCCD camera (Cascade 512, Princeton Instruments.). To reduce the pixel size, and hence improve the localization accuracy of a single particle a 4X magnifier (Nikon Inc.) is placed right in front

of the EMCCD. The final pixel size corresponds to 48nm/pixel. The exposure time of the camera is typically 20ms.

In both cases, within one field of view, which can be up to 1mm² multiple hot spots can be imaged in parallel (typically 5-10 hot spots will be visible) within the typical acquisition time of 20-80ms. This is much more efficient than raster scanning based techniques, such as near-field scanning optical microscopy and electron energy-loss spectroscopy.

Sample Preparation

The aluminum thin films samples were prepared by depositing a thin film of aluminum on the top of quartz slide using E-beam evaporation. Prior to the deposition, a 3"x1" quartz slide (Ted Pella Inc. or SPI Inc.) is thoroughly cleaned by first soaking it in a bath of RCA base solution (4:1:1 ratio of distilled water, hydrogen peroxide and ammonia hydroxide) for 15 minutes and then transferred to a RCA acid bath (6:1:1 ratio of distilled water, hydrogen peroxide and hydrogen chloride) for another 15mins, followed by 15mins of sonication in filtered distilled water (Milipore). The slide is then blow-dried with pure nitrogen gas and placed immediately inside an E-beam evaporation chamber (Torr International Inc.). The chamber is then pumped down to achieve vacuum and a 15nm Al film is deposited at a relatively fast rate of 0.1nm/s. The samples are then stored in the desiccator for up to 4 days.

To obtain sample with silver nano particle clusters - commercially synthesized nanoparticles were deposited on the top of glass cover slips. The glass cover slips (1.5 Fisher Scientific Inc.) were by first soaked in a bath of RCA base solution (4:1:1 ratio of distilled water, hydrogen peroxide and ammonia hydroxide) for 15 minutes, followed by RCA acid bath (6:1:1 ratio of distilled water, hydrogen peroxide and hydrogen chloride) for another 15mins-20min, followed by 15mins of sonication in filtered distilled water (Milipore). After cleaning, the cover slides were either immediately dried and used for an experiment or stored in a clean jar filled with filtered distilled water. Immediately before the experiment a drop of 0.1mL concentrated solution of 40nm silver colloids (Ted Pella Inc.) is spin coated on a cleaned cover glass forming a layer of nanoparticle clusters on the surface.

A flow chamber containing a sample was assembled immediately before the experiment by sandwiching the sample slide and a clean cover slide using 100 μ m-thick double sided tape. Then the sample is mounted on the top of the setup and filled with filtered distilled water (Milipore). Afterwards the water is exchanged for 10nM dye solution. Most experiments use 10nM Chromeo-542 dye (Active Motif) dye. However Cy3 (GE Healthcare), and Alexa-555 (Life technology) were used in control experiments and yielded similar results.

Data Analysis

Single Molecule Localization

When the dye gets temporarily adsorbed onto the sample its fluorescence stands above the background and its position can be localized. The molecule is localized by fitting the image of its point spread function (PSF) and finding its center. Since molecules are imaged one at a time they can be localized with resolution far exceeding diffraction limit. This is most typically done by using least-squares to fit a 2D gaussian to the fluorescent image [395, 213, 307, 29, 172, 34, 329, 248, 328, 37, 119, 355]. However, we have chosen to fit the fluorescent image with a two dimensional Gaussian by maximum likelihood estimation (MLE). We have selected MLE because MLE is capable of achieving theoretical fitting resolution based on the Fisher information theory [335, 260], which is higher than currently widely used least square fitting. Moreover it utilizes the available information most efficiently, while the least squares fitting wastes one third of the information contained within the raw images because, as opposed to least squares fitting, it doesn't treat shoulders and tails in the measured PSF as background [260].

The fluorescence signal from a dye reflects the intensity of the optical field at the location of the dye ($|E^2|$). Because Raman signal is much weaker than the fluorescence one, we choose fluorescence as the probe [266].

Data were analyzed using a home-written MATLAB script. The script performs single molecule localization in two steps: first we applied standard least square fitting or centroid fitting of the raw images to obtain the initial parameters and second we used those initial parameters in the maximum likelihood estimation routine to precisely determine the lateral position. To obtain the position we used the log likelihood function:

$$\sum_i (-E_i + n_i \log E_i - \log(n_i!)) \quad (2.1)$$

where n_i is the observed number of photons at pixel i , and E_i is the expected number of photons calculated from the fitting parameters, which is minimized during the fitting procedure. The accuracy of the estimation, determined from the variance using EMCCD camera, is:

$$\sigma^2(x) = 2 \frac{\sigma_\alpha^2}{N} \left(1 + \int dt \frac{\log t}{1 + t/\tau} \right) \quad (2.2)$$

where the width of the PSF is σ_α^2 . Since the PSF is imaged on a camera with fixed and not infinitesimally small pixels, their width of PSF as imaged on the camera is $\sigma_\alpha^2 = \sigma^2 + a^2/12$, where a is pixel width. N is the total number of photons acquired and $\tau = \frac{2\pi\sigma_\alpha^2 b^2}{Na^2}$, where b is the average background photon count.

Although the point spread function of a single molecule adsorbed at a hotspot appears as Airy function and the side lobes are clearly visible on Fig. 2.3B, the maximum likelihood

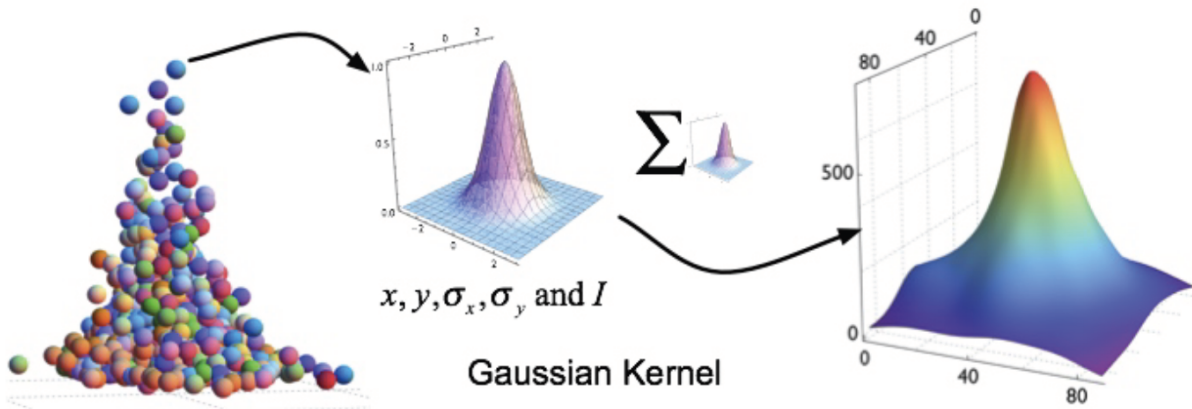


Figure 2.2: Gaussian Kernel Rendering Procedure. We start with the simple image where each ball represents one adsorption event with location at the x and y coordinates, and the fluorescence intensity as the z coordinate. Then each pixel X of the rendered image $I(X)$, is a weighted average of the intensity from all of the single molecule events, with molecules closer to X carrying more weight. The window size of the kernel is determined by the accuracy of the single molecule localization. The rendered image reports an averaged profile of the local fluorescence enhancement. A hotspot may have complex structures that are smaller than the size of the kernel; these fine structures are removed in the stochastic rendering process

estimation using Gaussian approximation to the true point spread function utilize the majority of the photons, and thus is able to provide localization accuracy of nearly theoretical limit (a cross section is shown in Fig. 2.3B as the red curve). To quantitatively test the single molecule localization accuracy, we measure the variance in position estimation among multiple consecutive position estimations of the same molecule adsorbed to the surface. The variation was 2.97nm and 2.68nm in x and y direction respectively (Fig. 2.3D, with the green and blue curves representing the deviation of the x and y from the mean for each frame of the entire time series). The theoretical variance calculated using the maximum likelihood estimated Eq. 2.2 provided the variance of 2.59nm (Fig. 2.3E red dash curve), which is in a good agreement with the measured value indicating that Eq.2.2 is sufficient for estimating the single molecule localization accuracy.

Gaussian Kernel Image Rendering

After all the single molecules for a given hot spot were localized they were used to predict the shape of the entire hot spot. The observed single molecule events were distributed randomly both in space and in time and were sparse in space allowing for single molecule localization beyond the diffraction limit. Each image spot is analyzed by a maximum likelihood estimation method explained above to predict its exact lateral position and intensity I . The

measured intensity I corresponds to the field enhancement at the $x - y$ position. We then assign each single molecule events to be represented by a color sphere in the 3D scatter plot (Fig. 2.2A), where the width of the sphere is the localization accuracy σ of a single molecule localization. To obtain smooth surface representative of field enhancement inside the hot spot we apply mesh to the scatter plot. However it is difficult to apply a fixed mesh directly in this case so we use a Gaussian Kernel rendering [34, 153], which gives us smooth surface (Fig. 2.2B). In Gaussian Kernel Rendering we take each of the molecular events denoted by a color sphere to represent the probability of finding the true location of the single molecule event in space. Multiplying each Gaussian function with the intensity I from the fitting, summing them up, and normalizing the sum by the mean number of events, using Eq. 2.3, provides a smooth 3D image of the enhancement profile, shown in the right panel of the figure 2.2, described as:

$$I(\vec{x}) = \frac{\sum I_i \exp(-(\vec{x} - \vec{x}_i)^2/2\sigma^2)}{\sum \exp(-(\vec{x} - \vec{x}_i)^2/2\sigma^2)} \quad (2.3)$$

Now each pixel X of the rendered image, $I(X)$, is a weighted average of the intensity from all of the single molecule events, with molecules closer to X carrying more weight. The window size of the kernel is determined by the accuracy of the single molecule localization. The rendered image reports an averaged profile of the local fluorescence enhancement. A hotspot may have complex structures that are smaller than the size of the kernel; these fine structures are removed in the stochastic rendering process. The rendering also decreases the confounding effect of a number of factors, including the molecules orientation relative to the polarization of local field, and stochastic photobleaching.

2.3 Results

Single Molecule Imaging

Estimating Lateral Localization of Single Molecules

First we conducted a control experiment to confirm that the events we are observing were indeed single molecule events and that the molecules are not diffusing during the acquisition time. There are two different kind of diffusion that could take place during this experiment - first the molecule could detach from the surface and diffuse into the liquid and second a molecule could diffuse on the surface of the aluminum film. If the molecule becomes detached from the surface and diffuses away in the liquid its diffusion would be extremely rapid (a 1-nm-diameter sphere diffuses through a 200-nm-wide spot in less than 0.1ms on average in water at room temperature, in contrast to an imaging time of typically 50-100 ms) and it would appear to us as the same as if the molecule bleached - as a sharp drop in fluorescence and as such would not affect the measurement. Since the diffusion coefficient of molecules adsorbed on a solid surface is very slow - less than 5nm^2 [73, 317] it will also not affect our imaging resolution. This can be seen more clearly by examining single molecule traces

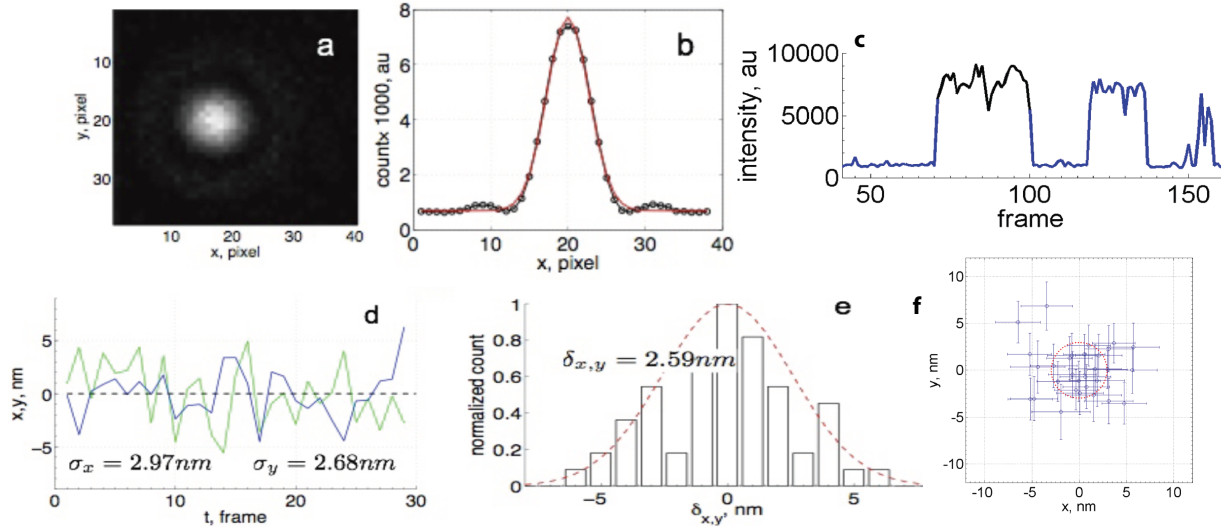


Figure 2.3: Single molecule localization in BEAST. (A) raw camera image of a hot spot with a fluorescent molecule adsorbed to it. The molecule appears as a round, bright spot that is roughly 10 pixels wide. (B) Cross section of the single molecule fluorescence intensity (black). The shape of the intensity is an Airy function with clearly visible side lobes. The 2D Gaussian that we used to fit the fluorescence profile (red) fits the fluorescence profile very well. (C) Fluorescence trace from a single hot spot over time. The black region indicates a 50ms time period when one molecule is adsorbed to the hot spot. Afterwards the molecule is bleached in a single step demonstrating that it was in fact a single molecule. (D) In order to estimate the localization accuracy we compare localization of a single molecule over time (green - x position estimation and blue - y position estimation). The standard deviation of the localization is less than 3nm. (E) Using Eq. 1.2 we estimated the maximum likelihood estimated variance of 2.59nm (red dash curve). There is a good agreement between the measured variance and the calculated variance. Therefore, Eq.1.2 is sufficient for estimating the single molecule localization accuracy. (F) We plot the centroid position from each frame within this period in the figure above. The error bar corresponds to the variance estimated from Eq. 1.2 The distribution of the data points provides an estimation of the surface diffusion. Most of the data points are located within a circle of 5nm. The standard deviation is only 2.6nm and 3.3nm in x and y direction respectively, which is smaller than the variance of the single molecule localization. Therefore, the effect of the surface diffusion of adsorbed molecule is not detectable.

from our experiments (Fig.2.3C) taken at a frame rate of 50 frames/s (exposure time 18ms for each frame). We can see that the molecule bleaches in one sharp step after it has been adsorbed to the surface (black portion of the trace). Additionally if we localize the molecule at each frame we can see that the distribution of the data points provides an estimation of the surface diffusion Fig.2.3E. Most of the data points are located within a circle of 5nm. The standard deviation is only 2.6nm and 3.3nm in x and y direction respectively, which is smaller than the variance of the single molecule localization estimated from an Equation 2.2 (denoted here as a blue error bar). Therefore, the effect of the surface diffusion of adsorbed molecule is not detectable and does not affect our measurement.

Estimating EM field enhancement based on intensity of single molecules

The estimation of EM field enhancement relies on correlating the intensity of EM field to fluorescence of the molecule. The fluorescence emission from single molecules is a stochastic variable and to verify that it correlates with the EM field intensity we performed a control experiment by measuring the intensity of single molecules that are randomly adsorbed on the surface of a quartz cover slide. A prism type total internal reflection fluorescence (TIRF) setup is used. A 0.1nM chromo-546nm dye (Active Motif Inc.) solution is flown into a chamber. The excitation intensity of the laser (532nm Lambda Inc.) is adjusted by changing the angle of a half wave plate sandwiched between two polarizers. Fig. 2.4A shows the histograms of the single molecule fluorescence intensity with excitation powers of 6.92mW, 7.97mW, 8.98mW and 10.05mW, respectively (bottom to top). The average fluorescence intensity is shown in Fig. 2.4B, which follows the excitation power in a linear manner quite well. However, underlying every point in panel B is a broad distribution of the intensities of single molecule events, as is shown in Fig. 2.4A. Fig. 2.4C depicts the relationship between the number of the single molecule events and the accuracy of the final averaged result. We randomly pick several groups of events collected at 10.05mW, and plot the average intensity of the groups against their size. The shaded region corresponds to a 15% level of uncertainty. From the figure, it is clear that about ≈ 10 events are sufficient for an accurate estimation of the final intensity.

Another factor that could affect the intensity of the molecule is its orientation with respect to the glass. The fluorescence intensity of a single molecule depends on the orientation of the molecule relative to the polarization of the local field, $\cos(\theta)$. Experiments have shown that a molecule undergoes hindered rotations on a metal surface [288, 259, 41], and that the wobbling axis can vary 90° from parallel to the surface of the metal to perpendicular to the metal surface [338, 339]. We consider two extreme cases to estimate the impact of the molecules orientations here: a molecule wobbling perpendicular, and parallel with respect to the polarization axis of the local field, with a cone angle of 45° ; these two extreme case situations yield fluorescence intensity of:

$$\frac{\int_0^{45} \cos(\theta)^2 \sin(\theta) d\theta}{\int_0^{45} \sin(\theta) d\theta} = 0.74 \quad (2.4)$$

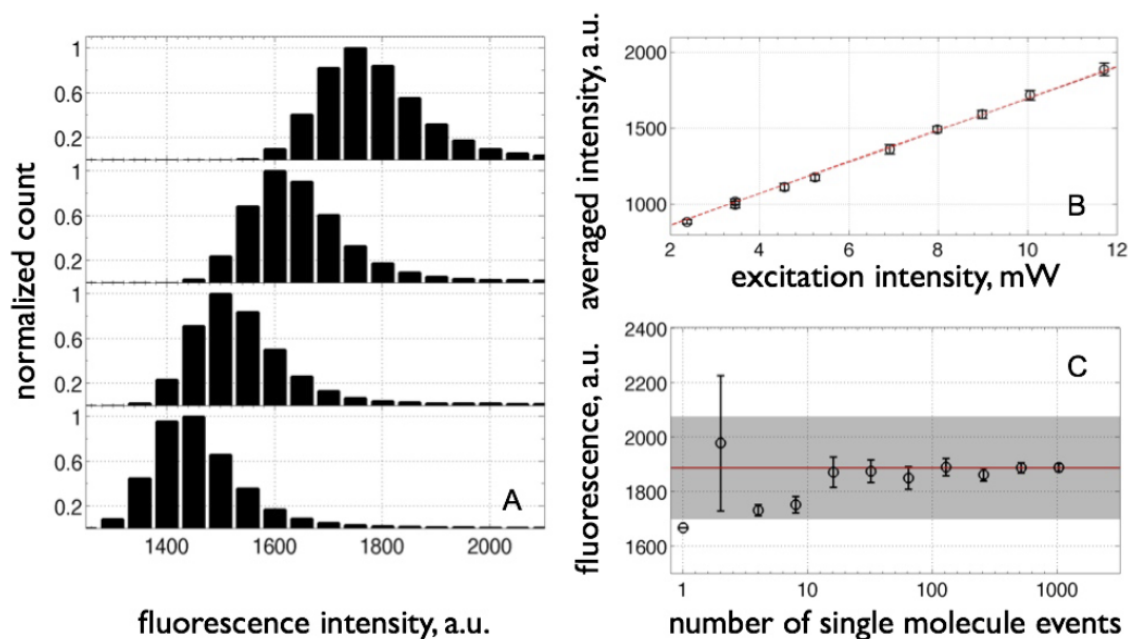


Figure 2.4: The relationship between molecule's fluorescence and EM field enhancement. (A) We varied the EM field intensity of the excitation light by changing the angle of a halfwave plate sandwiched between two polarizers and measured the fluorescence intensity of single molecules that are randomly adsorbed on the surface of a quartz cover slide. The histograms represent fluorescence counts of the single molecule fluorescence intensity excited with the excitation powers of 6.92mW, 7.97mW, 8.98mW and 10.05mW, respectively (bottom to top). (B) The average fluorescence intensity follows the excitation power in a linear manner. (C) Relationship between the number of the single molecule events and the accuracy of the final averaged result. Events collected at 10.05mW were picked at random and grouped into group of variable size then the average intensity of the groups was plotted against their size. The shaded region corresponds to a 15% level of uncertainty. From the figure, it is clear that about ≈ 10 events are sufficient for an accurate estimation of the final intensity.

and

$$\frac{\int_4^{90} 5 \cos(\theta)^2 \sin(\theta) d\theta}{\int_4^{90} 5 \sin(\theta) d\theta} = 0.26 \quad (2.5)$$

respectively. Therefore, due to the uncertainty of molecules orientation, the measured fluorescence emitted from a single molecule fluctuates to a degree that is within 26% - 74% of the true local enhancement. This should be viewed as an upper bound of the error bar. The final image is rendered by a kernel averaging method, therefore the intensity at each pixel represents a statistical average of several molecules sampling a broader distribution than that of a single molecule, which reduces/smooths the intensity fluctuations due to the uncertainty of the molecules orientation. Our control experiment on cover glass shows that averaging over 10 adsorption events could reduce the uncertainty down to less than 15% (Fig. 2.4C).

Imaging EM Enhancement of Single Hot Spots on Al Films

The hotspots are formed on the surface of a thin (12-15 nm) aluminum film deposited on a quartz substrate by electron-beam evaporation (Fig.2.5 A inset). Water facilitates the oxidization process [62]. An oxidized layer can form on the surface of the aluminum film and reach a thickness of up to 8 nm [62]. Each sphere in Fig. 2.5 A represents a single molecule adsorption event, with the x and y coordinates representing the location of the molecule, and the z coordinate corresponding to the intensity of the molecules fluorescence. Single molecules can be localized with accuracy down to 1.2 nm. The measured enhancement here exhibits a rapid exponential decay with a decay constant of 9.8 nm (Fig. 2.5 B and C). The standard deviation of the location of observed single molecule events was used as a model-independent measure of the width (15.4 nm) of the hotspot, as shown in Fig. 2.5 E. The existence of such a small hotspot demonstrates the presence of tight near-field optical confinement. After Gaussian image rendering the shape of the hot spot is more clear showing an exponential decaying field enhancement with the full-width at half-maximum (FWHM) measured as ≈ 20 nm (Fig 2.5 C). By comparing the fluorescence from the dye molecules adsorbed on the hotspot to that from the dye molecules immobilized on the surface of a quartz slide under the same conditions, we determined that the fluorescence enhancement is about 36 times greater at the center of the 20-nm hotspot. This modest enhancement results from the high ohmic loss of aluminum at the visible wavelength involved.

Among the total of 60 hotspots that were analyzed, we found a broad distribution of enhancement factors and sizes, with approximately 32 nm as the average size of the spots Fig. 2.6A . The maximum fluorescence enhancement factor of the hotspots was found to depend inversely on their size; the largest enhancement factor we observed was 54 times (for a 15-nm hotspot); this results from the tighter confinement of the electromagnetic field in a smaller hotspot Fig. 2.6B.

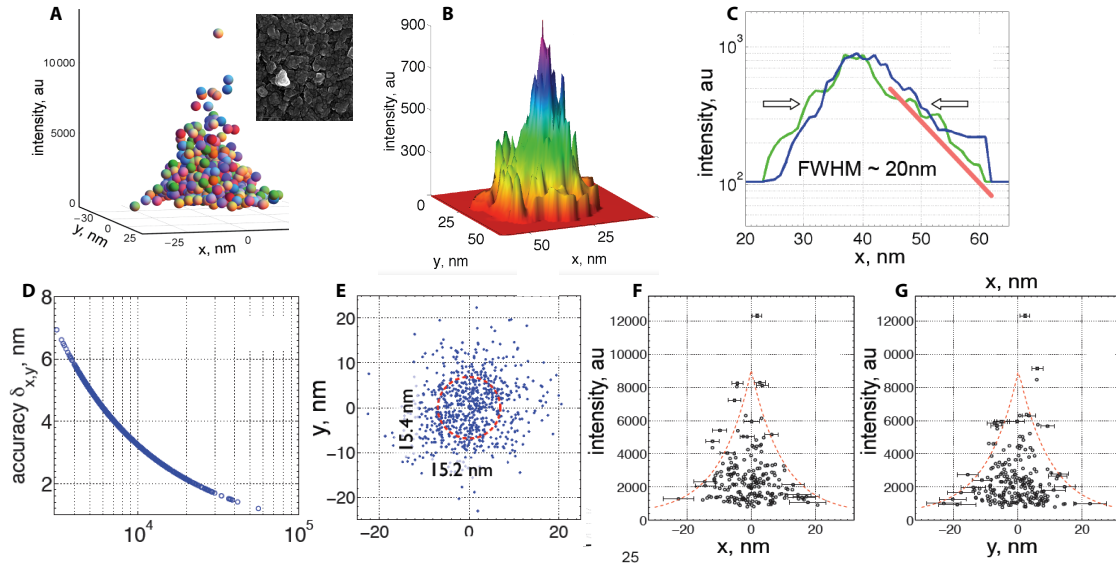


Figure 2.5: Imaging the EM field enhancement of a single hot spot. (A) By using the adsorption locations as the x and y coordinates, and the fluorescence intensity as the z coordinate, we obtain a 3D scatter plot of the fluorescence enhancement profile of the hotspot, with each sphere representing one single molecule event. The inset shows a SEM of a Al film from which the hot spots were imaged. (B) As the fluorescence of a single molecule is intrinsically stochastic, we remove this randomness by using a Gaussian kernel method to render the image of the field distribution. The field distribution of an example hot spot after the rendering is shown. Each pixel X of the rendered image corresponds to average intensity from all of the single molecule events, with molecules closer to X carrying more weight. The kernel window size is 2.1 nm; this small window size makes the image appear noisy. (C) Cross section of EM field enhancement of the hot spot. An exponential decay field profile is visible in the two cross-sections of the hotspot along x and y directions through the peak (blue and green curves respectively). The exponential shape is even more evident on a log scale where it clearly shows as a straight line (red solid line). The FWHM of the spot is ≈ 20 nm. (D) The accuracy of the reconstructed field profile, estimated from the variance of the maximum likelihood localization, depends on the number of photons collected from the molecules, with brighter single molecule events showing better accuracy, down to 1.2 nm. (E) The distribution of the single molecule events belonging to this hot-spot provides a direct measure of the size of the hotspot. The width of the hotspot characterized by the standard deviation of the single molecule events is 15.2 nm and 15.4 nm in x and y directions, respectively. (F) Cross-section of the hotspot at $y = 0$ nm. The molecules within $-2\text{nm} < y < 2$ nm are shown. (G) Cross-section of the hotspot at $x = 0$ nm. The envelope appears as an exponential decay with a constant of 9.83 nm (red dashed lines). To avoid crowding, only the single molecule localization variance of a few spheres near the envelope is shown.

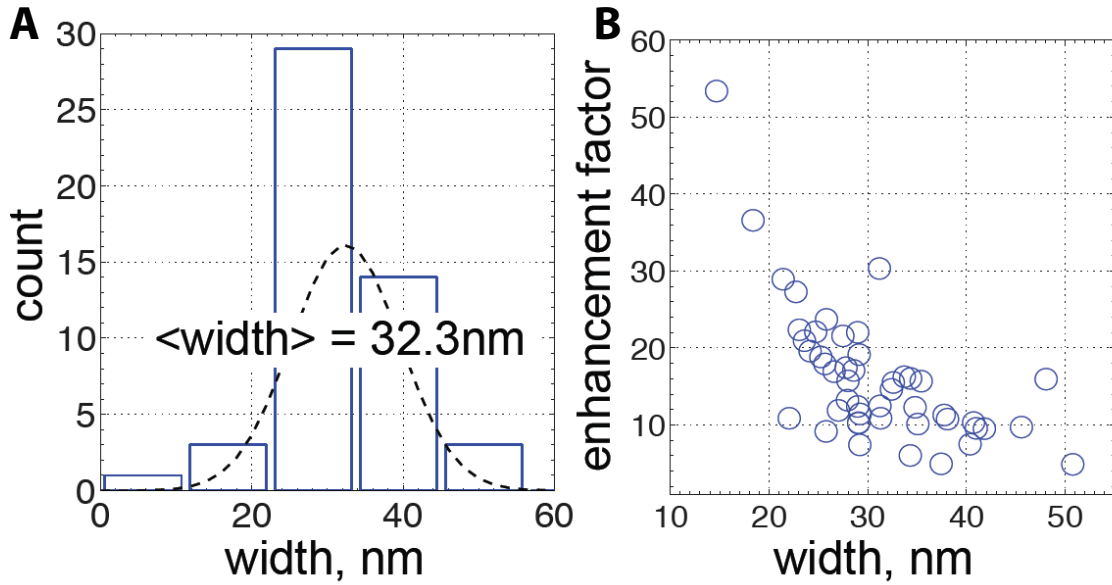


Figure 2.6: EM field enhancement statistics across multiple hot spots. (A) All of the hotspots observed are of deep sub-wavelength size, with an average width of 32.3 nm. (B) By plotting the enhancement factor of the hotspots against their width, an inverse relationship between the size and the enhancement factor is visible: tighter confinement leads to stronger enhancement.

Imaging EM Enhancement of Single Hot Spots on Ag NP clusters

As hotspots also appear in metal nanoparticle clusters [78, 261], and the mechanism has been postulated to be similar to that of the metal thin films, we investigated the hotspots that formed on silver clusters consisting of silver nanoparticles with average diameter of 40 nm. In addition to the oxidation layer of silver [388], the dispersing surfactant (that comes with the silver nanoparticle suspension) condenses on the surface of the silver nanoparticle clusters during the aggregation process. We found that the fluorescence enhancement profile of the hotspots formed in the silver clusters has an exponential shape, similar to that of hotspots on the surface of an aluminum film Fig. 2.7A. The electromagnetic field is strongly confined in a hotspot within an elliptical region of 13.2nm x 20.3nm, more than 30 times smaller than the wavelength of the excitation laser (Fig. 2.7B and C) and exhibits exponential decay (Fig. 2.6D).

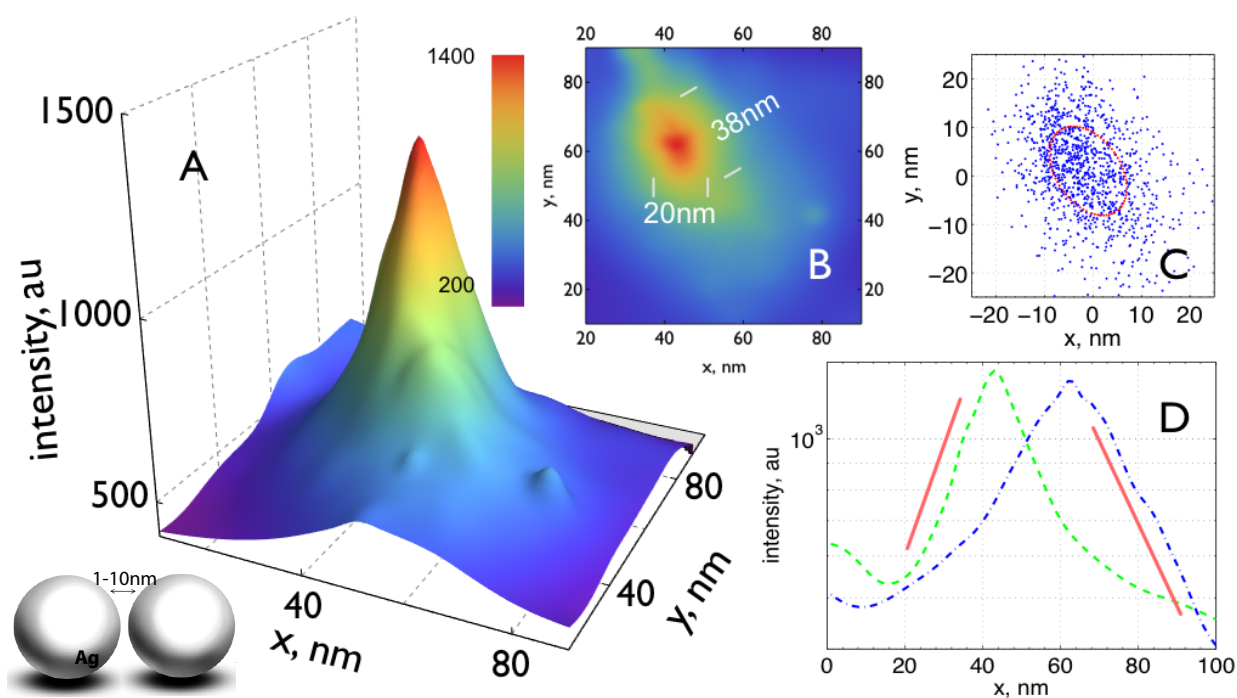


Figure 2.7: A hotspot formed on silver nanoparticle clusters appears similar to those formed on the aluminum film. A 644-nm laser is used for excitation, and Chromeo 642 dye (Active Motif) - whose emission centers around 660 nm - is used. The maximum enhancement factor at the center of the peak corresponds to 136x the fluorescence from the same dye molecules adsorbed on a glass surface. (B) The hotspot exhibits a similar exponential decay profile as those formed on the surface of the aluminum film. Two cross-sections of the hotspot along x (green) and y (blue) directions through the peak are plotted on a logarithmic scale, with the solid red lines as eye-guides for the exponential profile. (C) The widths of the hotspot, estimated from the distribution of the single molecule events on a scatter plot, are 13.2nm and 20.3nm along the two axes.

Three dimensional imaging of Hot Spots

In order to estimate the 3D profile of hot spots, the spacer was added after a single molecule image was recorded by flowing a 1% w/v bovine serum albumin (BSA) in phosphate buffer saline (PBS) solution into the chamber (Fig. 2.8A). After 30 minutes of incubation, long enough for the BSA to nonspecifically cover the surface of the silver nanoparticles [332], a second image was taken and compared with the previous image (Fig. 2.8B). A 36% drop in the enhancement and a 26% increase in the width were observed, with the shape remaining essentially the same as exponential (Fig. 2.8C). All 9 of the recorded hotspots show a similar order of magnitude of changes (Fig. 2.8D and E). Depending on the orientation of the BSA molecule, the thickness of the spacer layer varies from 4nm to 14nm [332]. If we use an average thickness of 9nm as an estimation, a change of 20 - 40% of the enhancement factor over 9nm puts the decay rate in a z direction similar to that in xy direction, suggesting a strong confinement of the local field in z direction as well.

2.4 Discussion

Using BEAST, we have demonstrated the first direct measurement of a single hotspot and observed that the EM field decays exponentially. This exponential profile sheds new light on the much-debated mechanism of extraordinary field confinement in a two-dimensional disordered system, where both Anderson-localized modes [348, 310] and localized plasmon modes could emerge. In Anderson localization, delocalized modes allow for transfer of energy over the entire extent of the system, while localized plasmon modes caused by strong interaction between the plasmonic resonances of the two particles permit concentration of energy in a small part of the system. It has been also suggested that plasmon eigenmodes may also simultaneously have properties of both localized and de-localized states: including hot spots on the small scale, but which are distributed and coherent over the large scale. The surface plasmons are extremely inhomogeneous in their oscillator strengths ranging over more than 10 orders of magnitude, which may explain a large variation in EM field enhancement from spot to spot. Although signatures of the Anderson-localized mode have been reported in two-dimensional disordered metallic systems [319], its hallmark, an exponential profile, had not been directly observed up until now.

The fluorescence field enhancement on the metal film arises as a result of interplay between local field enhancement and quenching. Since metal provides the fluorophores nonradiative pathways to the ground state it decreases their fluorescence by damping the dipole oscillations and thereby decreasing their quantum yield to $Q_0 = \Gamma/(\Gamma + k_{nr})$, where Γ is the radiative decay rate and k_{nr} is the non-radiative decay rate. It however doesn't have any significant effect on the rate of radiative decay, that is, the spontaneous rate at which fluorophores emit photons [59, 214]. The quenching is short-ranged and has a d^3 dependence where d is the distance between fluorophore and the metal. Fluorescence enhancement on the other hand

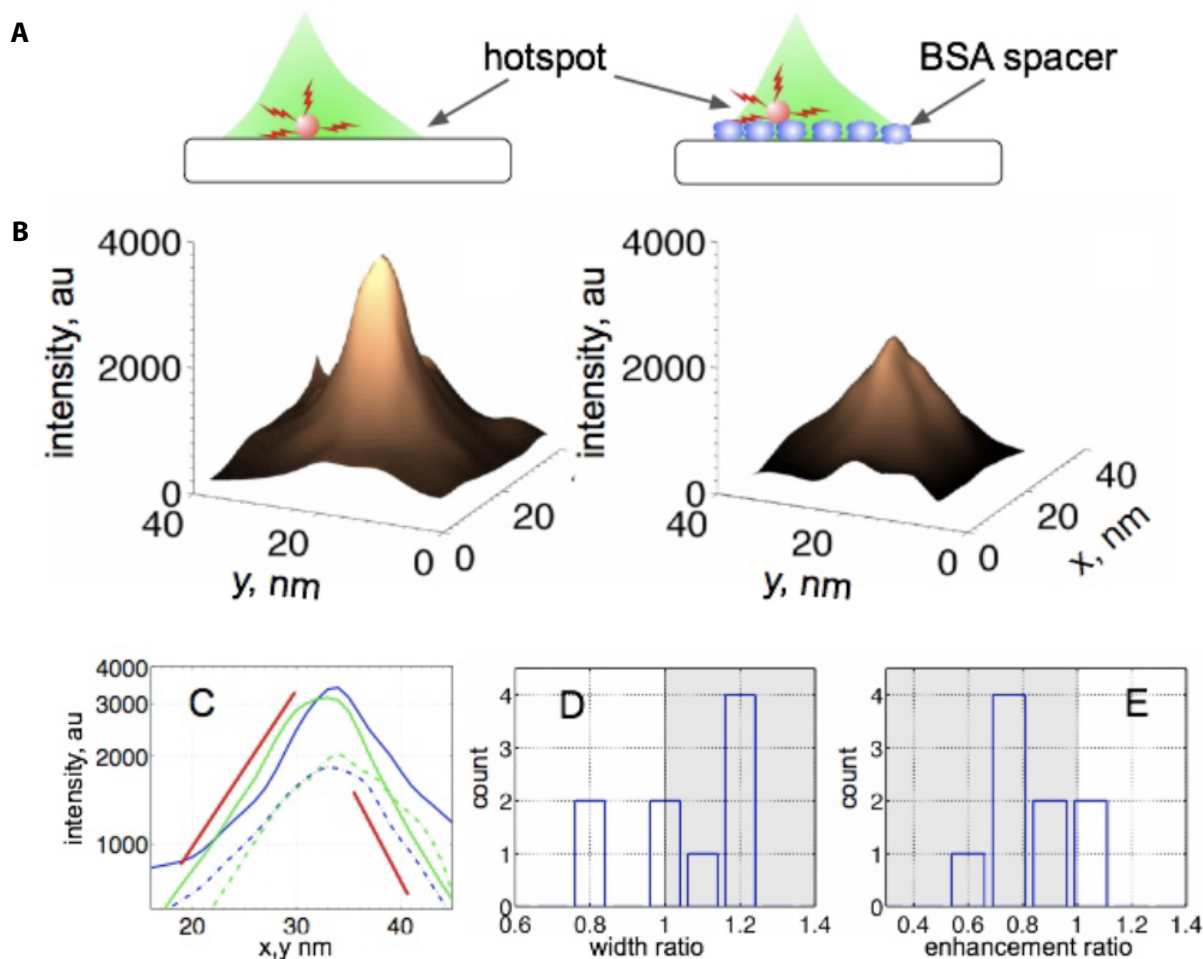


Figure 2.8: Measuring a 3D profile of a hot spot. (A) Experimental overview. A hot spot on a thin Al film is localized and imaged using standard BEAST technique (left), then BSA is flown and forms a 4-14nm layer. Then the hot spot is imaged again, however this time the intensity obtained is obtained 4-14nm above the surface of the metal. (B) Intensity before applying BSA (left) and after (right). The decrease in EM field enhancement is evident. (C) Cross section of the hot spot before BSA (solid line x -cross section green line and y -cross section blue line) and after (dashed line, x -cross section green line and y -cross section blue line). While the exponential decay is present in both cases there is a 36% drop in the enhancement and a 26% increase in the width were observed after BSA layer has been applied. (D) Statistics of width change across multiple hot spots showing that the increase in width ratio was comparable among them (E) Statistics of width change across multiple hot spots showing that the decrease in enhancement was comparable among them.

acts to amplify the incident field. This effect is much more long ranged and can extend many nm away from the metal surface [214]. Therefore there exists two distinct regimes above the surface of a metal: a quenching dominated regime near the surface, followed by a local field dominated regime further away from the surface [388, 19]. The transition point between the two regimes coincides with the peak of the fluorescence enhancement. This peak ranges from a few nanometres to tens of nanometres, depending on the materials and the geometry of the nanostructures [388, 19] depending most strongly on the shape and size of metallic structure. In our case the dielectric layers formed on the surface of the metal during the oxidation process provide a spacer between the metal surface and fluorescent molecule and shift the adsorbed layer of molecules into the local field dominant regime, contributing to the strong (up to 54 times (Al) and 136 times (Ag)) fluorescence enhancement observed. We explored the distance dependence of the enhancement by depositing a ≈ 9 -nm-thick spacer layer of self-assembled protein molecules on the surface of silver nanoparticle clusters *in situ*, in addition to the original dielectric layer. As the transition point of silver nanoparticle clusters is 2.5 nm above the surface in a similar system [19], the observation will be in the local field dominant regime. Comparing the same hotspot without and with the spacer layer, we found a $\approx 36\%$ drop in the fluorescence enhancement when the spacer was present which was accompanied by a $\approx 26\%$ increase in width of the hot spots indicating worse confinement. The characteristic exponential shape however remained essentially unchanged, which confirms that an exponential profile is a general feature of the local electromagnetic field.

2.5 Outlook

The single molecule super-resolution approach is a generic technique, which offers a unique, perturbation free capability for imaging the electromagnetic field enhancement of optical nanostructures with single-nanometre precision. Additionally, other imaging modalities can be integrated to provide spectroscopy as well as fluorescence lifetime information of the molecules. This approach could be used to investigate the strong-coupling regime such as one that occurs with resonant nano-antennas [352, 195]. In the strong-coupling regime, the distributed dipoles in the antenna could significantly affect the fluorescence of the molecules, and the strength of the coupling cannot be directly measured from the intensity of the fluorescence signals. A super-resolution measurement of the spatial distribution of the molecules fluorescence lifetime will help visualization and understanding of the coupling. Furthermore, with the development of brighter fluorophores, better photo-bleaching suppression methods, and more efficient three-dimensional super-resolution techniques, fully three-dimensional imaging will also be realized.

Chapter 3

Brownian Optical Imaging

3.1 Background and Motivation

Imaging three-dimensional (3D) topology is a key to understanding properties of nanomaterials, nanofabricated structures and investigating structure and function of biological systems. New imaging tools are mostly responsible for emergence of modern nanotechnology and material science. Atomic force microscopy (AFM) has been a workhorse for nanoscale topographic measurements due to its ability to map topology with resolution down to a few nanometers. It has proven itself a versatile and powerful instrument for imaging surface topology and has given scientists and engineers an unprecedented access to information about surface topology at the nanoscale. For example AFM has been instrumental in discovering microstructural properties of superalloys [131], investigating structure of soft polymers [374], DNA interactions and structure of proteins and cell [11]. While continuous improvements to AFM ensured that it remained a relevant and important technology, its performance is still limited by the serial nature of the single-tip scanning [104]. In a standard AFM a cantilever with a pyramidal downward pointing tip is scanned over an area on the top surface of the object. Since the AFM tip cannot reach down narrow trenches, inclined sidewalls or sharp corners of nanoscaled structures AFM imaging is limited to objects with low aspect ratio and prone to artifacts. Moreover AFM does not offer true three-dimensional imaging since the tip can scan only the topmost surface of the sample and hence AFM cannot image cavities, overhangs or structures shadowed by another object near or above them. Finally scanning of a single, macroscopic tip places severe limitations on the data rate and image size and might mechanically damage the sample (Fig. 3.1). Higher aspect ratio structures can be imaged by altering the tip geometry either by direct etching, frequently combined with focused ion beam [104, 372, 40, 48] or functionalization with carbon nanotubes, which are frequently added by direct growth by chemical vapor deposition [68, 147]. However, both techniques are still limited by the tip size, require laborious engineering of single tips and cannot image 3D overhang structures or cavities. To improve the throughput, arrays of parallel nanofabricated tips [342] or whole cantilevers [342, 60, 311, 113, 255, 8] have been designed. While

those novel tip designs allow to increase scanning speed and image larger area they are limited by the arrays size, engineering needed to fabricate them and are unable to image high aspect ratio structures. In addition, all tip-based imaging techniques are difficult to use in solution and the large probe combined with stiff cantilever may damage soft samples. This limitation can be addressed by replacing the AFM or NSOM probes by a metallic particle trapped in an optical tweezers [351, 186]. However scanning of a single, trapped particle is very slow severely limiting the throughput and requires a use of a powerful laser which could be damaging to the sample.

Other nanoscopic techniques such as scanning or transmission electron microscopy (SEM/TEM) are also often used to image geometry of nanoscopic structure. While they allow imaging with high-resolution and don't require scanning of a physical tip, these techniques suffer from other limitations. Chiefly they impose strong restrictions on the samples and their environments due to strong electron scattering and absorption. Additionally SEM and TEM require special preparation of samples and cannot be used with live biological samples, are highly invasive, require metal-based contrast, and typically make it possible to observe only the surface itself with limited ability to accurately measure structures with internal geometry (Fig. 3.1).

Minimally invasive optical tomography is suitable for the imaging of surface layers of highly scattering, nontransparent samples, as probing is based on backscattered photons. It is capable of imaging large three dimensional samples with complex geometries and has been most successfully used in medical and research setting for imaging soft biological tissues. However its resolution is limited to μm range and due to this limitation it has very few applications beyond biomedicine [148]. If the objects are highly scattering, tomography can be combined with non-linear inversion algorithms to image permittivity distribution at a sub- μm resolution, this however may not be directly related to shape and has not been so far shown to faithfully reproduce object's shape [243] (Fig. 3.1). Three dimensional wide-field images can also be obtained by time reversal technique, but it has a micrometer resolution due to the diffraction limit [49, 177].

In biology high-resolution imaging of fluorescently labeled biological samples can be also achieved by isolating multiple emitters residing within diffraction-limited volume either spectrally [72, 279] or temporarily by exploiting photocycling [35, 307], photo bleaching [296, 134] or blinking [227] and then imaging them one at the time. This suite of super-resolution imaging techniques is widely used to capture localization of fluorophores within biological tissue, which offers insights into biological structure and processes at the scale of single molecules. While these techniques are powerful, they require the imaged structure to be labeled with specific, surface-attached emitters, which limits the temporal resolution [35, 307] and makes it primarily applicable to imaging biological object with known molecular identity. Moreover they are prone to errors caused by artifacts that can arise from fixation, permeabilization

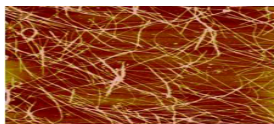
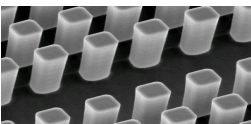
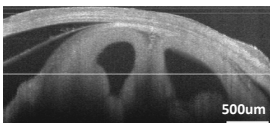
	SPM (AFM & NSOM)	EM (SEM & TEM)	OTC
			
Resolution	nm	nm	um
Throughput	low	high	high
Ambient Conditions	yes	No (vacuum)	yes
True 3D	No high aspect ratio, overhangs	yes	yes
BOM	True 3D Higher throughput	Ambient conditions/ liquid	nm -resolution

Figure 3.1: Summary and comparison of existing three-dimensional imaging techniques. AFM exhibits nanometric resolution and is capable of imaging samples in ambient conditions, however it does not offer true three-dimensional resolution and has a very low throughput due to the nature of tip scanning. Electron microscopies (SEM and TEM) also have great resolution and are capable of imaging some three dimensional objects, however they typically place stringent conditions on sample preparation and imaging conditions. Finally, optical coherence tomography (OCT) allows for wide-field truly three dimensional imaging, however its resolution is limited to the μm range. The technique presented here - Brownian Optical Microscopy (BOM) - allows for true three dimensional imaging in ambient conditions with nanometric resolution.

and light exposure of the sample [233]. To address this limitation, surface imaging by dynamic adsorption of single, freely diffusing molecules has been proposed. In these techniques interaction between the object and the emitter either enhances [324] or quenches [393] the fluorescence allowing to map the shape of the object by localization of adsorption events. These techniques provide only two-dimensional image and are limited to objects, which surfaces induce transient adsorption of an emitter and modulate its fluorescence, which are relatively uncommon. So far they have been used for mapping the surface of a lipid membrane which enhances fluorescence of the molecules adsorbed on it [324] or metal, which quenches the fluorescence upon direct adsorption [393].

Here we demonstrated a 3D super-resolution imaging technique based on fast, massively parallel scanning of surface with metal nanoparticles (NPs). Object surrounded by those

freely diffusing nanoparticles is placed in an evanescent field and as the NPs probe the volume around the object images of the optical scattering signal from all particles diffusing within a field of view are rapidly acquired, allowing their localization with nanometer accuracy in all three dimensions. NPs positions obtained from a series of imaging cycles are used to determine the volume excluded by the object and hence reconstruct its shape akin to scanning the surface with millions of freely diffusing AFM tips. We demonstrated that this technique is capable of imaging of three-dimensional objects including complex overhang structures with lateral and vertical resolution of 30nm. This wide field, all optical, super resolution imaging technique allows imaging of unlabeled, low contrast objects in ambient conditions. These unique advantages make this technique well suited for imaging biological objects as well as nanostructures (Fig. 3.2 A).

3.2 Methods

In BOM sample with low refractive index, which is often the case in biology, is surrounded by a solution of high uniformity gold nano particles with 50nm diameter, which is index matched with the object allowing the evanescent field to decay unperturbed exponentially away from the interface. The freely diffusing particles are localized in three dimensions by Gaussian fitting. The center of the Gaussian corresponds to the position of the particles while the height of the Gaussian, corresponding to the intensity of the particles relates sensitively to the height in the evanescent field (Fig. 3.2 A).

Nano-scale localization of freely diffusing particles requires rapid measurement of their lateral and vertical position before they diffuse a significant distance. NPs smaller than 40nm which are stationary or very slow moving can be localized with diffraction-limited resolution in three dimensions using heterodyne holography [3], however this does not work for freely diffusing particles. By using 50nm metal NPs as strong scatterers near plasmon resonance, BOM avoids bleaching and saturation and the scattering signal can be significantly enhanced, which enables us to collect sufficient amount of photons to accurately localize multiple diffusing particles simultaneously with resolution down to 30 nanometers.

To set up exponentially decaying field within the sample we took advantage of the fact that refraction of light, as it encounters the interface between two media having different refractive indices, results in confinement of a portion or all of the light to the higher-index medium. This phenomenon - total internal reflection (TIR) occurs when the light propagating at critical angle in a medium with higher refractive index (n_1) encounters a boundary with a medium of lower refractive index (n_2). The critical angle $\theta_c = \arcsin(n_2/n_1)$ can be calculated from Snell's law [155]. In the case of boundary formed between glass ($n_1=1.51$) and magnesium fluoride ($n_2=1.38$) or sapphire ($n_1=1.77$) and PMMA ($n_2=1.49$) the critical angle is $\theta_c = 66^\circ$ or $\theta_c = 57^\circ$ respectively. In the transmitted medium, this also produces an electromagnetic disturbance, called the evanescent wave, which propagates along the inter-

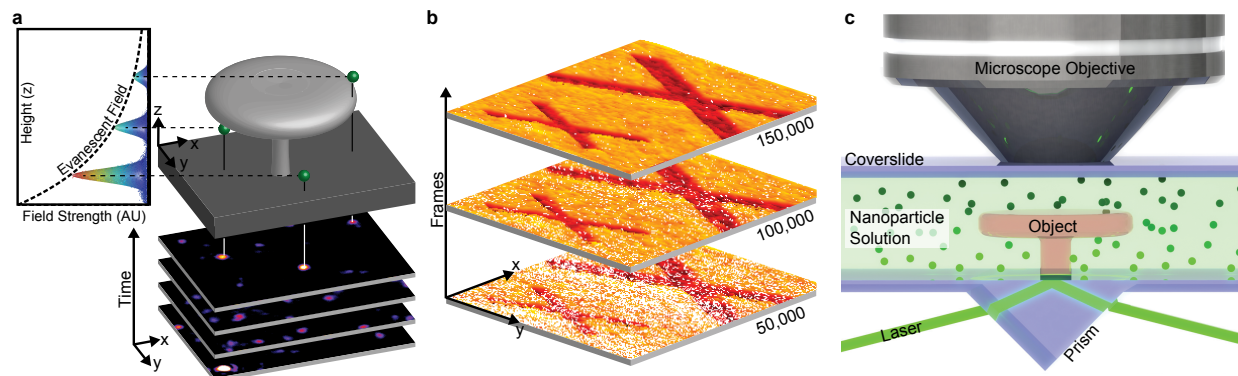


Figure 3.2: Principle of the BOM technique. A) BOM relies on three-dimensional localization of freely diffusing NPs. An object of arbitrary shape (gray) is placed in solution of randomly diffusing nanoparticles, denoted here by small green spheres, which are illuminated with an evanescent field established by total internal reflection (TIR) at the interface between the substrate and the object. A series of raw images of scattering from those particles is acquired and the NPs are individually localized in three dimensions as they randomly probe the volume around the object by Brownian diffusion. Images taken at different times will record different NPs randomly distributed around the field of view as the particles freely diffuse in the space around the object. The lateral localization is obtained by finding the center of the scattering signal by Gaussian fitting while the height of particle is estimated by measuring the intensity of the scattering signal (the height of the Gaussian). Since the evanescent field decays exponentially with the distance from the interface, the NPs close to the interface will interact with stronger field and hence appear brighter than ones further away from the boundary. Space occupied by the object is inaccessible to the NPs, and the resulting image of the excluded volume corresponds to the shape of the object. B) Once a large number of particle positions are recorded the volume excluded by the object can be estimated. The more particles are collected the finer the space sampling around the object and the better the shape of the object can be reconstructed. C) Experimental Setup. The sample, composed of glass cover slip with a MgF2 or PMMA structure nanofabricated on it enclosed in a flow chamber filled with a low density solution of freely diffusing 50nm NPs. The chamber is illuminated with a laser in such a way that evanescent field originates on the MgF2/glass or PMMA/sapphire interface and penetrates into the sample. The scattering signal is then detected on the other side of the sample using a 100X oil immersion objective.

face and exponentially decays away from the interface. The electrical field of the evanescent wave can be written as $E(z) = E_0 e^{-d_p z}$ where E_0 is the amplitude of the electric field at the interface and d_p is penetration depth and is a function of wavelength and illumination geometry, given by:

$$d_p = \frac{\lambda}{4\pi[n_1^2 \sin^2 \theta_t - n_2^2]^{1/2}} \quad (3.1)$$

where the θ_i is the incident angle [295]. Penetration depth determines depth of view in our method. We would like the depth of view to be between 200- 300nm, which sets d_p to be around 100nm-200nm and illumination angle to be $\theta_i = 55^\circ$ to $\theta_i = 60^\circ$ depending on desired penetration depth and sample design.

Mie theory is a set of exact solutions to Maxwell's equations for light interacting with small spherical particles and can be used as a model to predict behavior of nanoparticles in an evanescent field. Assuming that the sphere is not in immediate contact with the surface so that direct interaction of the sphere with the surface could be ignored, we can use Mie theory to predict the scattering profile of a non-absorbing sphere in an evanescent field [69]. Under these conditions, the scattering intensity follows the same exponential decay as an evanescent wave $I_s = I_0 e^{-d_p z}$, where I_0 is the scattering intensity at $z = 0$ when the particle is contact with the sample surface [158]. The deviation between this result and full treatment of evanescent wave scattering [346, 371] is estimated to be less than 2% using COMSOL simulation. Because the intensity of an evanescent wave decays exponentially with the distance to the interface, the intensity of light scattered by a metallic sphere will be a function of its separation distance from the interface.

At a specific frequency, coherent electron oscillations - plasmon resonance - can be excited on the nanoparticle and enhance its scattering cross section drastically. The resonant frequency depends on particle type and size as well as the type of dielectric medium it is in. We want to use 50nm nanoparticles as they show strong enhancement and have large scattering cross section. For 50nm diameter metal nanoparticles, the resonant frequency is around 530nm [286, 280, 290]. By matching laser frequency with the resonant wavelength of the particles, we can maximize its scattering cross-section, achieving a high signal to noise ratio (S/N). Therefore, we will use 532nm laser excitation light.

As the nanoparticles diffuse freely, they sample the available space by random walk. Mean diffusion time is given by

$$t_D = \sqrt{\frac{6L^2\pi\eta r}{2kT}} \quad (3.2)$$

where η is the viscosity of solution, L is mean free path and $r = 50\text{nm}$ is the radius of the sphere. In our case 80% glycerol solution or a mixture of 2,2-Thiodiethanol with water of similar density at 25°C has kinematic viscosity of mixture $0.08 \text{ m}^2/\text{ms}$ [66]. Mean free

path affects resolution, as the particle moves during acquisition time. In order to achieve resolution of 30nm or less we need to keep the acquisition time t to ≈ 3 ms or shorter, since the mean free path is around 60nm during this time. The spatial concentration of nanoparticles can be estimated to be around 1-5 particles per μm^3 , so that on average the distance between nanoparticles is 0.5-1 μm , indicating that the particles can be independently localized. For simplicity, we can assume that in order for a site to be sampled particle needs to cover at least this distance. Root mean square distance covered by a particle is $\sigma = \sqrt{2Dt}$ and it takes $t = \sigma^2/2D = 350$ ns [382]. This allows us to estimate the total imaging time with desired resolution by ensuring that a given number of particles sample the surface of the sample. The more particles are collected the smaller details of the object become visible (Fig. 3.2 B).

Optical Setup

A beam from a 200mW 532 nm laser (LambdaPro Technologies, Beijing, China) is directed via mirrors arranged in periscope setting onto a triangular sapphire prism ($n = 1.77$, Edmund Optics, New Jersey) at an angle $\approx 60^\circ$. The low index PMMA sample deposited on the top of thin sapphire slide is optically coupled to the top of the prism with immersion oil ($n = 1.77$, Cargille). The evanescent wave with penetration depth of ≈ 100 -250nm is formed at the sapphire-PMMA interface or glass-MgF₂ interface and penetrates into the PMMA or MgF₂ sample. A 2,2-Thiodiethanol-water1 (Sigma) suspension of 50nm unconjugated gold nanoparticles (Ted Pella), passivated with (Bis(p-sulfonatoatophenyl)phenylphosphine dihydrate dipotassium salt (1mg/ml, BSSP, Stern Chemicals) is index matched to the sample, and placed on the top on the sample and sealed using another cover slip (Fig. 3.2 C). The nanoparticles are concentrated, approximately 100x, by centrifugation and then water is replaced by index matched solution. Mixing 2,2-Thiodiethanol with water with different ratios allows to vary refractive index of solution from 1.33 to 1.5. The concentration of the particles is kept low enough so that the average distance between the particles is 0.5-1 μm . The imaging chamber is mounted on an inverted microscope (Zeiss Observer D1m) and laser light scattered from gold nanoparticles is collected via 100x high NA objective (Nikon Apo TIRF, NA=1.39) and sent to an EM-CCD camera (Hamamatsu, EM-CCD C9100). Raw data is collected either via HCIImage software (Hamamatsu) or through a custom written LabView (LabView, National Instruments) software. Typical acquisition times are 1-5ms.

Sample Fabrication

All samples were fabricated on glass coverslips or sapphire wafers depending on the required index range. Substrates were cleaned in hot Piranha for ten minutes, rinsed with isopropanol (IPA), and dried with nitrogen. After cleaning a 15 nm layer of ITO and 10nm layer of SiO₂ are deposited by electron sputtering, this provides a conduction pathway for later electron beam lithography steps. PMMA is spin-coated as an e-beam resist, the layer thickness can be tuned depending on the application. Typically PMMA A5 is spun at 3000 RPM for lift-off

applications, PMMA A2 is spun at 1800 RPM for direct imaging of the resist. The substrate is then patterned using electron-beam lithography (EBL). In the case of single layer samples this pattern can then be imaged directly or used as a lift off mask for a dielectric deposition. Dielectric deposition was performed using high vacuum electron-beam deposition of MgF₂ or SiO₂ with a maximum rate of 0.4 Angstroms/s.

To fabricate overhung PMMA structures the addition of MMA copolymer is required. MMA has much higher sensitivity than PMMA so it is possible to expose a layer of MMA through a layer of PMMA without exposing the PMMA [83]. In the case of overhang samples we imaged, we first fabricated a silicon dioxide smiley face structure using the above process. Subsequently, a thin layer of MMA (methyl methacryllate) is spun on the coverslide followed by a thicker layer of PMMA (poly methyl methacryllate). After patterning of the bilayer with EBL, the MMA was undercut in certain regions as a result of its lower required dose. In order to remove the resist from underneath the PMMA layer the sample is developed in an ice bath mounted onto a slowly moving shaker tray. The shaking action ensures circulation of the IPA:MIBK 3:1 developer. The samples must be allowed to develop for 4 to 12 hours depending on the feature size. The samples are then transitioned gradually from IPA to water by means of solvent exchange. The sample is then dried in all but the structure area, and nanoparticle solution is introduced. This process prevents the overhang structures from exposure to air which may cause them to collapse. The sample was then imaged using BOM, scanning electron microscope (SEM) and atomic force microscopy (AFM).

Data Analysis

After raw images were acquired and converted to 16bit .tif format, each of the detected particles was localized offline using custom written C++ and Matlab scripts. The algorithm first thresholds the images based either on user-determined threshold or automatically by Otsu thresholding [281] and subsequently finds all intensity clusters above the noise level, which correspond to the particles. The center of those nanoparticles is found using maximum likelihood estimation and the intensity at the center pixel is used to determine particle brightness. The standard deviation of the spot along the major and minor axis is also calculated and if the width of the spot along those two axes is not within 20% of each other i.e. the spot appears elongated, the particle is rejected. Particle position and height is then determined and after collecting sufficient number of particles the shape of the volume excluded by the object, and hence the object shape can be reconstructed. The larger number of particles collected per pixel the higher the accuracy of determining fine details in the excluded volume. If at each pixel the number of vertical surfaces is limited they can be localized more accurately with a smaller number of particles by taking all the particles collected at that pixel and looking at the cumulative probability distribution of their intensities. We utilize this method for all non-overhang samples. In this case the histogram of all the NPs intensities between $p=0.05$ and $p=0.95$ is fitted with straight line. The intersection of this line

with $y=0$ indicates the boundary beyond which NPs particles cannot access and indicates the height of the sample.

3.3 Results

Imaging Complex Topology

To demonstrate the ability of BOM to image unlabeled, low contrast sample in a parallel fashion with nanoscopic resolution we imaged an extruded CalNano nanostructure (Fig. 3.3A), which contains diverse feature sizes ranging from microns down to 100 nm. The sample was made out of PMMA on a sapphire support using E-beam lithography and its exact shape was first confirmed by scanning electron microscopy (Fig. 3.3B). Optical imaging of the sample using standard bright field microscopy does not allow us to resolve many fine details, although the overall shape of the writing is decipherable as it is somewhat darker (Fig. 3.3C). Using BOM we were able not only capture the full three dimensional nature of the structure (Fig. 3.3D), but also clearly resolve features as small as 100 nm over an entire 30x30um field of view (Fig. 3.3G). This also demonstrates how BOM was capable of imaging the entire, large field of view at once in contrast to probe scanning techniques that would require scanning the entire area point-by-point and would be very slow to image such a large area.

Resolution Characterization

Subsequently we wanted to systematically characterize both the lateral ($x - y$ -resolution) resolution as well as vertical resolution (z -resolution). Based on our theoretical estimations we believed that they both be mostly limited by the particle diffusion speed and equal to approximately half the diffusion distance 30nm.

Lateral Resolution

To characterize lateral resolution of BOM we imaged lines of progressively decreasing width ranging from 120 nm down to 20 nm and also with decreasing height. Just as before, the lines were fabricated using E-beam fabrication out of PMMA on sapphire cover slide. Similarly to the previous sample the lines were first characterized by SEM and shown to have expected thickness (Fig. 3.3E). However with SEM we were not able to see the height of the lines. Subsequently we imaged sample using BOM and demonstrated that BOM not only is able to reconstruct the three-dimensional image (Fig. 3.3H) of the lines, showing progressively decreasing heights, but also clearly shows almost all of the lines down to 30 nm Fig. 3.3F).

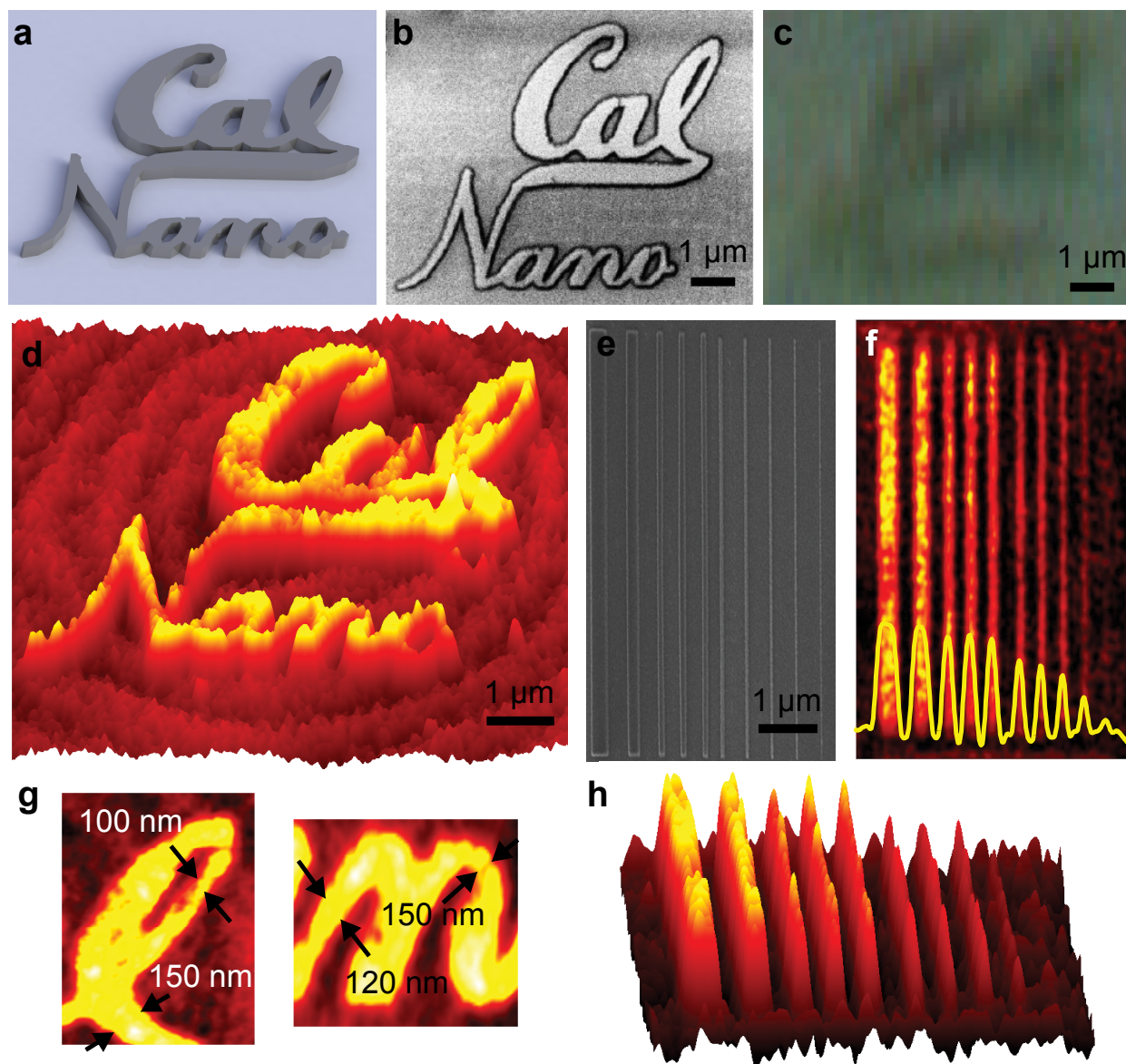


Figure 3.3: BOM can image three-dimensional topology of complex shapes with 30nm lateral resolution. (A) Schematics of the CalNano shape fabricated by E-beam lithography. (B) Two dimensional SEM image (C) Two dimensional optical image, which allows us to resolve only the large features of the shape (D) Three-dimensional BOM image in which the CalNano patterns geometry is clearly resolved. (E) SEM of fabricated lines with progressively decreasing width ranging from 120nm down to 20nm (F) BOM image of the lines including the averaged cross section (yellow) showing that the smallest 30nm line is clearly resolved. (G) Zoom-in highlighting the ability of BOM to resolve 100nm-150nm features in the letters "l" and "n" of the CalNano shape. (H) Three-dimensional reconstruction of the line sample.

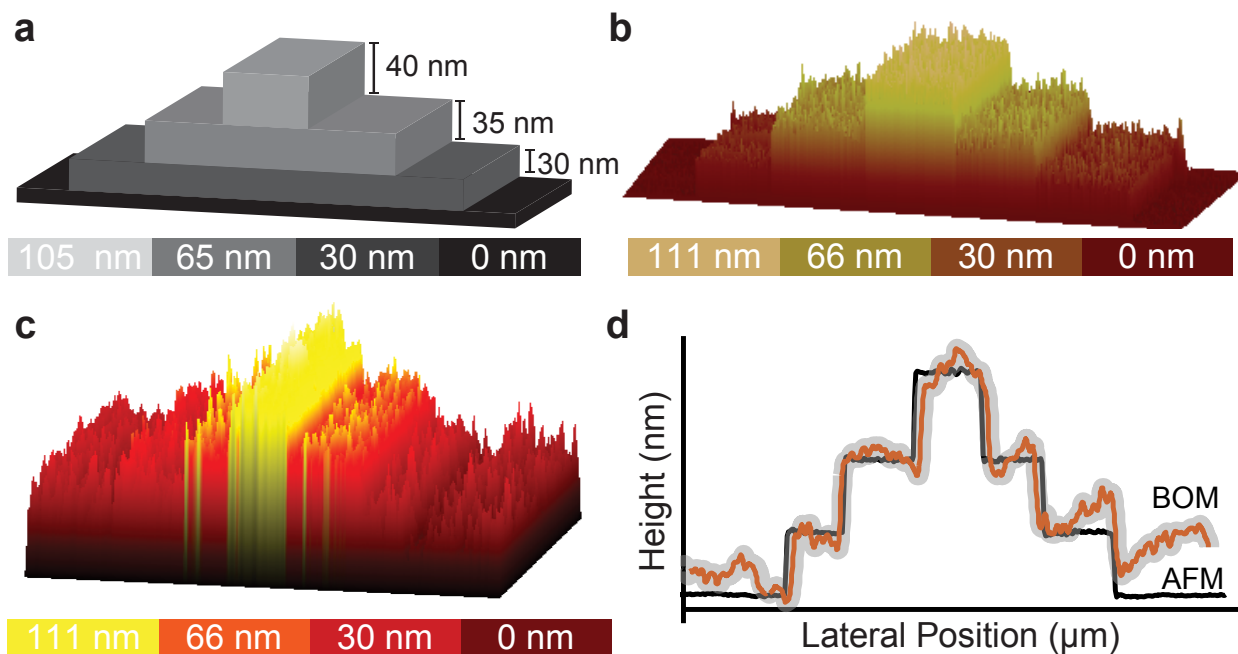


Figure 3.4: BOM can achieve 30nm vertical resolution. A) Schematics of a fabricated staircase pattern consisting of three steps with 30nm, 35nm and 40nm height respectively. B) AFM image of the sample. C) BOM image of the same sample showing three distinct steps. D) Averaged cross section of the AFM (black) and BOM images (orange) showing that BOM accurately resolved the heights of the steps with under 30nm resolution.

Vertical Resolution

To find out the vertical resolution limit of BOM we fabricated 3D staircase structures consisting of three steps with height of 30 nm, 35 nm and 40 nm, respectively (Fig. 3.4A). The structure is made of magnesium fluoride (MgF_2) covered by a thin glass film (5nm), which passivates the positively charged MgF_2 surface and prevents sticking of NPs which have negative surface potential. The sample was then imaged by AFM to confirm the step heights (Fig. 3.4B). Finally, we imaged the same sample using BOM. The smallest, 30 nm, step can be clearly resolved (Fig. 3.4B) and agrees well with the AFM measurement (Fig. 3.4D) as seen on the cross section. The cross section was obtained by averaging along the depth of the step (direction into the page) of both the BOM measurement (orange lines) as well as the AFM measurement (black line). The gray overlay represents standard error in the BOM measurement. The AFM and BOM measurement are generally in great agreement except on the bottom right-hand-side step where the BOM measurement appears to indicate higher height than AFM. This is most likely due to uneven illumination possibly caused by dirt on the cover slide which made some particles appear dimmer than they truly were.

Imaging Overhang Structures

Finally, we showed the unique ability of BOM to image topology of a three-dimensional complex shape with internal geometry such as overhung structures or cavities. A structure consisting of a silicon dioxide layer on a sapphire substrate was patterned into a smiley face that is covered by an overhanging structure made of PMMA (Poly(methyl methacrylate), (Fig. 3.5A). This structure is challenging to image with SEM due to the fact that the top thick PMMA layer shadows and obscures the underlying structures (Fig. 3.5B), so that while it is clear from SEM that there is a gap underneath PMMA roof it is not possible to see anything inside. Since BOM uses 50 nm particles to probe the surface of the object, those particles can easily probe underneath the overhang. BOM imaging clearly shows the smiley face structure as well as the overhang roof supported by a thick post (Fig. 3.5C, D). This allows BOM to capture not only the top surface of the object but also its internal cavity that is difficult to image for other nano imaging techniques such as AFM and SEM. The noise visible around the smiley face comes partially from inaccuracies in estimating the particle position and partially from scattering from unintended PMMA on or around the sample, which is an artifact of the fabrication procedure.

Imaging *E. Coli* Cells

BOM can also be used to image true three dimensional topology of biological structures and cells, which often have low refractive index contrast between them and the external medium. Additionally BOM is capable of imaging the topology of the cells without the need for staining them with fluorescent molecules or antibodies. Here, *E.coli* DH5 α were deposited by gel stamping [347] on a sapphire support coated with CellTak to ensure adhesion and passivated with a thin layer of PMMA deposited by spin casting to prevent NPs sticking. Then, the cells were imaged using AFM (Fig. 3.6A) and standard BOM technique (Fig. 3.5B). The characteristic elongated, round shape of *E. Coli* can be clearly distinguished using BOM indicating that this technique can be more broadly applicable to imaging biological objects. Appropriate NPs passivation with a polymer or a protein layer could be used in the future to prevent interactions between cells and NPs and remove the need for passivating the cells with PMMA.

3.4 Discussion

Localization and Sources of Uncertainty

Our results clearly demonstrate that BOM allows to optically image complex, three-dimensional shapes with 30 nm resolution. The vertical resolution depends on the sensitivity of intensity change with height, the diffusion distance and uniformity of NPs. The lateral resolution depends primarily on two factors: localization accuracy of any single particle and the amount each particle diffuses within single frame of acquisition. Accuracy of localization depends

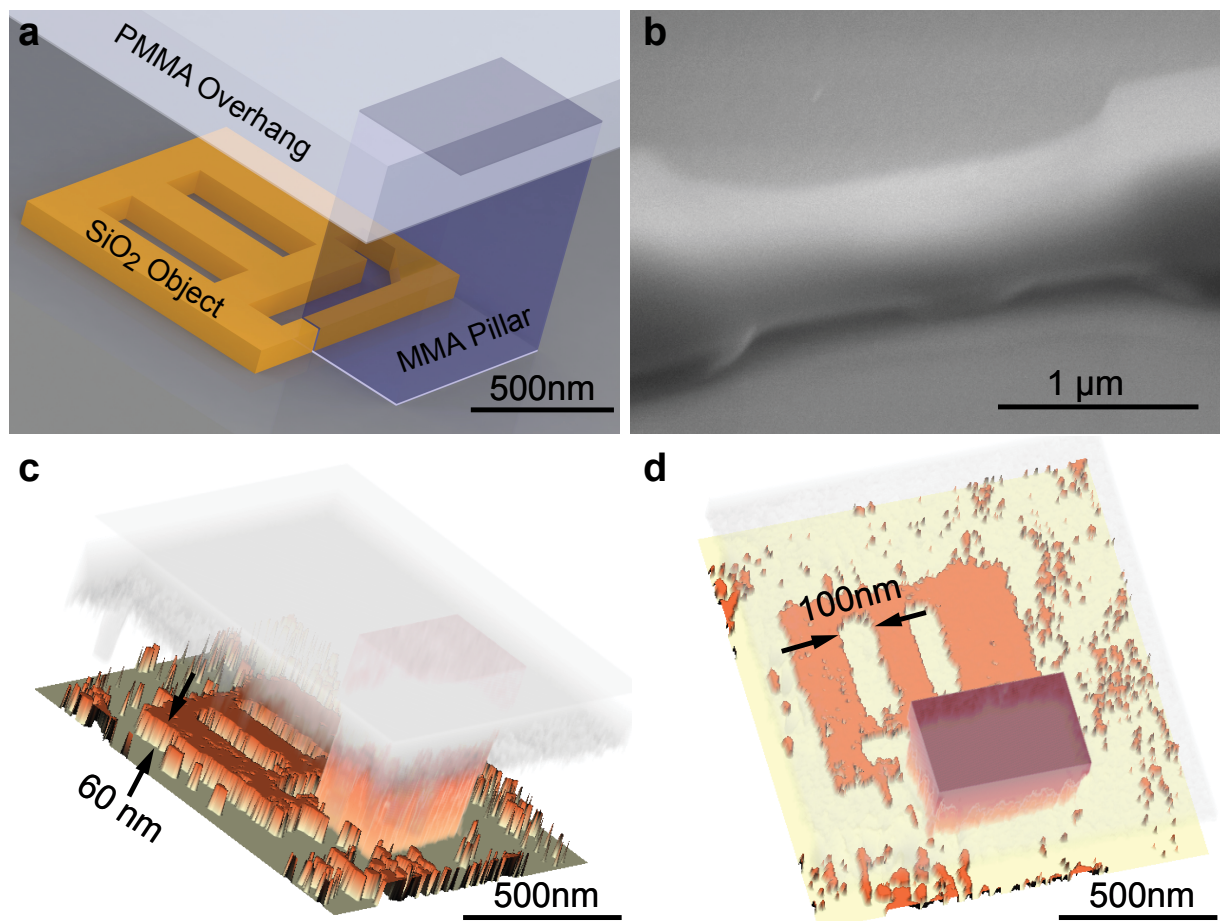


Figure 3.5: Imaging the topology of three-dimensional shapes with internal geometry A) Schematics of the fabricated structure consisting of a silicon dioxide layer on a sapphire substrate patterned into a smiley face in the first EBL step, and an overhanging PMMA structure fabricated from PMMA and MMA co-polymer in a second EBL step. B) SEM image of the structure on which a small gap can be seen but the top PMMA layer obscures the underlying smiley face. C-D) BOM images of the sample showing clearly the smiley face structure as well as the overhang roof supported by a thick post

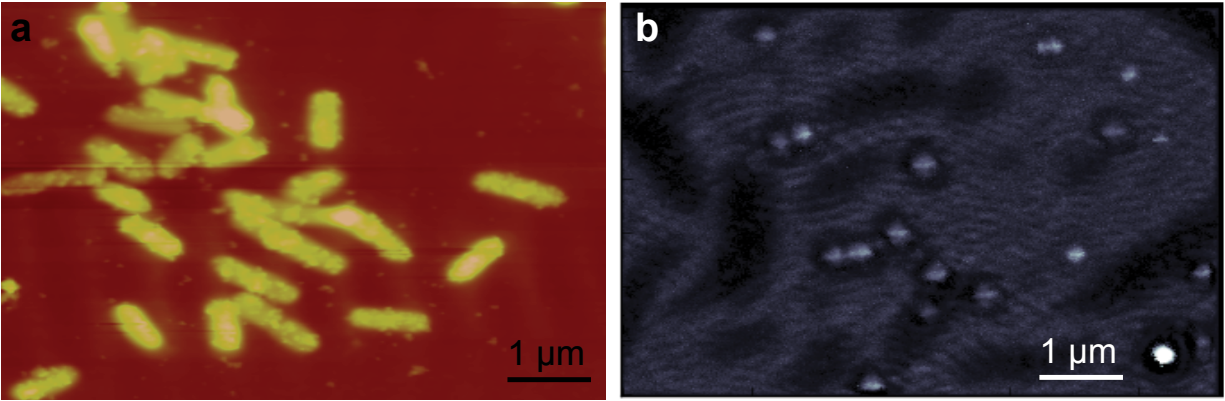


Figure 3.6: Imaging of topology of biological samples. A) AFM image of *E.Coli* deposited on sapphire surface B) BOM image of *E.Coli*

on the number of photons collected and is mainly limited by standard deviation (σ) of the Gaussian fit and the total number of photons collected N and in a lesser degree, by camera properties such as pixel size a and background noise b [355]:

$$\langle \Delta x \rangle = \sqrt{\frac{\sigma^2}{N} + \frac{a^2}{12N} + \frac{8\pi\sigma^4 b^2}{a^2 N^2}} \quad (3.3)$$

In our case the number of collected photons is directly related to the duration of acquisition, which is limited by the Brownian motion of the nanoparticles i.e. the longer the acquisition the more the particle will diffuse during this time. Due to strong plasmon resonance of the metal nanoparticles we can collect at least 6,000 photons during our standard 1ms-5ms acquisition time. During this time, the NPs can diffuse up to 60 nm. The background noise b is approximately 10 - 30 photons, $\sigma = 1$ pixel, size of the pixel $a=25$ nm and in 1ms we are collecting around 6000 photons. This gives localization accuracy of 1-2nm, so that the resolution is mostly determined by diffusion distance, not localization accuracy. The lateral resolution limit is then mostly limited by approximately half of the diffusion distance and could be improved by limiting this distance. The amount of diffusion during acquisition can be shortened over 20x by decreasing the acquisition time using either a more sensitive camera or stronger pulsed illumination. Improvements in camera system and illumination will also improve the temporal resolution of the system, decreasing the total acquisition time needed to reconstruct an image to ≈ 10 s. The accuracy of determining vertical position relates to the decay of the evanescent field and can be tuned by varying the incident angle of total internal reflection.

The vertical resolution depends on the sensitivity of scattering intensity change with height, the diffusion distance the NPs diffuse within single frame and uniformity of NPs. NPs uni-

formity affects the z -resolution since particles with larger cross-section will scatter more strongly than particles with a smaller one even at the same height. In order to minimize the errors arising from particle inhomogeneity we are using highly uniform 50nm Ted Pella Nanoparticles. Those NPs have size coefficient of variation $\approx 4-8\%$ corresponding to $\approx 15\%$ variation in intensity, which translates to 15nm standard error in height determination for each particle. However, as discussed before, the particle will diffuse around 60nm during this time. Since diffusion of NPs during the acquisition is also the limiting factor determining the vertical resolution of BOM. Improving the setup so that the acquisition time would be shortened would result in large improvements in BOMs resolution in all three dimensions. While BOM provides an unparalleled 3D resolution, the total height of the sample is constrained by the depth of the evanescent field, typically 300-700 nm. This concept can be however extended to imaging thicker samples by using highly axially-dependent illumination [93], bi-plane detection [181] or point spread function engineering [75, 171] for vertical localization.

The error in determining sample shape will be decreased if more particles were localized within the same area. Since the plasmonic NPs never bleach, unlimited number of events can be imaged until desired image resolution is achieved. If the number of vertical layers of the object is known, then rather than using particles at each voxel, cumulative distribution of all particles collected at that pixel at all heights can be used to find out what the excluded levels are. In order to estimate how many particles are needed to predict a height of an object where there is only one level at each pixel (i.e. there is no overhang) we run a Monte Carlo simulation in which particles with a size distribution of 1%, 10% and 20% were randomly generated at different heights between 0 and 300nm. The illumination field was assumed to be exponentially decaying with a penetration depth of 120nm and the intensity of the particle at a given height was calculated using Mie theory [280, 39] and analyzed using our standard analysis code. For each simulation the accuracy of localization was calculated and then averaged for 1,000 simulations run at the same conditions (Fig. 3.7). The simulations allowed us to estimate that we need to collect 15-20 particles at each voxel to estimate the height of the level with 0.95 probability within 30 nm given the inhomogeneity of our particles. Collecting more particles would result in increasing the sampling accuracy, but also would require increasing the acquisition time. Typically, to collect 20 particles per pixel we acquire 100,000 frames, which means our total acquisition time is 300-500s. Additional time during the experiment is however required to save the data onto the hard drive. If the acquisition time was shortened and also more uniform particles were used the total acquisition time could be shortened resulting in 20-30x improvements in temporal resolution. Additionally improvements to the computer system can be made to support either in-line graphics processing unit (GPU) based data analysis without saving the image file or multi-disk array to save the images in parallel to decrease the additional overhead time required during the experiment.

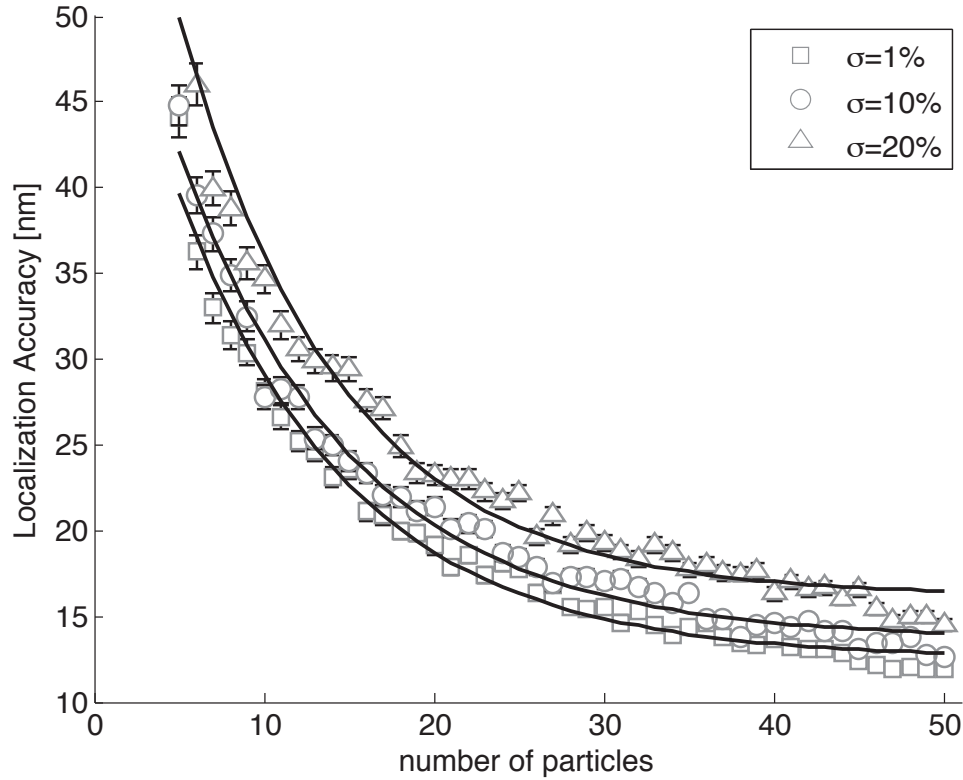


Figure 3.7: Dependence of accuracy of localization of a single surface on number of particles and standard deviation deviation of their size. For the particles with size deviation of 10%, which is similar to the particles used in experiment, we need to collect ≈ 20 particles to achieve localization of $\approx 20\text{-}25\text{nm}$.

Summary and Outlook

The BOM technique exploits the resonant plasmonic interaction between NPs and evanescent field used to excite them, to image three dimensional complex contour of an object with a resolution of 30nm in all three dimensions. Since BOM is using massively parallel scanning of NPs around the object, it does not require raster scanning and can image large field of view with high resolution. BOM is a non-invasive optical technique that can be applied to a wide range of samples including samples that cannot be fluorescently labeled and have low optical contrast such as imaging of 3D nanostructures, cells or even large molecular ensembles *in vitro*. Large field, high spatial resolution imaging is applicable to a wide variety of systems and offers great potential in dynamically imaging 3D structure of assemblies in nano-science and biology. Incorporation of stronger laser or more sensitive detection technique would allow the particle size to be further decreased likely increasing their ability to penetrate and image smaller object features or decrease image acquisition time to improve

BOM's temporal resolution in order to image dynamical processes. This technique could also be in the future combined with fluorescence measurements to allow for imaging functional properties of biological or man-made nano structures with three dimensional resolution.

Chapter 4

Synaptically Independent Dendritic Plasticity

4.1 Background and Motivation

One of the most significant challenges in neuroscience is to understand processes underlining learning and memory formation. While plasticity, which is thought to underlay learning and memory, is typically associated with persistent modifications of synaptic strengths [375, 184], recent studies indicated that modulations of dendritic excitability may form the other part of the physical signature of memory - the engram [263, 238]. However it remains unknown whether modulation of dendritic excitability is controlled by synaptic changes or whether it can be distinct from them. Here we show the first observation of the induction of a localized, activity-based, persistent plastic decrease in dendritic excitability decoupled from synaptic stimulation. This local plasticity decrease is conferred by CamKII phosphorylated A-type potassium channels upon interaction of a back propagating action potential (bAP) with dendritic depolarization.

Role of Non-Synaptic Plasticity in Learning and Memory

Persistent modifications of neuronal function, in response to repetitive and precisely timed stimuli, are believed to underlie learning, memory formation and storage [375, 184]. Such persistent modifications are based on the modulation of synaptic strengths and typically involve either modulation of the release machinery at the pre-synaptic terminal or modulation of receptor properties at the postsynaptic cell [245, 250, 71]. However, synaptic inputs are actively shaped and integrated by dendrites before reaching the soma and currently it is widely believed that different forms of synaptic plasticity can alter local dendritic excitability by modulating both resting and voltage-gated channels along the length of the dendrites[334].

One of earliest reports showing learning-dependent nonsynaptic plasticity dates back to 1973, when Woody and colleagues [390] showed that classical conditioning of the cat eye-

blink reflex was associated with increased excitability and input resistance in the neurons in sensorymotor cortical areas and in facial nucleus. Later it was showed that non-synaptic changes were in fact associated with learning during classical conditioning in the mollusk *Hermisenda*. In those experiments the conditioning produced changes in several membrane properties of the photoreceptors, including increases in spontaneous firing and input resistance due to reduction of A-type potassium current and IK_{Ca} [13, 112, 14, 80]. More recent studies revealed that all major forms of nonassociative and associative learning produced modifications that were not limited to synaptic function in a wide variety of organisms including *Aplysia*, rabbits and monkeys [263].

Several lines of evidence indicate that both LTP and LTD are accompanied by modifications of intrinsic excitability. In 1973 Bliss and Lmo observed an increase in the population spike that could not be entirely explained by the increase in the EPSP [38]. This phenomenon termed EPSP-to-spike potentiation (E-S potentiation) has been later found in several other brain regions [63, 2]. E-S potentiation in CA1 pyramidal neurons was associated with a shift in the activation curve of voltage-gated Na^+ channels reducing the AP threshold and increasing excitability [394]. The changes in excitability shared a similar signaling pathway with LTP, including activation of NMDA receptors, Ca^{2+} influx and activity of CaMKII [394, 127]. In addition to the hippocampus, synergistic changes in synaptic strength and excitability were found in the cerebellar cortex. High-frequency stimulation of mossy fibers led to both LTP and an enhancement of intrinsic excitability of granule cells [22]. Recently a long term potentiation (LTP) protocol was shown to increase dendritic excitability [225, 242] favoring backpropagation of APs into stimulated dendrites and enhancing coupling between synaptic potentials and postsynaptic spiking [122, 238]. However LTP can also be associated with h-channel regulated decrease in cellular excitability, which is thought to be stimulated by back propagating AP and be calcium/calmodulin-dependent protein kinase II (CaMKII) [109]. Similar decrease of excitability following LTP has been observed during classical conditioning of feeding in *Aplysia*, which strengthened the excitatory synaptic input to neuron B51, which is responsible for feeding response, but decreased the excitability of the B51 itself [237, 218]. The occurrence of such a reduction in cellular excitability in parallel with LTP would be a negative feedback mechanism to normalize neuronal output firing and thus promote network stability. It has been hypothesized that whether LTP procedures increased or decreased excitability might depend on the degree of LTP.

Interestingly changes in excitability are not always temporarily reassembling modifications of synaptic strengths [263]. Temporal dissociation between nonsynaptic changes and the memory trace was observed in *Lymnaea* during classical conditioning of feeding [191, 192]. After the conditioning the increased excitability persisted after the classical response was extinguished and perhaps could function as a mechanism for storing the memories. On the contrary during rabbit trace eyelid conditioning [262, 357] and olfactory discrimination learning [308] the excitability of hippocampal neurons was increased [262, 357], but this response decayed before than synaptic trace did. A computational model suggested that changes in

excitability could regulate the threshold for the induction of synaptic plasticity [359], thus proposing intrinsic plasticity as a mechanism to prime circuits to a more permissive state for modification during learning [308] suggesting that they are involved in rule learning rather than memory storage per se. These findings suggest that nonsynaptic and synaptic changes might play distinct roles in the expression of the different temporal domains of the memory.

Additionally plasticity of dendritic excitability and integration is associated with spike timing dependent plasticity (STDP). STDP is unique in the sense that whether it produces potentiation or depression depends sensitively on the timing between pre- and post- synaptic pulses. STDP may provide important functional features such as synaptic competition, predictive coding, and the functional development of neural circuits [334]. Interestingly changes in dendritic excitability during STDP have analogues temporal specificity - STDP-LTP facilitated dendritic excitability in CA1 pyramidal neurons whereas STDP-LTD depressed dendritic excitability (ES depression) [54]. Suggesting that there might exist a common learning rule for both synaptic plasticity and plasticity of dendritic excitability. Recently an investigation of STDP in neurodevelopmental learning disorders using Fragile X syndrome as a model allowed to make a compelling argument that alterations in dendritic excitability underlie deficits seen in STDP that leads to altered synapse development and in turn diseases such as Fragile X syndrome [253].

To date, localized modulations of dendritic excitability in the absence of synaptic stimulation have not been reported, leaving many key questions about the role of dendritic excitability in plasticity unsolved. Is dendritic excitability contingent upon synaptic processes or can dendrites detect spatio-temporal patterns of activation independently? Are dendrites able to store plastic changes on their own or do they only facilitate synaptically based storage?

A-type potassium channels

K⁺ channels serve a variety of functions in neurons and other excitable cells. In general, activation of K⁺ channels leads to dampening of membrane excitability due to the negative, often hyperpolarized reversal potential of K⁺ ions across the plasma membrane. Voltage-dependent K⁺ (Kv) channels act as potent modulators of diverse excitatory events such as action potentials, excitatory synaptic potentials, and Ca²⁺ influx [36]. The fast inactivating A-type potassium current is primarily encoded by Kv4.2 subunit in most neurons throughout the nervous system, and it also contributes to the transient outward currents of cardiac myocytes [398]. A potassium channel of this type is a molecular complex consisting not only of pore forming α subunits but also of multiple additional subunits and scaffold proteins that change the conductivity and kinetic properties of potassium channels, their transport, and their subcellular localization [208]. The transient, A-type K⁺ current (IA) controls the excitability of CA1 pyramidal neuron dendrites by regulating the back-propagation of action potentials and by shaping synaptic input. Moreover Kv4.2 channels serve as molecular signal integration devices, allowing the cell to integrate a variety of cell-surface signals into

a coordinated output in terms of membrane electrical properties [36]. Notably Kv4.2 channels are present through hippocampus and cortex with a high density in the dendrites of CA1 and CA3 pyramidal neurons [362, 326, 246] and the density of the A-type K⁺ channels increases with distance from the soma [166] which appears to underlie amplitude attenuation of back-propagating action potentials. Because these channels are at high density in dendrites where the neurons receive synaptic input, rapid voltage-dependent activation of these channels can limit the peak amplitude of back-propagating action potentials as well as modulate incoming synaptic information [4]. Thus these currents can exert profound effects on hippocampal network communication [166].

Kv4.2 channels play crucial role in controlling neuronal excitability by mediating transient A-type potassium currents. Localizing Kv channels near the synapse might allow neurons to mold their intrinsic excitability in the vicinity of active synapses. NMDA (N-methyl-D-aspartate) receptor activation in hippocampal CA1 neurons either directly [122] or through glutamate receptor activation [193, 222] causes a local increase of dendritic excitability, because of rapid internalization of A-type potassium channels that probably contain Kv4.2. In addition to NMDA receptor, activation Ca²⁺ influx is also necessary for Kv4.2 internalization. Similarly induction of LTP by synaptic stimulation also results in the internalization of the Kv4.2 channels increasing dendritic excitability [149]. Mechanistically it has been shown that during LTP induction (by short term glycine application and direct activation of synaptic inputs) the inclusion of GluR1 AMPA receptors responsible for potentiation of the synapses was coupled with Kv4.2 channel internalization [193]. However potentiation of synaptic inputs may also be associated with the decrease in dendritic excitability. In a culture of cortical neurons, the potentiation of excitatory inputs with glutamate, K⁺, or electrical stimulation was associated with an increase in output potassium current. The authors hypothesized that this effect is related to the translocation of Kv4.2 subunits into cytoplasmic membrane. This effect was also mediated by the activation of NMDA receptors [325].

K⁺ channels have also been shown to play a crucial role in inducing and controlling STDP-LTP by influencing the amplitude of dendritic back-propagating action potentials. Typically dendritic back-propagating action potentials are small and do not cause a significant Ca²⁺ influx. However during STDP, when EPSPs and back-propagating action potentials are paired within a critical time window the EPSP-mediated depolarization inactivates the A-current and thereby prevents a K⁺ channel-mediated dampening of the bAPs. Consequently, voltage-gated Ca²⁺ channels can be activated, which leads to Ca²⁺ influx through these channels. This induces large membrane depolarization which serves to unblock NMDA receptors allowing further influx of Ca²⁺ through NMDA receptors leading to long-term potentiation at those synapses [383, 241]. In addition to contributing to the induction of LTP and STDP-LTP, dendritic A-type K⁺ current is also involved in maintenance of the plasticity by locally increasing dendritic excitability at the synapses where LTP has been induced. This increase of excitability is spatially limited to the vicinity of the stimulated

synapses, and is related to a negative shift of the inactivation curve of A-type K⁺ currents [122]. Recently in addition to processes on cellular level, Kv4.2 channels have been directly associated with spatial memory in rats performing radial maze task [360].

The alterations of dendritic excitability, such as those observed after and during induction of LTP and STDP-LTP are typically regulated by either by alterations of density of potassium channels on the membrane surface or alterations of conductance of individual channels. This can be achieved by phosphorylation or by modulating influence of β subunits or other channel-associated proteins [208].

The conductance of A-type K⁺ currents can be regulated by phosphorylation. Activation of either PKA or PKC through ERK/MEK-specific MAPK (mitogen-activated protein kinase) pathway decreases the probability of A-type K⁺ channel opening and increases the dendritic excitability and hence the amplitude of back-propagating action potentials in distal dendrites. However, direct phosphorylation of the Kv4.2 α -subunit by PKA was not sufficient to modulate channel function and the effects of phosphorylation require the presence of the KChIP ancillary subunit [397]. MEK is known to regulate Kv4.2 phosphorylation by activating ERK which can then directly phosphorylate Kv4.2 at T602, T607, and S616 leading to increased channel conductance and decreased excitability [354]. However MEK can also phosphorylate CamKII [130, 189] which can then directly phosphorylate Kv4.2. CamKII phosphorylates Kv4.2 at Ser438. This type of phosphorylation leads to increase in local cellular Kv4.2 and potentiation of A-type current [368] and hence decreases dendritic excitability by approximately 12%. It has been hypothesized that CaMKII is responsible for the integration of channels into the membrane surface while protein kinase A regulates their internalization. The direct importance of Kv4.2 phosphorylation and excitability changes is underscored by the fact that inhibition of MEK interferes with LTP and STDP-LTP induction by reducing the boosting of the action potential [383, 303]. Moreover the Kv4.2 internalization in hippocampal spines and dendrites is induced rapidly upon glutamate receptor stimulation [193].

Kv4.2 channels can also be modulated by interactions with multiple modulatory and scaffolding proteins, which influence their conductivity and kinetics as well as their transport and sub-cellular localization. One of those are cytosolic Kv channel-interacting proteins- KChIPs - which belong to a family of calcium binding proteins that form a natural complex with the Kv4 subunit and their specific binding with the N-terminus of Kv4 subunit influences the gating properties of the channels, surface location and structural composition [208]. Specifically they have been shown to increase the density of the potassium A-current and decrease the activation threshold and resistance to inactivation causing more rapid restoration of the active state of the channels, which can be explained by either more active integration of channels or more effective stabilization of the channels within the membrane [16]. A second major class of auxiliary subunits that play distinct roles in modulating the biophysical properties of Kv4.2 are dipeptidyl-peptidase-like type II transmembrane proteins typified by DPPX [269]. DPPX also affects activation of Kv4.2 channel integration into membrane surface [399, 178]

and plays a critical role in regulating membrane excitability in hippocampal CA1 pyramidal neurons [194]. Additionally KvB may interact with Kv4.2 channels. KvB1 and KvB2 contribute to an increase in channel density without any effect on their biophysical properties.

The translocation may be mechanistically achieved by interaction of Kv4.2 with cytoskeleton. It has been shown that Kv4.2 interacts with filamin, a member of the α -actinin family of actin-binding proteins and integrins which are hypothesized to be responsible for Kv4.2 localization to somatodendritic compartments of neurons and their removal results in altered clustering and spatial distribution of Kv4.2 expression [381, 289].

Kv4.2 channels play an important role in both learning and memory as well as dendritic information and processing and disruption of their correct function can lead to serious disease states. The K⁺ channel blocker 4-aminopyridine (4-AP) induces epileptiform activity *in vitro* and seizures *in vivo*. Mutations in some K⁺ channel-associated proteins have also been linked to an epilepsy phenotype. Decrease in Kv4.2 expression is seen in several animal models of epilepsy especially after seizures. Kv4.2 channels have also been implicated in a number of hyperexcitability and neurodegenerative diseases such as epilepsy [363, 58, 222], ischemia [70, 407] and Fragile X mental retardation [142, 219]. Thus understanding the role of changes in dendritic excitability in the processing of the incoming information would allow to more deeply understand the principles of the organization and training of neural networks under normal and pathological conditions.

4.2 Methods

Cell Culture and Transfection

Animal euthanasia procedures were conducted according to guidelines approved by the Office of Laboratory Animal Care (OLAC) at the University of California, Berkeley. Hippocampi were dissected from P1-2 Sprague Dawley rats, and kept in ice-cold HEPES buffered Hanks' Balanced Salt Solution (HBSS, GIBCO) at all times. Cells were dissociated with trypsin for 10 min at 37C, followed by gentle trituration. The dissociated cells were then transfected with EYFP-ChR2 construct using Nucleofector-II (Amaxa Biosystems) in accordance with manufacturers protocol (Rat Neuron Nucleofector For Primary Rat Hippocampal or Cortical Neurons) and plated at a density of 25,000/50,000/cm² on poly-l-lysine-coated glass coverslips. Dissociated neurons were cultured in Neurobasal medium (GIBCO) supplemented with B-27 (Invitrogen) and penicillin-streptomycin (10U/ml, GIBCO). Experiments were done on morphologically identified pyramidal neurons 1418 d *in vitro* (DIV).

Electrophysiology

Individual coverslips were placed in a recording chamber (Biosciences) and submerged in room temperature ACSF (145 mM NaCl, 3 mM KCl, 10 mM HEPES, 20 mM glucose, 2

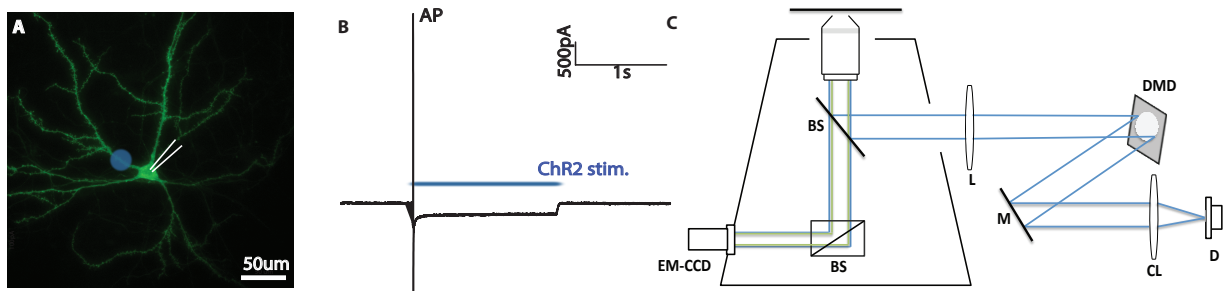


Figure 4.1: Experimental setup to achieve decoupling of synaptic and dendritic processes. (A) EYFP-ChR2 expressing hippocampal neuron is stimulated with 28 μm light spot (blue circle) applied on the proximal dendrites coupled with somatically induced spike. (B) The stimulation protocol where 2s photostimulation of proximal dendrite is coupled with a spike. (C) Schematics of the optical setup. Patterned ChR2 stimulation is achieved by a 470nm LED is collimated by a lens (CL) and directed using a mirror (M) to Digital Micromirror Device (DMD). The light reflected from DMD is collimated and scaled using a lens system (L) and coupled into the microscope via a beam splitter (BS).

CaCl₂ and 1 MgCl₂) supplemented with 0.1mM picrotoxin (Sigma), 0.01mM DNQX (Sigma) at 322 mOsm, pH 7.4. Voltage or current clamp recordings were performed in the perforated patch-clamp configuration. Electrodes (2-5 M Ω) were pulled from borosilicate glass tubing (World Precision Instruments) using a laser based micropipette puller (Sutter Instrument P-2000). The pipette tip was dipped in an intracellular solution containing (in mM) 68 K-gluconate, 68mM KCl, 0.2mM EGTA, 2 MgSO₄, 20 HEPES, 3 ATP, 0.2mM GTP (322 mOsm, pH 7.4) and then backfilled with the same solution but containing 0.12 mg/ml amphotericin B (Sigma); final osmolarity was about 290 mOsm/kg H₂O and open pipette resistance when filled was 2 - 5 M Ω . Currents were recorded using patch-clamp amplifier Axopatch 200B-2 in conjunction with Digitizer 1440A, sampled at 10 kHz. The holding potential in voltage-clamp mode was 70 mV (Fig. 4.1A), uncorrected for any liquid junction potential between internal and external solutions. Recordings were analyzed using pClamp v10 software or custom written Matlab code. For pharmacological experiments all drugs were obtained from Sigma-Aldrich with an exception of Stomatotoxin-II which was obtained from Alome Labs. All drugs were bath applied and handled according to manufacturer recommendations. Dendritic excitability decrease was achieved by coupling thirty 2s sub-threshold ChR2 photodepolarizations with thirty APs which were delivered somatically 20ms after the onset of light (Fig. 4.1B).

Optical Setup for Optogenetic Stimulation

Hippocampal neurons were placed in a perfusion chamber and visualized using inverted Nikon TE-2000E microscope and Andor EM-CCD (Andor). The cell plane was illuminated with X-Cite 120 lamp (Lumen Dynamics) and only neurons, which expressed EYFP, were chosen for experiments. To generate patterned illumination, a 470nm LED (Phillips) was expanded, collimated and reflected directly from digital mirror device (DMD, InFocus LP435Z) coupled into the microscope. The diode was synchronized with electrical stimulation through a TTL signal and DMD was controlled using VGA signal from a computer. DMD patterns were generated via custom written MATLAB (Mathworks) software, which allowed user to position an arbitrary light pattern over the displayed cell image (Fig. 4.1C). For a majority of the experiments, a circular pattern of $28\mu\text{m}$ in diameter was positioned over the imaged proximal section of the dendrite. A set of previously determined affine transformations were applied to the pattern, so that after passing through the optical path of the microscope, it would be correctly positioned with respect to the cell. To stimulate the cell we paired thirty 2s photocurrent injections (or 100ms in case of data presented in Figure 4.4) into proximal dendritic compartment, with APs (20ms after the onset of the light).

Immunofluorescence Staining

Dendritic excitability decrease was induced as described previously with the exception that 10ms 70mV action potentials were delivered using Iso Flex Unit Stimulator (A.M.P.I) rather than patch pipette. Cells were fixed immediately after stimulation with 4% paraformaldehyde (Sigma) in PBS for 20 minutes before being permeabilized (1% Triton-X, Sigma) and blocked in block solution (PBS containing 5% BSA). Then cells were incubated for 4h with anti-pKv4.2 Ser 438 monoclonal antibodies (Santa Cruz Biotechnology) and then Alexa Fluor 568 secondary antibodies (Invitrogen). Coverslips were mounted using Fluoromount-G (SouthernBiotech) and sealed with nail polish. Cells were visualized using a Nikon TE-2000 inverted epifluorescence microscope through 60x 0.8 NA Nikon or 100x 1.3NA Zeiss objective. Images were digitally captured using EMCCD Andor. Excitation was via X-Cite lamp with appropriate filter cubes. Images were analyzed using ImageJ and custom written Matlab (Mathworks) software.

Live Cell Imaging

Dendritic excitability decrease was induced as described previously with the exception that 2ms stimulations at 70V were delivered using Iso Flex Unit Stimulator (A.M.P.I). This stimulation protocol was sufficient to induce a single action potential in the hippocampal neurons, reliably and without affecting cell viability as confirmed by electrical recordings. Cells were transfected with mCherry-Kv4.2 plasmid (kind gift from Prof. Manuel Covarrubias) as described before and visualized immediately before and after stimulation using a Nikon TE-2000 inverted epifluorescence microscope through 60x 0.8 NA Nikon or 100x

1.3NA Zeiss objective. Images were obtained using an X-Cite lamp with appropriate filter cubes and digitally captured using Andor EMC-CD. Images were analyzed using custom written Matlab (Mathworks) software. For each cell, we obtained the ChR2 distribution (YFP fluorescence), the Kv4.2 distribution, and the stimulation pattern and registered all these images with each other to ensure accurate comparison. The images were corrected for bleaching and dendritic clusters were manually identified and counted. By comparing the positions of the clusters before and after the stimulation the direction of the movement was assessed. The re-distribution of Kv 4.2 clusters on the soma was visualized by comparing images before and after the stimulation as well as by calculating differential images: $Kv4.2_{before}-Kv4.2_{after}$ and $Kv4.2_{after}-Kv4.2_{before}$.

4.3 Results

Demonstration of dendritic excitability decrease (DED)

To study the relationship between dendritic excitation and synaptic memory and elucidate their interdependence, we developed a technique to decouple the dendritic excitability changes from synaptic strength changes by stimulating dendrites with a protocol similar to spike timing dependent plasticity (STDP) substituting presynaptic cell stimulation with localized photostimulation of ChR2 using a digital micromirror device (DMD). The use of a DMD allowed us to photostimulate multiple sub-cellular locations simultaneously and to vary the locations of the depolarizations with millisecond resolution (Fig. 4.1) [379]. Synaptic transmission was completely blocked by 2-amino-3-hydroxy-5-methyl-4-isoxazolepropionic acid (AMPA) and gamma-aminobutyric acid (GABA) receptor antagonists ($10\mu\text{M}$ DNQX and $100\mu\text{M}$ PTX).

We observed that even in the absence of synaptic inputs, pairing thirty 2s photocurrent injections into proximal dendritic compartment, with APs (20ms after the onset of the light) resulted in a persistent ($>15\text{min}$) decrease in dendritic excitability as indicated by the decrease of amplitude of evoked current at the soma (Fig. 4.2 A-B), $\text{DED}=13\%\pm 1.7\%$ $p<0.001$, $n=12/12$, no stimulation = $0.74\%\pm 2.0\%$ $p=0.14$ $n=6/6$). We will refer to this phenomenon as dendritic excitability depression (DED). DED requires a coincident interaction of dendritic stimulation and neither APs alone ($\text{DED}=0.2\%\pm 2.8\%$ $p=0.35$, $n=7/7$) nor dendritic stimulation alone ($\text{DED}=0.0\%\pm 1.9\%$, $p=0.43$, $n=6/6$) induced DED (Fig. 4.3A). Similarly no stimulation of any kind also does not result in a change of excitability ($0.74\%\pm 2.0\%$ $p=0.14$ $n=6/6$, Fig. 4.3A). This suggests that dendrites can detect coincident dendritic stimulation and APs independently of synaptic AMPA and GABA receptors. We observed no change in intrinsic, whole-cell excitability accompanying DED, as indicated by unchanged Spike-Current relationship ((Fig. 4.2B), two tailed t-test $p=0.49$ between before and after stimulation, $p=0.49$ between APs only stimulation and no stimulation $n=3/3$). This suggests that DED was the result of localized dendritic excitability modulation.

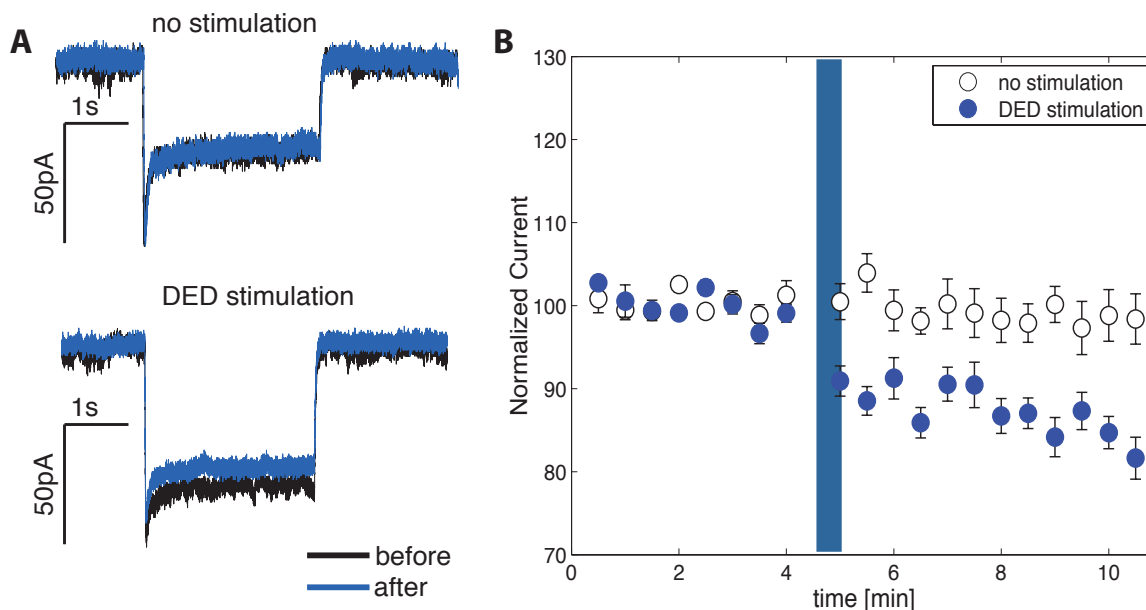


Figure 4.2: Persistent decrease in dendritic excitability following paired stimulation. (A) An example trace for 2s photo depolarization before (black trace) and after (blue trace) the treatment. When no stimulation was applied (top) no change in dendritic excitability is observed, however after paired stimulation (bottom) excitability decreased (B) Dendritic excitability prior to paired stimulation, shows a steady basal level of dendritic excitability as assessed by measuring the peak magnitude of the ChR2-induced photo current. After paired stimulation the current decreases by 13% for 2s report as compared to 0.74% for no stimulation.

Spatial dependence of DED

To investigate how different sub-cellular compartments respond to DED we induced DED at one of the proximal sites and measured the excitabilities at other dendrites, soma and integrated over the entire cell. Since 2s photo-stimulation, which we previously used to determine dendritic excitability before and after stimulation and to induce DED, injected too much current when applied on the cell body or over the entire cell we used 100ms stimulation in this experiment. First we stimulated a proximal dendrite and observed a change of excitability on that dendrite, just as before, but using 100ms photo-stimulation. DED was smaller in magnitude but still robustly induced (Fig. 4.4A, $DED=2.65\% \pm 2\%$, $p < 0.05$). When the whole cell was photo-stimulated the excitability was not affected ($DED=1.6\% \pm 1.9$, $n=6/6$, Fig. 4.4D), supporting the observation that intrinsic excitability does not change and somatic current increased (Fig. 4.4B increase of $6.3\% \pm 2.1$ $n=6/6$). Finally unstimulated dendritic branches were unaffected by the stimulation of another branch (Fig 2b.

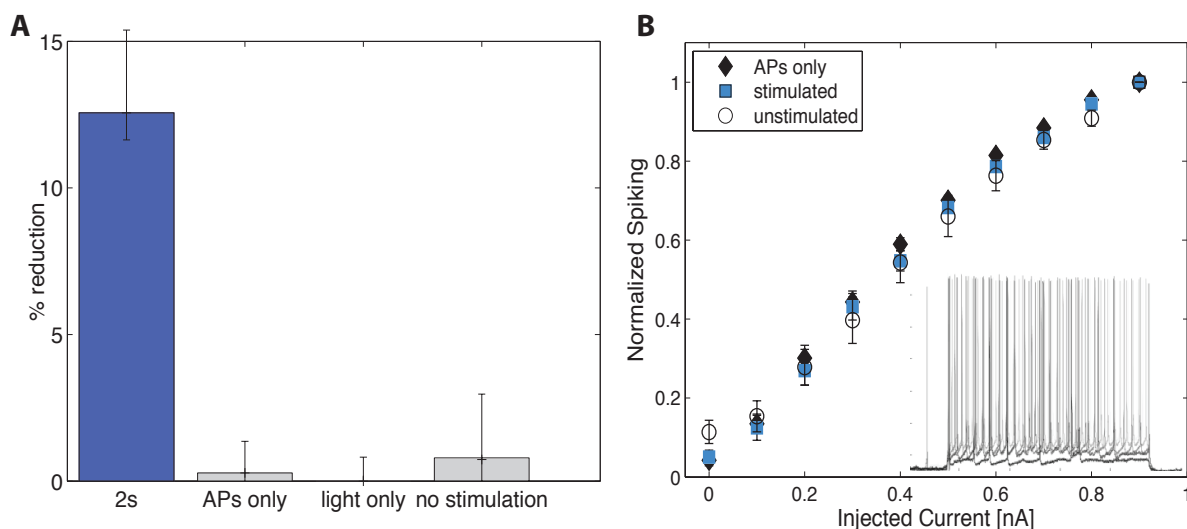


Figure 4.3: Persistent decrease in dendritic excitability following paired stimulation. (A) Only stimulation by paired APs and dendritic depolarization causes DED= 12.6% ($p < 0.05$). Controls, where no stimulation takes place or either APs or light alone are delivered show no significant DED ($p > 0.05$ in all cases). (B) There is no change in spike-current relationship between stimulated (blue square) and unstimulated neurons (open circle) or neurons stimulated only with APs (black filled rhombus) indicating no change in intrinsic excitability.

$\%DED = 0.26\% \pm 2.16\%$, $p = 0.07$, $n = 7/7$). Taken together, these results show that DED is confined to a stimulated dendrite and coupled with modulation of somatic excitability, ensuring that overall neuronal excitability remains unchanged, akin to homeostatic plasticity mechanism observed in other systems [364].

Mechanism

Since voltage-gated channels regulate dendritic processing by dynamically modulating membrane excitability in a spatially restricted manner as well as play a key role in induction of long term plasticity including STDP [36, 398], we tested their involvement in DED. Application of non-selective voltage-gated potassium channel inhibitor (20mM TEA) eliminated most of the DED (DED=1.7% \pm 1.1%, $p < 0.05$, $n = 10/10$, Fig. 4.5A and C). Stromatotoxin (100 nM), which specifically inhibits delayed rectifier and A-type potassium channels [108] (Kv2.1, Kv4.2, Kv2.2 and Kv2.1/9.3), significantly reduced DED (Fig. 4.5A and C, DED=1.6% \pm 1.0%, $p < 0.01$, $n = 5/5$). To distinguish between Kv2.1 and Kv4.2 channels, we bath-applied Heteropodatoxin-2 (Hptx, 100nM) which specifically blocks Kv4.2, Kv4.1 and Kv4.3 but not Kv2.1[400]. Hptx completely eliminated DED (Fig. 4.5A and C. DED=

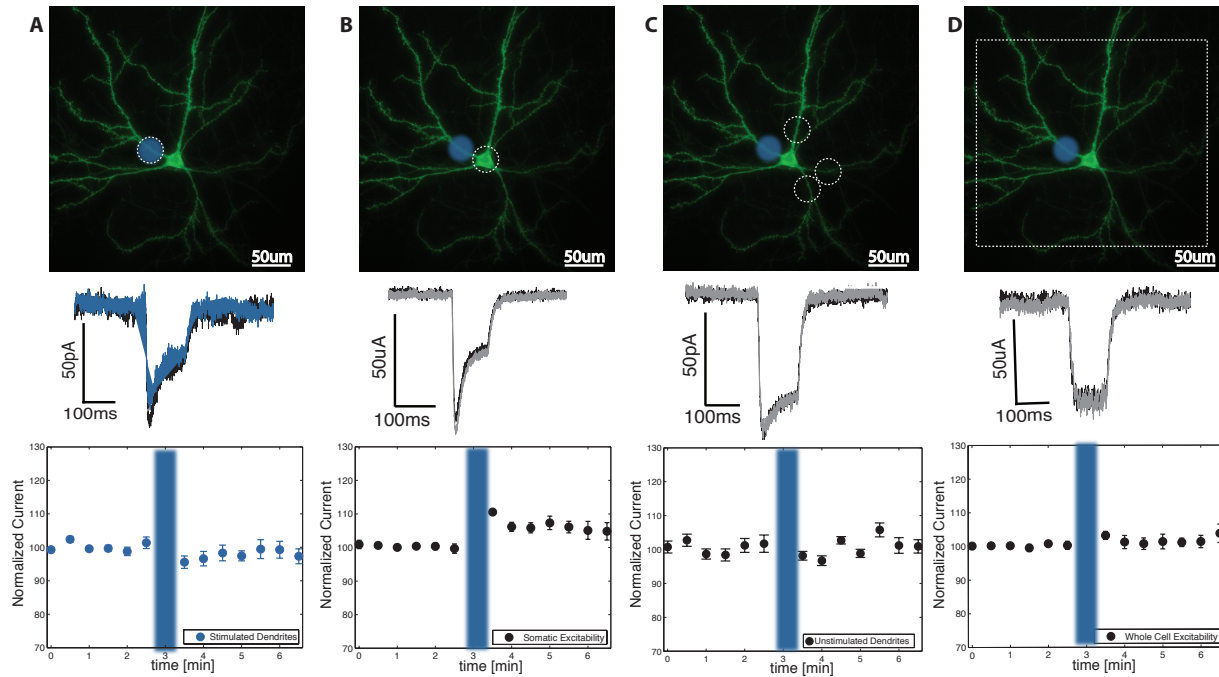


Figure 4.4: DED is spatially localized. (A, B, C and D) Top panels display the dendritic location used for dendritic stimulation (blue circle) and the range of possible report locations (white dotted lines). Bottom panels show example current measurements before (black) and after stimulation (grey or blue) as well normalized current before and after stimulation. Following proximal dendritic stimulation, (A) proximal dendritic current decreases (DED=2.65%, $p < 0.05$) (B) somatic current shows increase in excitability by $6.2\% \pm 2.1\%$. (C) Un-stimulated dendrites don't show DED (DED= 0.28% \pm 3.4%, $p=0.84$) and (D) Current resulting from whole cell photo-stimulation does not change significantly (increase= $1.6\% \pm 1.9$).

$0.2\% \pm 2.9\%$, $p=0.45$, $n=10/10$). This data indicates that decrease of dendritic excitability is conferred by changes in A-type potassium currents mediated by Kv4.2 channels.

Since Kv4.2 channels also control bAPs [404], we further investigated whether bAPs are essential for induction of DED. If an interaction between bAPs and dendritic stimulation is required for DED, then it is reasonable to assume that abolishing spikes by bath application of sodium channel blockers should reduce DED [350, 241]. Application of $1\mu\text{M}$ tetrodotoxin (TTX) precluded induction of DED (Fig. 4.5A,C. DED= $2.2\% \pm 1.5\%$, $p=0.18$, $n=5/5$), suggesting that DED requires coincident interaction of bAPs and dendritic depolarization, which would be consistent with the proposed mechanism of involvement of Kv4.2 in STDP.

Subsequently we wanted to investigate if calcium, which is essential for many neurological processes and plays a key part in controlling STDP, is necessary for DED. To determine

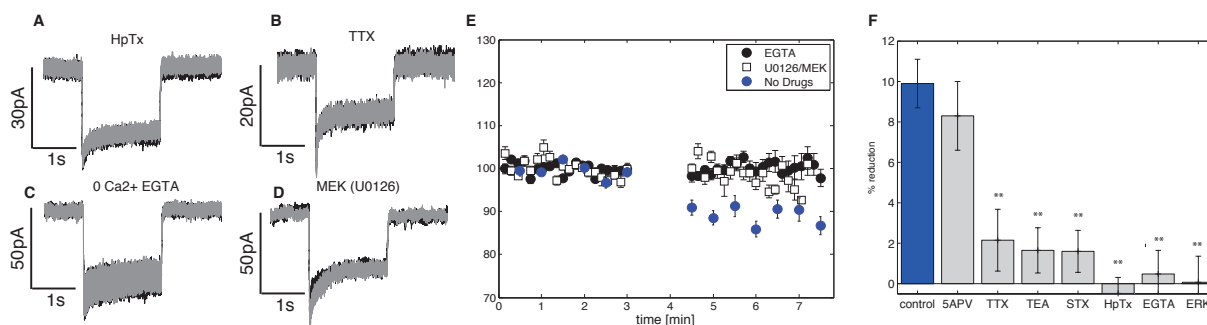


Figure 4.5: K_v4.2 channels are responsible for DED and the process requires Ca²⁺ and MEK. (A-D) Example current measurements before (black) and after stimulation (grey) showing that DED is blocked by HpTx (A) and TTX (B). Moreover DED does not happen in the absence of Ca²⁺ (C) and is blocked by MEK inhibitor U0126 (D). (E) Time trace showing the effect of chelating calcium (by EGTA) and MEK by (U0126) showing that blocking their action clearly abolished DED as compared to its normal magnitude (blue circles). (F) Bar graph summarizing effect of different drugs. When no drugs are applied 10% DED is observed. Application of TTX (1 μM), TEA (20mM) and Stromatotoxin-II (100nM) reduced the amount of DED to 3% while application of Hptx (100mM) or U0126 (10 μM) or removal of calcium from external solution completely abolishes DED.

this we attempted to induce DED in 0 Ca²⁺ with 2mM EGTA. Dendritic excitability didn't change in the absence of calcium (DED=0.48% ±1.2%, p=0.56, Fig. 4.5B,C) indicating that it does in fact play a key part in induction of DED.

Since translocation and conductance of K_v4.2 channels is tightly controlled by phosphorylation to gain more insight about the mechanism of DED we turned our attention to MEK, which is a key component of K_v4.2 phosphorylation cascade and has been previously implicated in learning and memory in behaving animals and shown to be necessary for many forms of synaptic plasticity although its precise role is unknown. Blocking MEK using 10 μM of U0126 abolished induction of DED (DED=0.07±0.3, p=0.28, Fig. 4.5B,C).

Finally, to ensure that DED is not a result of synaptic process where NMDA receptors are activated by local depolarization and Glu released from synapses or ambient Glu in the cleft we induced DED in the presence of NMDA blocker 5APV (50 μM). Dendritic excitability decreased 8.3%±3.4% (p<0.001) indicating that NMDA receptors are not involved in DED and that the process is independent of synaptic receptors.

Taken together this data suggest DED stimulation induces interaction of bAP with local dendritic depolarization leading to an increase in intracellular calcium. Elevated calcium activates a signaling cascade involving MEK, which then affects the K_v4.2 channels leading

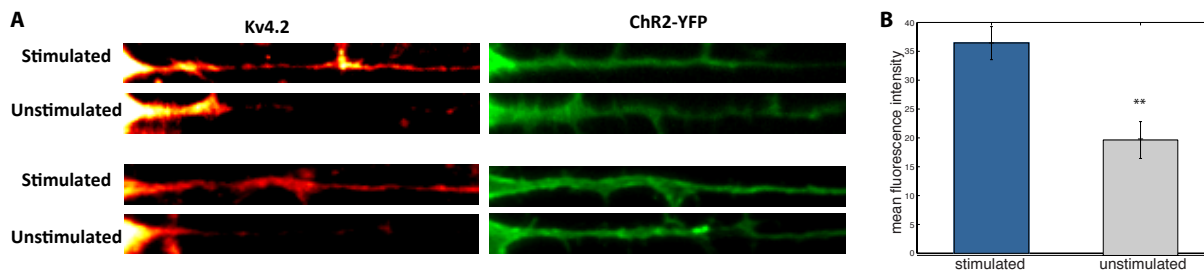


Figure 4.6: Kv4.2 phosphorylation is enhanced along the stimulated dendrite. (A) Immunostaining against Kv4.2 phosphorylated at Ser 438 shows enhanced phosphorylation at the stimulated dendrite as compared with the un-stimulated dendrite of the same cell. The dendrites have comparable amounts of ChR-YFP. Dendrites from two representative cells are shown (top and bottom). (B) Mean immunofluorescence of pKv4.2 along the stimulated dendrite is much higher (mean fluorescence = 36.5 ± 2.84) than along the non-stimulated dendrite (mean fluorescence = 19.8 ± 3.17), $p=0.01$.

to an increased A-type current and decreased excitability.

To gain further insight into the physical mechanism, that allows Kv4.2 channels to modulate dendritic excitability dynamically, we performed immunostaining against Ser 438 phosphorylated Kv4.2. The density of phosphorylated Kv4.2 along the stimulated dendrite was significantly higher (increased 16.7%, $p=0.01$) than along a comparable, unstimulated dendrite on the same cell (Fig. 4.6). This suggests that DED is associated with differential phosphorylation of Kv4.2. This phosphorylation increases Kv4.2 current [368] and also affects translocation direction and turnover rate of Kv4.2 [274, 306].

We observed that DED is associated with increased Kv4.2 phosphorylation which increases the conductance of Kv4.2 channel leading to increased A-type current and decreased excitability [368]. Phosphorylation of Kv4.2 was also shown to affect translocation direction and turnover rate [274, 306] so to gain further insight into the physical mechanism of DED, we investigated their translocation using mCherry-Kv4.2 (Fig. 4.7). We tracked 251 clusters taken from $n=16$ cells. Kv4.2 clusters on stimulated dendrites ($n=118$) either stayed stationary (61%) or moved distally (33%) while clusters on unstimulated dendrites ($n=133$) mostly moved towards the soma (38%) or remained in place (45%), Fig. 4.6A-B. The clusters that did move, moved on average at $0.16 \pm 0.04 \mu\text{m}/\text{min}$ and moved a total of $1.3 \pm 0.3 \mu\text{m}$. The total displacement of clusters that were classified as non-moving was on average $0.12 \mu\text{m}$, which is close to the resolution limit of our microscope. This slow translocation dynamics is consistent with previous studies [193, 274]. Additionally, rearrangements of somatic Kv4.2 distribution were visible; resulting in increased somatic Kv4.2 clustering (Fig. 4.7C).

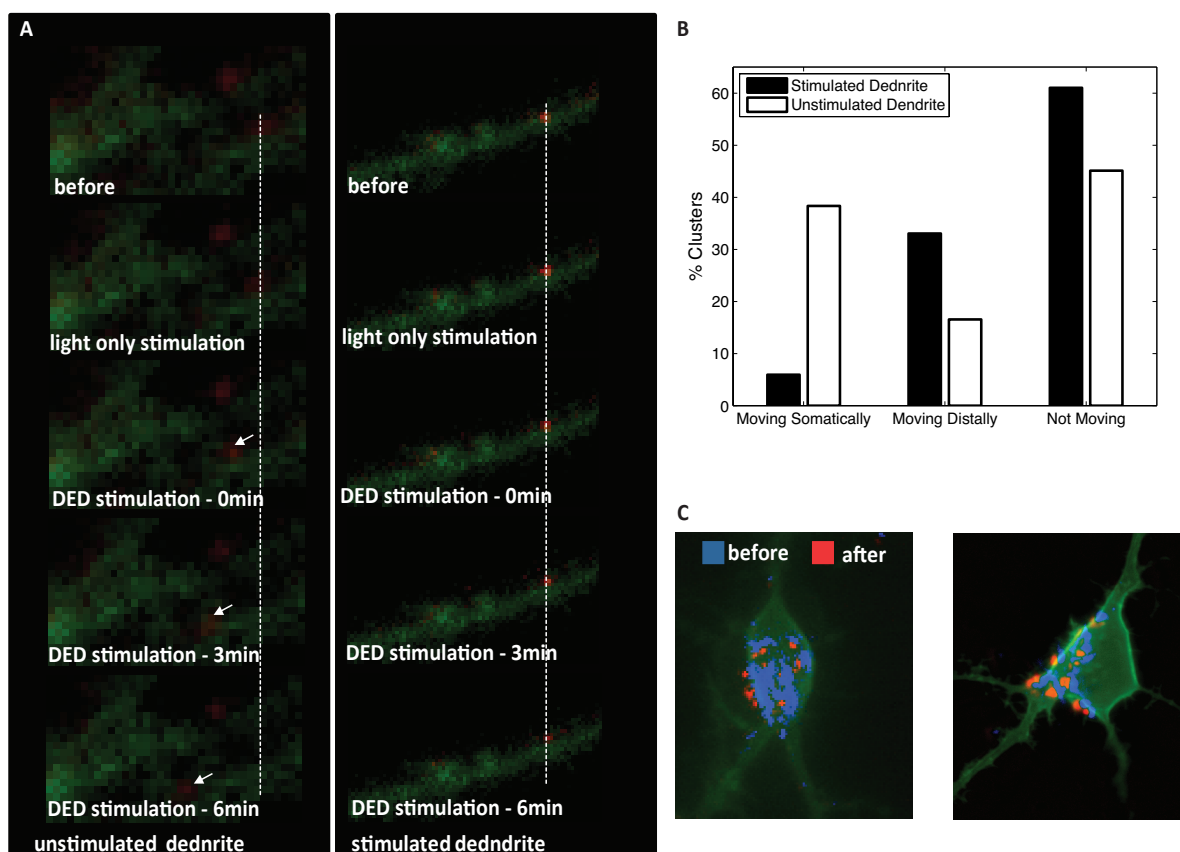


Figure 4.7: : Kv4.2 channels are responsible for DED. (A) Example time trace showing clusters on unstimulated dendrite moving somatically and ones on stimulated dendrites not moving (B) Summary of cluster movement on stimulated and unstimulated dendrites. Clusters on stimulated dendrites preferentially move distally (33%) or remain in place (61%) with only 5% moving somatically. Clusters on unstimulated dendrites preferentially move somatically (38%) or remain in place (45%) with only 17% moving distally (C) Example images of showing clustering of somatic Kv4.2 channels.

4.4 Discussion

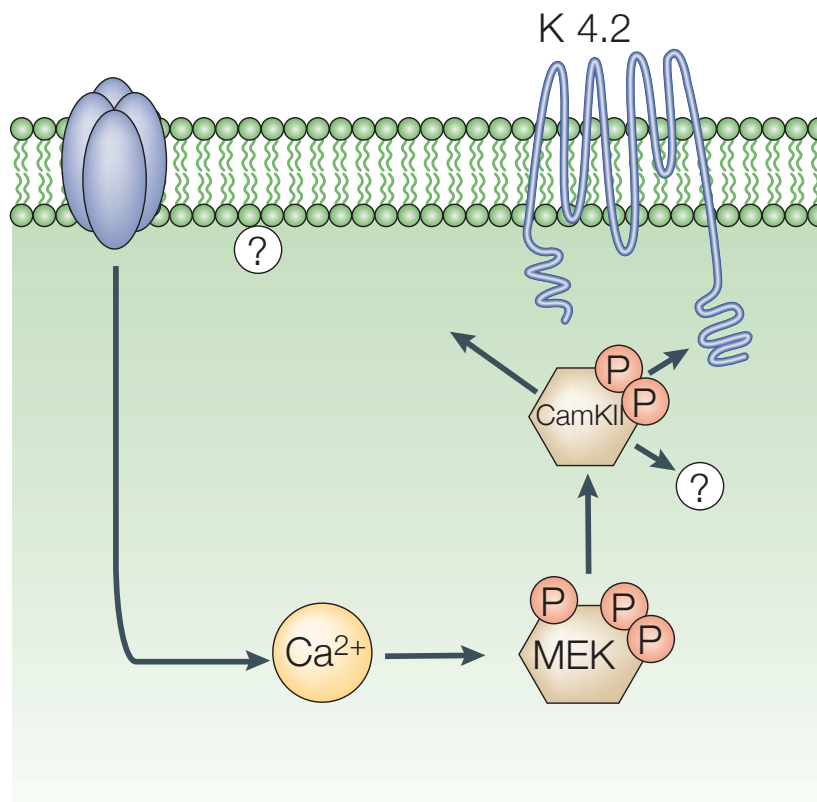


Figure 4.8: Possible Mechanism behind DED. MEK regulates Kv4.2 phosphorylation by activating CamKII which can then directly phosphorylate Kv4.2. CamKII phosphorylates Kv4.2 at Ser438 which increases the inactivating A-type potassium current and hence decreased dendritic excitability.

Activity dependent modulations in dendritic excitability are central to information processing and storage but so far have only been seen in addition to synaptic plasticity. Here we show that localized depression of dendritic excitability can be decoupled from synaptic processing and can be induced in response to stimulatory activity only. This process of dendritic excitability decrease (DED) is confined to the stimulated dendrite and brought about by interaction of bAPs with dendritic depolarization. This interaction induced increase in intracellular calcium, which results in MEK-regulated phosphorylation of Kv4.2 at Ser 438 residue.

MEK is known to regulate Kv4.2 phosphorylation by activating either ERK [354] or CamKII

[130, 189] which can then directly phosphorylate Kv4.2. CamKII phosphorylates Kv4.2 at Ser438 while ERK phosphorylates Kv4.2 at T602, T607, and S616. DED leads to increased levels of Kv4.2 phosphorylated at Ser438 at the stimulated dendrite, suggesting that increased calcium causes MEK activation, which in turn activates CamKII which directly phosphorylates Kv4.2. Ser438 Kv4.2 phosphorylation leads to increase in local cellular Kv4.2 and potentiation of A-type current [368] and hence decreased dendritic excitability.

While previously redistribution of A-type potassium channels was shown to accompany various forms of LTP [36, 222, 368] here we show, for the first time, that Kv4.2 channels are responsible for localized DED in the absence of any synaptic potentiation. Since A-type K^+ currents are the major modulator of back-propagating action potentials (bAP) [404] increase in A-type current, such as one caused by DED, decreases both the bAP [404, 18, 64] and forward propagating sub-threshold photocurrent. This leads to depression of dendritic current reaching the soma but also limits further development of DED by decreasing the magnitude of bAPs. Such compartmentalized and active excitability modulation may be a general feature of dendritic information storage and would greatly increase neuronal storage capacity [220, 133]. Moreover altering Kv4.2 levels leads to a rapid, bidirectional remodeling of CA1 synapses by altering synaptic NR2B/NR2A subunit composition which in turn affects LTP induction. This synaptic remodeling was mimicked in experiments manipulating intracellular Ca^{2+} and dependent on spontaneous activation of NMDA receptors and CaMKII activity [182].

Take together these findings suggests that dendrites can play a far more crucial and independent role than previously believed by self-organizing in response to activity rather than being synaptically controlled and might themselves play a role in controlling synapses.

Chapter 5

Conclusions and Outlook

The work done in this thesis was largely motivated by the desire to extend the current imaging and light actuation methodologies by utilizing principles from plasmonics and photonics. In this dissertation I present a development and applications of two novel, plasmonic-aided imaging techniques (BOM and BEAST) and describe discovery of a new activity driven plastic alteration of dendritic excitability, which was made possible by utilizing new dynamic light modulation scheme for controlling ChR2 inside cells.

The first technique described here is a novel single molecule super-resolution technique termed Brownian Emitter Adsorption Superresolution Technique (BEAST). We used it to conduct the first-time mapping of electromagnetic field within single hotspots of 15nm on a metal surface with a resolution of 1.2 nm. We discovered that the field distribution in this nanometer scale hotspot follows an exponential decay - a strong experimental evidence for Anderson localization mechanism of the hotspots, which has been extensively debated over last decades. The hotspots are localized optical modes on the surface of noble metals exhibiting giant enhancement effect, which have attracted a broad interest from understanding their mechanism to developing practical applications. However, characterizing these hotspots has been difficult, due to the limited resolution of current imaging techniques including NSOM (near-field-scanning-optical-microscopy), EELS (electron-energy-loss-spectroscopy), and CL (cathode-luminescence imaging). Our method improves the resolution significantly to single nanometer level, which enables imaging the EM field inside single hotspots for the first time. Besides, this approach is significantly more efficient, simpler to operate, perturbation-free, and therefore appealing to a broad audience including chemists, physicists and engineers interested in nanoscopic light matter interactions. In the future we envision that other imaging modalities can be integrated with BEAST to expand its imaging capabilities to spectroscopic as well as fluorescence lifetime measurement. Then this approach will be perfectly suited to investigate the strong-coupling regime such as occurs with resonant nano-antennas, since in the strong-coupling regime, the distributed dipoles in the antenna could significantly affect the fluorescence of the molecules, and the strength of the coupling cannot be directly measured from the intensity of the fluorescence signals, but some insight can be

gained from measuring fluorescence lifetime. Furthermore, BEAST's performance including the spatiotemporal resolution and S/N will be improved with the development of brighter fluorophores and better photo-bleaching suppression methods. Additionally, it would be fascinating to make a more detailed three dimensional profile of a hot spot and attempt to correlate the EM field profile to the exact material features creating it.

The second imaging technique described here - Brownian Optical Microscopy (BOM) - is the first technique to offer true three dimensional imaging with nano-resolution, which we strongly believe is critical to advancing our understanding of nano-materials and complex biological and physical systems. Currently there is no technique that would offer such capabilities. Scanning probe microscopy (SPM) is a primary way to image topology of nano-structures. While SPM offers nanoscopic resolution the use of the tip and slow scanning speed limits its throughput and makes it unable to image high aspect ratio or complex overhung samples. Optical tomography is able to image complex three-dimensional shapes but its resolution is limited to the micron range, while electron microscopy offers higher resolution but often requires imaging in stringent conditions such as vacuum. On the other hand BOM does not suffer from those limitations. It is an all-optical imaging technique, which relies on Brownian motion of gold nanoparticles to sample the shape of the object akin to scanning the sample in parallel by millions of small, freely diffusing SPM tips. In BOM an object of arbitrary shape is placed in solution of randomly diffusing nanoparticles, which are illuminated with an evanescent field so that the scattering intensity of resonant NPs correlates with their vertical position. We demonstrate that BOM is capable of imaging complex shapes with 30nm resolution in all three dimensions, including overhang samples, which cannot be imaged with any other technique. We believe that this major development of BOM will impact our imaging capabilities and will provide a flexible platform, which can be further extended. It has a potential to profoundly impact our fundamental understanding of complex materials. In the future we hope to both incrementally improve BOM's spatiotemporal resolution by engineering a better optical system and fundamentally extend it to include additional imaging modalities such as fluorescence or EM field.

The last chapter of this thesis uses optogenetics combined with dynamics light modulation to explore plasticity of dendritic excitability. It was long believed that that plasticity, which plays a crucial role in formation of neural circuits, is based on alteration of synaptic weights. Recent studies indicate that modulations of dendritic excitability may contribute the other part of the engram and critically impact the emergence of complex network behavior. However, a fundamental question remained whether dendritic excitability is controlled by synaptic inputs or arises independently of any synaptic modifications, purely as a result of activity. We used a novel optical system which offers high spatiotemporal control over neural stimulation to observe for the first time the plasticity of local dendritic excitability, which is autonomous from synaptic plasticity and arises only as a result of local activity. This persistent change in dendritic excitability is as a result of a back propagating action potential interacting with simultaneous dendritic depolarization. We identified a number of

mechanistic steps in the process and showed that MEK-regulated phosphorylation Kv4.2 by CamKII is responsible for this local decrease in dendritic excitability. This major discovery of activity dependent dendritic plasticity sheds a new light on the role of dendrites in memory formation and storage. Our research suggests that through reshaping subcellular excitability upon local activity, dendrites may play a far more important and independent role in neuronal plasticity and circuitry than previously thought and might autonomously contribute to forming physical representation of memory. This scientific breakthrough may profoundly impact our fundamental understanding of neural plasticity and memory and might have impact on understanding basis of neural networks and neurodevelopmental and neurodegenerative diseases where Kv4.2 channel deregulation is thought to play a crucial role. While this experiments answer many questions they also pose many. It would be fascinating to further elucidate the molecular interactions underlining the reaction as well as explore in details changes in excitability in different cellular compartments.

In the history of science, developments of new instruments resulted in new understanding of nature, opened up new fields and allowed scientists to push the frontier of unknown a little bit. I believe that new interdisciplinary approaches merging classical photonics with other fields have a great potential to provide novel techniques to advance medicine, biology, physics, chemistry and engineering. In particular I believe that neurophotonics is posed to drive remarkable advances in minimally invasive brain stimulation and monitoring, laser therapies, restore vision and reverse damage to sensitive neural tissues, and improve surgical accuracy. These advances will not only help researchers understand the functioning of the brain, but they will act more broadly to help reduce health care costs by providing better methods for patient management that minimize costly procedures and extended hospital stays. On the other hand nanophotonics will help provide microscopes that rival the resolution only thought possible using electrons or x rays a few short years ago, enabling study of material surfaces, physics of nanostructures as well as early detection and efficacious treatment of disease.

Bibliography

- [1] Ernst Abbe. Beitrage zur Theorie des Mikroskops und der mikroskopischen Wahrnehmung. *Arch. Mikr. Anat*, 9:413–468, 1873.
- [2] W C Abraham, B Gustafsson, and H Wigström. Long-term potentiation involves enhanced synaptic excitation relative to synaptic inhibition in guinea-pig hippocampus. *The Journal of physiology*, 394:367–80, December 1987.
- [3] E Absil, G Tessier, M Gross, M Atlan, N Warnasooriya, S Suck, M Coppey-Moisan, and D Fournier. Photothermal heterodyne holography of gold nanoparticles. *Optics express*, 18(2):780–6, January 2010.
- [4] C. D. Acker and S. D. Antic. Quantitative Assessment of the Distributions of Membrane Conductances Involved in Action Potential Backpropagation Along Basal Dendrites. *Journal of Neurophysiology*, 101(3):1524–1541, December 2008.
- [5] Gwen Acton, Alicia Gómez-yafal, and Emily Walsh. building a business From academic solos to industrial symphonies. pages 1–3, 2011.
- [6] Antoine R Adamantidis, Feng Zhang, Alexander M Aravanis, Karl Deisseroth, and Luis de Lecea. Neural substrates of awakening probed with optogenetic control of hypocretin neurons. *Nature*, 450(7168):420–4, November 2007.
- [7] Hillel Adesnik and Massimo Scanziani. Lateral competition for cortical space by layer-specific horizontal circuits. *Nature*, 464(7292):1155–60, April 2010.
- [8] Yoomin Ahn, Takahito Ono, and Masayoshi Esashi. Micromachined Si cantilever arrays for parallel AFM operation. *Journal of Mechanical Science and Technology*, 22(2):308–311, May 2008.
- [9] C D Aizenman and D J Linden. Rapid, synaptically driven increases in the intrinsic excitability of cerebellar deep nuclear neurons. *Nature neuroscience*, 3(2):109–11, February 2000.
- [10] M. Grant Albrecht and J. Alan Creighton. Anomalously intense Raman spectra of pyridine at a silver electrode. *Journal of the American Chemical Society*, 99(15):5215–5217, June 1977.

- [11] Andrea Alessandrini and Paolo Facci. AFM: a versatile tool in biophysics. *Measurement Science and Technology*, 16(6):R65–R92, June 2005.
- [12] A. Paul Alivisatos, Anne M. Andrews, Edward S. Boyden, Miyoung Chun, George M. Church, Karl Deisseroth, John P. Donoghue, Scott E. Fraser, Jennifer Lippincott-Schwartz, Loren L. Looger, Sotiris Masmanidis, Paul L. McEuen, Arto V. Nurmikko, Hongkun Park, Darcy S. Peterka, Clay Reid, Michael L. Roukes, Axel Scherer, Mark Schnitzer, Terrence J. Sejnowski, Kenneth L. Shepard, Doris Tsao, Gina Turrigiano, Paul S. Weiss, Chris Xu, Rafael Yuste, and Xiaowei Zhuang. Nanotools for Neuroscience and Brain Activity Mapping. *ACS Nano*, 7(3):130320113921003, March 2013.
- [13] D L Alkon, M Sakakibara, R Forman, J Harrigan, I Lederhendler, and J Farley. Reduction of two voltage-dependent K⁺ currents mediates retention of a learned association. *Behavioral and neural biology*, 44(2):278–300, September 1985.
- [14] Shoukimas JJ Alkon DL, Lederhendler I. Primary changes of membrane currents during retention of associative learning. *Science*, pages 693–695, 1982.
- [15] R. a. Álvarez Puebla and L. M. Liz-Marzán. Environmental applications of plasmon assisted Raman scattering. *Energy & Environmental Science*, 3(8):1011, 2010.
- [16] W F An, M R Bowlby, M Betty, J Cao, H P Ling, G Mendoza, J W Hinson, K I Mattsson, B W Strassle, J S Trimmer, and K J Rhodes. Modulation of A-type potassium channels by a family of calcium sensors. *Nature*, 403(6769):553–6, February 2000.
- [17] Jun Ando, Katsumasa Fujita, Nicholas I Smith, and Satoshi Kawata. Dynamic SERS Imaging of Cellular Transport Pathways with Endocytosed Gold Nanoparticles. *Nano letters*, 11:5344–5348, 2011.
- [18] B K Andrásfalvy, J K Makara, D Johnston, and J C Magee. Altered synaptic and non-synaptic properties of CA1 pyramidal neurons in Kv4.2 knockout mice. *The Journal of physiology*, 586(16):3881–92, August 2008.
- [19] Pascal Anger, Palash Bharadwaj, and Lukas Novotny. Enhancement and Quenching of Single-Molecule Fluorescence. *Physical Review Letters*, 96(11):3–6, March 2006.
- [20] Igor Antonov, Irina Antonova, Eric R Kandel, and Robert D Hawkins. Activity-dependent presynaptic facilitation and hebbian LTP are both required and interact during classical conditioning in Aplysia. *Neuron*, 37(1):135–47, January 2003.
- [21] Alexander M Aravanis, Li-Ping Wang, Feng Zhang, Leslie A Meltzer, Murtaza Z Mogri, M Bret Schneider, and Karl Deisseroth. An optical neural interface: in vivo control of rodent motor cortex with integrated fiberoptic and optogenetic technology. *Journal of neural engineering*, 4(3):S143–56, September 2007.

- [22] E Armano, S., Rossi, P., Taglietti, V., D'Angelo. Long-term potentiation of intrinsic excitability at the mossy fibergranule cell synapse of rat cerebellum. *Journal of neuroscience*, 20(14):5208–5216, 2000.
- [23] Deniz Atasoy, Yexica Aponte, Helen Hong Su, and Scott M Sternson. A FLEX switch targets Channelrhodopsin-2 to multiple cell types for imaging and long-range circuit mapping. *The Journal of neuroscience : the official journal of the Society for Neuroscience*, 28(28):7025–30, July 2008.
- [24] Malvin Carl Teich Bahaa E. A. Saleh. *Fundamentals of Photonics*. Wiley-Interscience, 2007.
- [25] K Bahlmann, S Jakobs, and S W Hell. 4Pi-confocal microscopy of live cells. *Ultramicroscopy*, 87(3):155–64, April 2001.
- [26] Christian Bamann, Ronnie Gueta, Sonja Kleinlogel, Georg Nagel, and Ernst Bamberg. Structural guidance of the photocycle of channelrhodopsin-2 by an interhelical hydrogen bond. *Biochemistry*, 49(2):267–78, January 2010.
- [27] Natalia Bastrikova, Gregory A Gardner, Jeff M Reece, Andreas Jeromin, and Serena M Dudek. Synapse elimination accompanies functional plasticity in hippocampal neurons. *Proceedings of the National Academy of Sciences of the United States of America*, 105(8):3123–7, February 2008.
- [28] Mark Bates, Timothy R Blosser, and Xiaowei Zhuang. Short-range spectroscopic ruler based on a single-molecule optical switch. *Physical review letters*, 94(10):108101, March 2005.
- [29] Mark Bates, Bo Huang, Graham T Dempsey, and Xiaowei Zhuang. Multicolor super-resolution imaging with photo-switchable fluorescent probes. *Science (New York, N. Y.)*, 317(5845):1749–53, September 2007.
- [30] Nadine Becker, Corette J Wierenga, Rosalina Fonseca, Tobias Bonhoeffer, and U Valentin Nägerl. LTD induction causes morphological changes of presynaptic boutons and reduces their contacts with spines. *Neuron*, 60(4):590–7, November 2008.
- [31] André Berndt, Matthias Prigge, Dietrich Gradmann, and Peter Hegemann. Two open states with progressive proton selectivities in the branched channelrhodopsin-2 photocycle. *Biophysical journal*, 98(5):753–61, March 2010.
- [32] André Berndt, Ofer Yizhar, Lisa A Gunaydin, Peter Hegemann, and Karl Deisseroth. Bi-stable neural state switches. *Nature neuroscience*, 12(2):229–34, February 2009.
- [33] E Betzig and J K Trautman. Near-field optics: microscopy, spectroscopy, and surface modification beyond the diffraction limit. *Science (New York, N. Y.)*, 257(5067):189–95, July 1992.

- [34] Eric Betzig, George H Patterson, Rachid Sougrat, O Wolf Lindwasser, Scott Olenych, Juan S Bonifacino, Michael W Davidson, Jennifer Lippincott-Schwartz, and Harald F Hess. Imaging intracellular fluorescent proteins at nanometer resolution. *Science (New York, N. Y.)*, 313(5793):1642–5, September 2006.
- [35] Eric Betzig, George H Patterson, Rachid Sougrat, O Wolf Lindwasser, Scott Olenych, Juan S Bonifacino, Michael W Davidson, Jennifer Lippincott-schwartz, and Harald F Hess. Imaging Intracellular Proteins at Nanometer Resolution. 1642(2006), 2012.
- [36] Shari G Birnbaum, Andrew W Varga, Li-Lian Yuan, Anne E Anderson, J David Sweatt, and Laura a Schrader. Structure and function of Kv4-family transient potassium channels. *Physiological reviews*, 84(3):803–33, July 2004.
- [37] Julie S Biteen, Michael A Thompson, Nicole K Tselentis, Grant R Bowman, Lucy Shapiro, and W E Moerner. Super-resolution imaging in live *Caulobacter crescentus* cells using photoswitchable EYFP. *Nature methods*, 5(11):947–9, November 2008.
- [38] T Bliss, T.V.P., Lomo. Long lasting potentiation of synaptic transmission in the dentate area of the anaesthetized rabbit following stimulation of the perforant path. *Journal of Physiology*, 232(2):331–356, 1973.
- [39] Craig F. Bohren and Donald R. Huffman. *Absorption and Scattering of Light by Small Particles (Wiley Science Paperback Series)*. Wiley-VCH, 2012.
- [40] Anja Boisen, Ole Hansen, and Siebe Bouwstra. AFM probes with directly fabricated tips. *Journal of Micromechanics . . .*, 6(1):58–62, March 1999.
- [41] M Bonn, C Hess, S Funk, Jh Miners, Bn Persson, M Wolf, and G Ertl. Femtosecond surface vibrational spectroscopy of CO adsorbed on Ru(001) during desorption. *Physical review letters*, 84(20):4653–6, May 2000.
- [42] Edward S Boyden, Feng Zhang, Ernst Bamberg, Georg Nagel, and Karl Deisseroth. Millisecond-timescale, genetically targeted optical control of neural activity. *Nature neuroscience*, 8(9):1263–8, September 2005.
- [43] SI Bozhevolnyi and Brian Vohnsen. Direct observation of surface polariton localization caused by surface roughness. *Optics . . .*, 4018(95), 1995.
- [44] Darrin H Brager and Daniel Johnston. Plasticity of intrinsic excitability during long-term depression is mediated through mGluR-dependent changes in I(h) in hippocampal CA1 pyramidal neurons. *The Journal of neuroscience : the official journal of the Society for Neuroscience*, 27(51):13926–37, December 2007.
- [45] Siberian Branch and Siberian Branch. Atoms , Molecules and Clusters Fractals : optical susceptibility and giant raman scattering. 79:71–79, 1988.

- [46] Björn Brembs, Fred D Lorenzetti, Fredy D Reyes, Douglas a Baxter, and John H Byrne. Operant reward learning in Aplysia: neuronal correlates and mechanisms. *Science (New York, N.Y.)*, 296(5573):1706–9, May 2002.
- [47] C.D. Brons, J.F., Woody. No TitleLong-term changes in excitability of cortical neurons after Pavlovian conditioning and extinction. *Journal of Neurophysiology*, 44(3):605–615, 1980.
- [48] J. Brugger, R.a. Buser, and NF De Rooij. Silicon cantilevers and tips for scanning force microscopy. *Sensors and Actuators A: Physical*, 34(3):193–200, September 1992.
- [49] T. Buma and T. B. Norris. Time reversal three-dimensional imaging using single-cycle terahertz pulses. *Applied Physics Letters*, 84(12):2196, 2004.
- [50] C Bustamante, C Rivetti, and D J Keller. Scanning force microscopy under aqueous solutions. *Current opinion in structural biology*, 7(5):709–16, October 1997.
- [51] Hans-Jürgen Butt, Brunero Cappella, and Michael Kappl. Force measurements with the atomic force microscope: Technique, interpretation and applications. *Surface Science Reports*, 59(1-6):1–152, October 2005.
- [52] Jon P Camden, Jon A Dieringer, Jing Zhao, and Richard P Van Duyne. Controlled plasmonic nanostructures for surface-enhanced spectroscopy and sensing. *Accounts of chemical research*, 41(12):1653–61, December 2008.
- [53] Emilie Campanac, Gaël Daoudal, Norbert Ankri, and Dominique Debanne. Down-regulation of dendritic I(h) in CA1 pyramidal neurons after LTP. *The Journal of neuroscience : the official journal of the Society for Neuroscience*, 28(34):8635–43, August 2008.
- [54] Emilie Campanac and Dominique Debanne. Spike timing-dependent plasticity: a learning rule for dendritic integration in rat CA1 pyramidal neurons. *The Journal of physiology*, 586(3):779–93, February 2008.
- [55] Hu Cang, Anna Labno, Changgui Lu, Xiaobo Yin, Ming Liu, Christopher Gladden, Yongmin Liu, and Xiang Zhang. Probing the electromagnetic field of a 15-nanometre hotspot by single molecule imaging. *Nature*, 469(7330):385–8, January 2011.
- [56] Hu Cang, Anna Labno, Changgui Lu, Xiaobo Yin, Ming Liu, Christopher Gladden, Yongmin Liu, and Xiang Zhang. Probing the electromagnetic field of a 15-nanometre hotspot by single molecule imaging. *Nature*, 469(7330):385–8, January 2011.
- [57] Jessica A Cardin, Marie Carlén, Konstantinos Meletis, Ulf Knoblich, Feng Zhang, Karl Deisseroth, Li-Huei Tsai, and Christopher I Moore. Targeted optogenetic stimulation and recording of neurons in vivo using cell-type-specific expression of Channelrhodopsin-2. *Nature protocols*, 5(2):247–54, February 2010.

- [58] P a Castro, E C Cooper, D H Lowenstein, and S C Baraban. Hippocampal heterotopia lack functional Kv4.2 potassium channels in the methylazoxymethanol model of cortical malformations and epilepsy. *The Journal of neuroscience : the official journal of the Society for Neuroscience*, 21(17):6626–34, September 2001.
- [59] R R Chance, A Prock, R Silbey, and I Introduction. Comments on the classical theory of energy transfer*. 62(6), 1975.
- [60] Ami Chand and MB Viani. Microfabricated small metal cantilevers with silicon tip for atomic force microscopy. *Journal of Microelectromechanical Systems*, 9(1):112–116, 2000.
- [61] C C Chang, D B Fraser, M J Grieco, T T Sheng, S E Haszko, R E Kerwin, R B Marcus, A K Sinha, Bell Laboratories, Murray Hill, and I May. Aluminum Oxidation in Water. pages 1–6.
- [62] CC Chang, DB Fraser, and MJ Grieco. Aluminum oxidation in water. *Journal of The . . .*, pages 1–6, 1978.
- [63] L.E. Chavez-Noriega, T.V.P. Bliss, and J.V. Halliwell. The EPSP-spike (E-S) component of long-term potentiation in the rat hippocampal slice is modulated by GABAergic but not cholinergic mechanisms. *Neuroscience Letters*, 104(1-2):58–64, September 1989.
- [64] Xixi Chen, Li-Lian Yuan, Cuiping Zhao, Shari G Birnbaum, Andreas Frick, Wonil E Jung, Thomas L Schwarz, J David Sweatt, and Daniel Johnston. Deletion of Kv4.2 gene eliminates dendritic A-type K⁺ current and enhances induction of long-term potentiation in hippocampal CA1 pyramidal neurons. *The Journal of neuroscience : the official journal of the Society for Neuroscience*, 26(47):12143–51, November 2006.
- [65] Yu-chen Karen Chen, Yong S. Chu, JaeMock Yi, Ian McNulty, Qun Shen, Peter W. Voorhees, and David C. Dunand. Morphological and topological analysis of coarsened nanoporous gold by x-ray nanotomography. *Applied Physics Letters*, 96(4):043122, 2010.
- [66] Nian-Sheng Cheng. Formula for viscosity of glycerol-water mixture. *Industrial and Engineering Chemistry Research*, 47:3285–3288, 2008.
- [67] C L Cheung, J H Hafner, and C M Lieber. Carbon nanotube atomic force microscopy tips: direct growth by chemical vapor deposition and application to high-resolution imaging. *Proceedings of the National Academy of Sciences of the United States of America*, 97(8):3809–13, April 2000.
- [68] CL Cheung. Carbon nanotube atomic force microscopy tips: Direct growth by chemical vapor deposition and application to high-resolution imaging. *Proceedings of the . . .*, 97(8):3809–13, April 2000.

- [69] H Chew, D S Wang, and M Kerker. Elastic scattering of evanescent electromagnetic waves. *Applied optics*, 18(15):2679–87, August 1979.
- [70] Xian Xuan Chi and Zao C Xu. Differential Changes of Potassium Currents in CA1 Pyramidal Neurons After Transient Forebrain Ischemia Differential Changes of Potassium Currents in CA1 Pyramidal Neurons After Transient Forebrain Ischemia. *Journal of neurophysiology*, 84:2834–2843, 2000.
- [71] DB Chklovskii, BW Mel, and K Svoboda. Cortical rewiring and information storage. *Nature*, 431(OCTOBER), 2004.
- [72] L Stirling Churchman, Zeynep Okten, Ronald S Rock, John F Dawson, and James a Spudich. Single molecule high-resolution colocalization of Cy3 and Cy5 attached to macromolecules measures intramolecular distances through time. *Proceedings of the National Academy of Sciences of the United States of America*, 102(5):1419–23, February 2005.
- [73] Kevin Claytor, Saumyakanti Khatua, Jason M Guerrero, Alexei Tcherniak, James M Tour, and Stephan Link. Accurately determining single molecule trajectories of molecular motion on surfaces. *The Journal of chemical physics*, 130(16):164710, April 2009.
- [74] L J Cleary, W L Lee, and J H Byrne. Cellular correlates of long-term sensitization in Aplysia. *The Journal of neuroscience : the official journal of the Society for Neuroscience*, 18(15):5988–98, August 1998.
- [75] Donald B Conkey, Rahul P Trivedi, Sri Rama, Prasanna Pavani, Ivan I Smalyukh, and Rafael Piestun. Three-dimensional parallel particle manipulation and tracking by integrating holographic optical tweezers and engineered point spread functions. 19(5):11785–11790, 2011.
- [76] P Rui Costa and Jesper Sjöström. One cell to rule them all , and in the dendrites bind them. *Neuroscience*, 3(September):1–2, 2011.
- [77] Donald R. Huffman Craig F. Bohren. *Absorption and Scattering of Light by Small Particles*. Wiley Science Paperback Series, 2012.
- [78] J. Alan Creighton, Christopher G. Blatchford, and M. Grant Albrecht. Plasma resonance enhancement of Raman scattering by pyridine adsorbed on silver or gold sol particles of size comparable to the excitation wavelength. *Journal of the Chemical Society, Faraday Transactions 2*, 75:790, 1979.
- [79] J.H Critz, S.D., Baxter, D.A., Byrne. Modulatory effects of serotonin, FMRFamide, and myomodulin on the duration of action potentials, excitability, and membrane currents in tail sensory neurons of Aplysia. *Journal of neurophysiology*, 66(6):1912–1926, 1991.

- [80] T J Crow and D L Alkon. Associative behavioral modification in hermissenda: cellular correlates. *Science (New York, N.Y.)*, 209(4454):412–4, July 1980.
- [81] Scott J Cruikshank, Hayato Urabe, Arto V Nurmikko, and Barry W Connors. Pathway-specific feedforward circuits between thalamus and neocortex revealed by selective optical stimulation of axons. *Neuron*, 65(2):230–45, January 2010.
- [82] Robert H Cudmore and Gina G Turrigiano. Long-term potentiation of intrinsic excitability in LV visual cortical neurons. *Journal of neurophysiology*, 92(1):341–8, July 2004.
- [83] Zheng Cui. *Nanofabrication: Principles, Capabilities and Limits*. Springer, 2008.
- [84] Yang Dan and Mu-Ming Poo. Spike timing-dependent plasticity of neural circuits. *Neuron*, 44(1):23–30, September 2004.
- [85] W R D’Angelo, S J Sterbing, E-M Ostapoff, and S Kuwada. Role of GABAergic inhibition in the coding of interaural time differences of low-frequency sounds in the inferior colliculus. *Journal of neurophysiology*, 93(6):3390–400, June 2005.
- [86] Niels de Jonge and Frances M Ross. Electron microscopy of specimens in liquid. *Nature nanotechnology*, 6(11):695–704, November 2011.
- [87] Mathias De Roo, Paul Klausner, and Dominique Muller. LTP promotes a selective long-term stabilization and clustering of dendritic spines. *PLoS biology*, 6(9):e219, September 2008.
- [88] Dominique Debanne and Mu-Ming Poo. Spike-timing dependent plasticity beyond synapse - pre- and post-synaptic plasticity of intrinsic neuronal excitability. *Frontiers in synaptic neuroscience*, 2(June):21, January 2010.
- [89] Karl Deisseroth. Optogenetics. *Commentary*, 8(1):26–29, 2011.
- [90] Niraj S Desai, Lana C Rutherford, and Gina G Turrigiano. BDNF Regulates the Intrinsic Excitability of Cortical Neurons BDNF Regulates the Intrinsic Excitability of Cortical Neurons. pages 284–291, 1999.
- [91] Jacques Désarménien. How to run T_EX in french. Technical Report SATN-CS-1013, Computer Science Department, Stanford University, Stanford, California, August 1984.
- [92] Product Description. Amaxa Rat Neuron Nucleofector Kit. pages 2–6.
- [93] Moerner WE, Dickson RM, Norris DJ, TzengYL. Three-dimensional imaging of single molecules solvated in pores of poly(acrylamide) gels. *Science*, 8(274), 1996.
- [94] Moerner WE, Dickson RM, Norris DJ, TzengYL. Three-dimensional imaging of single molecules solvated in pores of poly(acrylamide) gels. *Science*, 8(274), 1996.

- [95] Eric D. Diebold, Paul Peng, and Eric Mazur. Isolating Surface-Enhanced Raman Scattering Hot Spots Using Multiphoton Lithography. *Journal of the American Chemical Society*, 131(45):16356–16357, November 2009.
- [96] Jon a. Dieringer, Adam D. McFarland, Nilam C. Shah, Douglas a. Stuart, Alyson V. Whitney, Chanda R. Yonzon, Matthew a. Young, Xiaoyu Zhang, and Richard P. Van Duyne. Introductory Lecture : Surface enhanced Raman spectroscopy: new materials, concepts, characterization tools, and applications. *Faraday Discussions*, 132:9, 2006.
- [97] Gerald Donnert, Jan Keller, Rebecca Medda, M Alexandra Andrei, Silvio O Rizzoli, Reinhard Lührmann, Reinhard Jahn, Christian Eggeling, and Stefan W Hell. Macromolecular-scale resolution in biological fluorescence microscopy. *Proceedings of the National Academy of Sciences of the United States of America*, 103(31):11440–5, August 2006.
- [98] Gerald Donnert, Jan Keller, Christian A Wurm, Silvio O Rizzoli, Volker Westphal, Andreas Schönle, Reinhard Jahn, Stefan Jakobs, Christian Eggeling, and Stefan W Hell. Two-color far-field fluorescence nanoscopy. *Biophysical journal*, 92(8):L67–9, April 2007.
- [99] B Drake, C B Prater, A L Weisenhorn, S A Gould, T R Albrecht, C F Quate, D S Cannell, H G Hansma, and P K Hansma. Imaging crystals, polymers, and processes in water with the atomic force microscope. *Science (New York, N.Y.)*, 243(4898):1586–9, March 1989.
- [100] Arnaud Dubois, Kate Grieve, Gael Moneron, Romain Lecaque, Laurent Vabre, and Claude Boccara. Ultrahigh-resolution full-field optical coherence tomography. *Applied optics*, 43(13), 2004.
- [101] J V Duncia, J B Santella, C a Higley, W J Pitts, J Wityak, W E Fietze, F W Rankin, J H Sun, R a Earl, a C Tabaka, C a Teleha, K F Blom, M F Favata, E J Manos, a J Daulerio, D a Stradley, K Horiuchi, R a Copeland, P a Scherle, J M Trzaskos, R L Magolda, G L Trainor, R R Wexler, F W Hobbs, and R E Olson. MEK inhibitors: the chemistry and biological activity of U0126, its analogs, and cyclization products. *Bioorganic & medicinal chemistry letters*, 8(20):2839–44, October 1998.
- [102] R C Dunn. Near-field scanning optical microscopy. *Chemical reviews*, 99(10):2891–928, October 1999.
- [103] Marcus Dyba, Stefan Jakobs, and Stefan W Hell. Immunofluorescence stimulated emission depletion microscopy. *Nature biotechnology*, 21(11):1303–4, November 2003.
- [104] P. Eaton, Peter, West. *Atomic Force Microscopy*. 2010.
- [105] Émile Verdet. *Leçons d'optique physique*. 1869.

- [106] A Engel and C Colliex. Application of scanning transmission electron microscopy to the study of biological structure. *Current opinion in biotechnology*, 4(4):403–11, August 1993.
- [107] F Engert and T Bonhoeffer. Dendritic spine changes associated with hippocampal long-term synaptic plasticity. *Nature*, 399(6731):66–70, May 1999.
- [108] Pierre Escoubas, Sylvie Diochot, Marie-Louise Célérier, Terumi Nakajima, and Michel Lazdunski. Novel tarantula toxins for subtypes of voltage-dependent potassium channels in the Kv2 and Kv4 subfamilies. *Molecular pharmacology*, 62(1):48–57, July 2002.
- [109] Yuan Fan, Desdemona Fricker, Darrin H Brager, Xixi Chen, Hui-Chen Lu, Raymond a Chitwood, and Daniel Johnston. Activity-dependent decrease of excitability in rat hippocampal neurons through increases in I(h). *Nature neuroscience*, 8(11):1542–51, November 2005.
- [110] Nicholas Fang, Hyesog Lee, Cheng Sun, and Xiang Zhang. Sub-diffraction-limited optical imaging with a silver superlens. *Science (New York, N.Y.)*, 308(5721):534–7, April 2005.
- [111] J N Farahani, D W Pohl, H-J Eisler, and B Hecht. Single quantum dot coupled to a scanning optical antenna: a tunable superemitter. *Physical review letters*, 95(1):017402, July 2005.
- [112] Joseph Farley. Associative Training Results in Persistent Reductions in a Calcium-Activated Potassium Current in Hermissenda Type B Photoreceptors. *Behavioral Neuroscience*, 102(5):784 – 802, 1988.
- [113] Mélanie Favre and J PoleselâMaris. Parallel AFM imaging and force spectroscopy using two-dimensional probe arrays for applications in cell biology. *Journal of Molecular . . .*, 24(3):446–52, 2011.
- [114] Lief Fenno, Ofer Yizhar, and Karl Deisseroth. The development and application of optogenetics. *Annual review of neuroscience*, 34:389–412, January 2011.
- [115] Marta Fernández-Suárez and Alice Y Ting. Fluorescent probes for super-resolution imaging in living cells. *Nature reviews. Molecular cell biology*, 9(12):929–43, December 2008.
- [116] Lucia Ferrari, Josef Kaufmann, Frank Winnefeld, and Johann Plank. Interaction of cement model systems with superplasticizers investigated by atomic force microscopy, zeta potential, and adsorption measurements. *Journal of colloid and interface science*, 347(1):15–24, July 2010.

- [117] Ann E Fink and Thomas J O'Dell. Short trains of theta frequency stimulation enhance CA1 pyramidal neuron excitability in the absence of synaptic potentiation. *The Journal of neuroscience : the official journal of the Society for Neuroscience*, 29(36):11203–14, September 2009.
- [118] M Fleischmann. [io]. ... 2. 26(2):2–5, 1974.
- [119] Jonas Fölling, Mariano Bossi, Hannes Bock, Rebecca Medda, Christian A Wurm, Birka Hein, Stefan Jakobs, Christian Eggeling, and Stefan W Hell. Fluorescence nanoscopy by ground-state depletion and single-molecule return. *Nature methods*, 5(11):943–5, November 2008.
- [120] Danielle S. Fonseca. *Potassium Channels: Types, Structure and Blockers*. 2012.
- [121] Heinrich G Frey, Susanne Witt, Karin Felderer, and Reinhard Guckenberger. High-resolution imaging of single fluorescent molecules with the optical near-field of a metal tip. *Physical review letters*, 93(20):200801, November 2004.
- [122] Andreas Frick, Jeffrey Magee, and Daniel Johnston. LTP is accompanied by an enhanced local excitability of pyramidal neuron dendrites. *Nature neuroscience*, 7(2):126–35, February 2004.
- [123] David Fuchs. The format of T_EX's DVI files version 1. *TUGboat*, 2(2):12–16, July 1981.
- [124] David Fuchs. Device independent file format. *TUGboat*, 3(2):14–19, October 1982.
- [125] Richard K. Furuta and Pierre A. MacKay. Two T_EX implementations for the IBM PC. *Dr. Dobb's Journal*, 10(9):80–91, September 1985.
- [126] L.D Gandhi, C.C., Matzel. Modulation of presynaptic action potential kinetics underlies synaptic facilitation of type B photoreceptors after associative conditioning in *Hermisenda*. *Journal of neuroscience*, 20(5):2022–2035, 2000.
- [127] K Ganguly, L Kiss, and M Poo. Enhancement of presynaptic neuronal excitability by correlated presynaptic and postsynaptic spiking. *Nature neuroscience*, 3(10):1018–26, October 2000.
- [128] Bertram Gerber, Hiromu Tanimoto, and Martin Heisenberg. An engram found? Evaluating the evidence from fruit flies. *Current opinion in neurobiology*, 14(6):737–44, December 2004.
- [129] Joel Gersten. Electromagnetic theory of enhanced Raman scattering by molecules adsorbed on rough surfaces eo e. 73(7), 1980.

- [130] M G Giovannini, R D Blitzler, T Wong, K Asoma, P Tsokas, J H Morrison, R Iyengar, and E M Landau. Mitogen-activated protein kinase regulates early phosphorylation and delayed expression of Ca²⁺/calmodulin-dependent protein kinase II in long-term potentiation. *The Journal of neuroscience : the official journal of the Society for Neuroscience*, 21(18):7053–62, September 2001.
- [131] M Göken and M Kempf. Microstructural properties of superalloys investigated by nanoindentations in an atomic force microscope. *Acta Materialia*, 47(3):1043–1052, 1999.
- [132] Claire Goldsbury and Simon Scheuring. Introduction to atomic force microscopy (AFM) in biology. *Current protocols in protein science / editorial board, John E. Coligan ... [et al.]*, Chapter 17:Unit 17.7, November 2002.
- [133] Leonardo L Gollo, Osame Kinouchi, and Mauro Copelli. Active dendrites enhance neuronal dynamic range. *PLoS computational biology*, 5(6):e1000402, June 2009.
- [134] Matthew P Gordon, Taekjip Ha, and Paul R Selvin. Single-molecule high-resolution imaging with photobleaching. *Proceedings of the National Academy of Sciences of the United States of America*, 2004:15–18, 2004.
- [135] Reuven Gordon, David Sinton, Karen L Kavanagh, and Alexandre G Brolo. A new generation of sensors based on extraordinary optical transmission. *Accounts of chemical research*, 41(8):1049–57, August 2008.
- [136] Arvind Govindarajan, Inbal Israely, Shu-Ying Huang, and Susumu Tonegawa. The dendritic branch is the preferred integrative unit for protein synthesis-dependent LTP. *Neuron*, 69(1):132–46, January 2011.
- [137] Viviana Gradinaru, Kimberly R Thompson, and Karl Deisseroth. eNpHR: a *Neisseria meningitidis* halorhodopsin enhanced for optogenetic applications. *Brain cell biology*, 36(1-4):129–39, August 2008.
- [138] Viviana Gradinaru, Kimberly R Thompson, Feng Zhang, Murtaza Mogri, Kenneth Kay, M Bret Schneider, and Karl Deisseroth. Targeting and readout strategies for fast optical neural control in vitro and in vivo. *The Journal of neuroscience : the official journal of the Society for Neuroscience*, 27(52):14231–8, December 2007.
- [139] Viviana Gradinaru, Feng Zhang, Charu Ramakrishnan, Joanna Mattis, Rohit Prakash, Ilka Diester, Inbal Goshen, Kimberly R Thompson, and Karl Deisseroth. Molecular and cellular approaches for diversifying and extending optogenetics. *Cell*, 141(1):154–65, April 2010.
- [140] Duncan Graham, David G Thompson, W Ewen Smith, and Karen Faulds. Control of enhanced Raman scattering using a DNA-based assembly process of dye-coded nanoparticles. *Nature nanotechnology*, 3(9):548–51, September 2008.

- [141] M Grant. Plasma Resonance Enhancement of Raman Scattering by Pyridine Adsorbed on Silver or Gold Sol Particles of Size. pages 790–798, 1978.
- [142] Christina Gross, Xiaodi Yao, Dan L Pong, Andreas Jeromin, and Gary J Bassell. Fragile X mental retardation protein regulates protein expression and mRNA translation of the potassium channel Kv4.2. *The Journal of neuroscience : the official journal of the Society for Neuroscience*, 31(15):5693–8, April 2011.
- [143] Nir Grossman, Vincent Poher, Matthew S Grubb, Gordon T Kennedy, Konstantin Nikolic, Brian McGovern, Rolando Berlinguer Palmieri, Zheng Gong, Emmanuel M Drakakis, Mark a a Neil, Martin D Dawson, Juan Burrone, and Patrick Degenaar. Multi-site optical excitation using ChR2 and micro-LED array. *Journal of neural engineering*, 7(1):16004, February 2010.
- [144] Lisa A Gunaydin, Ofer Yizhar, André Berndt, Vikaas S Sohal, Karl Deisseroth, and Peter Hegemann. Ultrafast optogenetic control. *Nature neuroscience*, 13(3):387–92, March 2010.
- [145] M G Gustafsson, D A Agard, and J W Sedat. I5M: 3D widefield light microscopy with better than 100 nm axial resolution. *Journal of microscopy*, 195(Pt 1):10–6, July 1999.
- [146] Mats G L Gustafsson. Nonlinear structured-illumination microscopy: wide-field fluorescence imaging with theoretically unlimited resolution. *Proceedings of the National Academy of Sciences of the United States of America*, 102(37):13081–6, September 2005.
- [147] JH Hafner and CL Cheung. Structural and functional imaging with carbon nanotube AFM probes. *Progress in biophysics and . . .*, 77(1):73–110, January 2001.
- [148] Christoph Haisch. Optical tomography. *Annual review of analytical chemistry (Palo Alto, Calif.)*, 5:57–77, January 2012.
- [149] Rebecca S Hammond, Lin Lin, Michael S Sidorov, Andrew M Wikenheiser, and Dax a Hoffman. Protein kinase a mediates activity-dependent Kv4.2 channel trafficking. *The Journal of neuroscience : the official journal of the Society for Neuroscience*, 28(30):7513–9, July 2008.
- [150] Jin-Hee Han, Steven A Kushner, Adelaide P Yiu, Christy J Cole, Anna Matynia, Robert A Brown, Rachael L Neve, John F Guzowski, Alcino J Silva, and Sheena A Josselyn. Neuronal competition and selection during memory formation. *Science (New York, N. Y.)*, 316(5823):457–60, April 2007.
- [151] Jin-Hee Han, Steven A Kushner, Adelaide P Yiu, Hwa-Lin Liz Hsiang, Thorsten Buch, Ari Waisman, Bruno Bontempi, Rachael L Neve, Paul W Frankland, and Sheena A Josselyn. Selective erasure of a fear memory. *Science (New York, N. Y.)*, 323(5920):1492–6, March 2009.

- [152] Christopher D Harvey and Karel Svoboda. Locally dynamic synaptic learning rules in pyramidal neuron dendrites. *Nature*, 450(7173):1195–200, December 2007.
- [153] J Hastie, T., Tibshirani, R. & Friedman. *The Elements of Statistical Learning*. Springer, 2001.
- [154] Michael Hausmann, Bodo Liebe, Birgit Perner, Martin Jerratsch, Karl-Otto Greulich, and Harry Scherthan. Imaging of human meiotic chromosomes by scanning near-field optical microscopy (SNOM). *Micron (Oxford, England : 1993)*, 34(8):441–7, January 2003.
- [155] Eugene Hecht. *Optics*. Addison-Wesley, 4th edition, 2001.
- [156] Birka Hein, Katrin I Willig, and Stefan W Hell. Stimulated emission depletion (STED) nanoscopy of a fluorescent protein-labeled organelle inside a living cell. *Proceedings of the National Academy of Sciences of the United States of America*, 105(38):14271–6, September 2008.
- [157] Rainer Heintzmann, Thomas M. Jovin, and Christoph Cremer. Saturated patterned excitation microscopy concept for optical resolution improvement. *Journal of the Optical Society of America A*, 19(8):1599, August 2002.
- [158] Laurent Helden, Elena Eremina, Norbert Riefler, Christopher Hertlein, Clemens Bechinger, Yuri Eremin, and Thomas Wriedt. Single-particle evanescent light scattering simulations for total internal reflection microscopy. *Applied optics*, 45(28):7299–308, October 2006.
- [159] S. W Hell. *Single Molecule Spectroscopy in Chemistry, Physics and Biology*. Springer Series in Chemical Physics, Springer, 2009.
- [160] S. W. Hell and M. Kroug. Ground-state-depletion fluorescence microscopy: A concept for breaking the diffraction resolution limit. *Applied Physics B Lasers and Optics*, 60(5):495–497, May 1995.
- [161] Stefan Hell and Ernst H.K. Stelzer. Fundamental improvement of resolution with a 4Pi-confocal fluorescence microscope using two-photon excitation. *Optics Communications*, 93(5-6):277–282, October 1992.
- [162] Stefan W. Hell and Jan Wichmann. Breaking the diffraction resolution limit by stimulated emission: stimulated-emission-depletion fluorescence microscopy. *Optics Letters*, 19(11):780, June 1994.
- [163] Samuel T Hess, Thanu P K Girirajan, and Michael D Mason. Ultra-high resolution imaging by fluorescence photoactivation localization microscopy. *Biophysical journal*, 91(11):4258–72, December 2006.

- [164] Peter Hinterdorfer and Yves F Dufrêne. Detection and localization of single molecular recognition events using atomic force microscopy. *Nature methods*, 3(5):347–55, May 2006.
- [165] Primary Mouse Hippocampal, Cortical Neurons, and Product Description. Amaxa Mouse Neuron Nucleofector Kit. pages 1–5.
- [166] D A Hoffman, J C Magee, C M Colbert, and D Johnston. K⁺ channel regulation of signal propagation in dendrites of hippocampal pyramidal neurons. *Nature*, 387(6636):869–75, June 1997.
- [167] Christiane Höppener and Lukas Novotny. Antenna-based optical imaging of single Ca²⁺ transmembrane proteins in liquids. *Nano letters*, 8(2):642–6, February 2008.
- [168] Julia W P Hsu. Near-field scanning optical microscopy studies of electronic and photonic materials and devices. 33:1–50, 2001.
- [169] Juan Hu and Chun-yang Zhang. Single base extension reaction-based surface enhanced Raman spectroscopy for DNA methylation assay. *Biosensors & bioelectronics*, 31(1):451–7, January 2012.
- [170] Min Hu, Fung Suong Ou, Wei Wu, Ivan Naumov, Xuema Li, Alexander M. Bratkovsky, R. Stanley Williams, and Zhiyong Li. Gold Nanofingers for Molecule Trapping and Detection. *Journal of the American Chemical Society*, 132(37):12820–12822, September 2010.
- [171] Bo Huang, Mark Bates, and Xiaowei Zhuang. Super-resolution fluorescence microscopy. *Annual review of biochemistry*, 78:993–1016, January 2009.
- [172] Bo Huang, Wenqin Wang, Mark Bates, and Xiaowei Zhuang. Three-Dimensional Super-Resolution Reconstruction Microscopy. (February):810–813, 2008.
- [173] James a Hutchison, Silvia P Centeno, Hideho Odaka, Hiroshi Fukumura, Johan Hofkens, and Hiroshi Uji-I. Subdiffraction limited, remote excitation of surface enhanced Raman scattering. *Nano letters*, 9(3):995–1001, March 2009.
- [174] Anatoli Ianoul, Melissa Street, Donna Grant, John Pezacki, Rod S Taylor, and Linda J Johnston. Near-field scanning fluorescence microscopy study of ion channel clusters in cardiac myocyte membranes. *Biophysical journal*, 87(5):3525–35, November 2004.
- [175] Emad L Izake. Forensic and homeland security applications of modern portable Raman spectroscopy. *Forensic science international*, 202(1-3):1–8, October 2010.
- [176] David L Jeanmaire and Richard P V A N Duyne. Surface Raman spectroelectrochemistry: Part I. Heterocyclic, aromatic, and aliphatic amines adsorbed on the anodized silver electrode. *Electroanal. Chem.*, 84, 1977.

- [177] P.U. Jepsen, D.G. Cooke, and M. Koch. Terahertz spectroscopy and imaging - Modern techniques and applications. *Laser & Photonics Reviews*, 5(1):124–166, January 2011.
- [178] Henry H Jerng, Paul J Pfaffinger, and Manuel Covarrubias. Molecular physiology and modulation of somatodendritic A-type potassium channels. *Molecular and cellular neurosciences*, 27(4):343–69, December 2004.
- [179] Lonnie Dee Russell John J. Bozzola. *Electron Microscopy*. Jones & Bartlett Learning, 1999.
- [180] Sheena A Josselyn. Continuing the search for the engram: examining the mechanism of fear memories. *Journal of psychiatry & neuroscience : JPN*, 35(4):221–8, July 2010.
- [181] MF Juette, TJ Gould, and MD Lessard. Three-dimensional sub100 nm resolution fluorescence microscopy of thick samples. *Nature . . .*, 5(6):527–529, 2008.
- [182] Sung-Cherl Jung, Jinhyun Kim, and Dax a Hoffman. Rapid, bidirectional remodeling of synaptic NMDA receptor subunit composition by A-type K⁺ channel activity in hippocampal CA1 pyramidal neurons. *Neuron*, 60(4):657–71, November 2008.
- [183] R Juskaitis, T Wilson, M A Neil, and M Kozubek. Efficient real-time confocal microscopy with white light sources. *Nature*, 383(6603):804–6, October 1996.
- [184] E R Kandel. The molecular biology of memory storage: a dialogue between genes and synapses. *Science (New York, N.Y.)*, 294(5544):1030–8, November 2001.
- [185] Shigeki Kato, Kenta Kobayashi, Ken-ichi Inoue, Masahito Kuramochi, Tomoaki Okada, Hiroyuki Yaginuma, Kinjiro Morimoto, Takashi Shimada, Masahiko Takada, and Kazuto Kobayashi. A lentiviral strategy for highly efficient retrograde gene transfer by pseudotyping with fusion envelope glycoprotein. *Human gene therapy*, 22(2):197–206, February 2011.
- [186] S Kawata, Y Inouye, and T Sugiura. Near-field scanning optical microscope with a laser trapped probe. *Japanese journal of applied . . .*, 33:1725–1727, 1994.
- [187] Satoshi Kawata, Yasushi Inouye, and Prabhat Verma. Plasmonics for near-field nano-imaging and superlensing. *Nature Photonics*, 3(7):388–394, July 2009.
- [188] Satoshi Kawata, Atsushi Ono, and Prabhat Verma. Subwavelength colour imaging with a metallic nanolens. *Nature Photonics*, 2(7):438–442, June 2008.
- [189] Raymond J Kelleher, Arvind Govindarajan, Hae-Yoon Jung, Hyejin Kang, and Susumu Tonegawa. Translational control by MAPK signaling in long-term synaptic plasticity and memory. *Cell*, 116(3):467–79, February 2004.

- [190] R R Kellner, C J Baier, K I Willig, S W Hell, and F J Barrantes. Nanoscale organization of nicotinic acetylcholine receptors revealed by stimulated emission depletion microscopy. *Neuroscience*, 144(1):135–43, January 2007.
- [191] Ildikó Kemenes, György Kemenes, Richard J Andrew, Paul R Benjamin, and Michael O’Shea. Critical time-window for NO-cGMP-dependent long-term memory formation after one-trial appetitive conditioning. *The Journal of neuroscience : the official journal of the Society for Neuroscience*, 22(4):1414–25, February 2002.
- [192] Ildikó Kemenes, Volko A Straub, Eugeny S Nikitin, Kevin Staras, Michael O’Shea, György Kemenes, and Paul R Benjamin. Role of delayed nonsynaptic neuronal plasticity in long-term associative memory. *Current biology : CB*, 16(13):1269–79, July 2006.
- [193] Jinhyun Kim, Sung-Cherl Jung, Ann M Clemens, Ronald S Petralia, and Dax a Hoffman. Regulation of dendritic excitability by activity-dependent trafficking of the A-type K⁺ channel subunit Kv4.2 in hippocampal neurons. *Neuron*, 54(6):933–47, June 2007.
- [194] Jinhyun Kim, Marcela S Nadal, Ann M Clemens, Matthew Baron, Sung-Cherl Jung, Yoshio Misumi, Bernardo Rudy, and Dax A Hoffman. Kv4 accessory protein DPPX (DPP6) is a critical regulator of membrane excitability in hippocampal CA1 pyramidal neurons. *Journal of neurophysiology*, 100(4):1835–47, October 2008.
- [195] Anika Kinkhabwala, Zongfu Yu, Shanhui Fan, Yuri Avlasevich, Klaus Müllen, and W. E. Moerner. Large single-molecule fluorescence enhancements produced by a bowtie nanoantenna. *Nature Photonics*, 3(11):654–657, October 2009.
- [196] Robert J Kittel, Carolin Wichmann, Tobias M Rasse, Wernher Fouquet, Manuela Schmidt, Andreas Schmid, Dhananjay A Wagh, Christian Pawlu, Robert R Kellner, Katrin I Willig, Stefan W Hell, Erich Buchner, Manfred Heckmann, and Stephan J Sigrist. Bruchpilot promotes active zone assembly, Ca²⁺ channel clustering, and vesicle release. *Science (New York, N. Y.)*, 312(5776):1051–4, May 2006.
- [197] Samuel L Kleinman, Renee R Frontiera, Anne-Isabelle Henry, Jon a Dieringer, and Richard P Van Duyne. Creating, characterizing, and controlling chemistry with SERS hot spots. *Physical chemistry chemical physics : PCCP*, 15(1):21–36, January 2013.
- [198] Katrin Kneipp, Yang Wang, Harald Kneipp, Lev Perelman, Irving Itzkan, Ramachandra Dasari, and Michael Feld. Single Molecule Detection Using Surface-Enhanced Raman Scattering (SERS). *Physical Review Letters*, 78(9):1667–1670, March 1997.
- [199] Donald E. Knuth. The WEB system for structured documentation, version 2.3. Technical Report STAN-CS-83-980, Computer Science Department, Stanford University, Stanford, California, September 1983.

- [200] Donald E. Knuth. Literate programming. *The Computer Journal*, 27(2):97–111, May 1984.
- [201] Donald E. Knuth. A torture test for T_EX, version 1.3. Technical Report STAN-CS-84-1027, Computer Science Department, Stanford University, Stanford, California, November 1984.
- [202] Donald E. Knuth. *T_EX: The Program*, volume B of *Computers & Typesetting*. Addison-Wesley, Reading, Massachusetts, 1986.
- [203] Lena Fitting Kourkoutis, Jürgen M. Plitzko, and Wolfgang Baumeister. Electron Microscopy of Biological Materials at the Nanometer Scale. *Annual Review of Materials Research*, 42(1):33–58, August 2012.
- [204] Lena Fitting Kourkoutis, Jürgen M. Plitzko, and Wolfgang Baumeister. Electron Microscopy of Biological Materials at the Nanometer Scale. *Annual Review of Materials Research*, 42(1):33–58, August 2012.
- [205] Alexxai V Kravitz, Benjamin S Freeze, Philip R L Parker, Kenneth Kay, Myo T Thwin, Karl Deisseroth, and Anatol C Kreitzer. Regulation of parkinsonian motor behaviours by optogenetic control of basal ganglia circuitry. *Nature*, 466(7306):622–6, July 2010.
- [206] Atsushi Kubo, Yun Suk Jung, Hong Koo Kim, and Hrvoje Petek. Femtosecond microscopy of localized and propagating surface plasmons in silver gratings. *Journal of Physics B: Atomic, Molecular and Optical Physics*, 40(11):S259–S272, June 2007.
- [207] Atsushi Kubo, Yun Suk Jung, Hong Koo Kim, and Hrvoje Petek. Femtosecond microscopy of localized and propagating surface plasmons in silver gratings. *Journal of Physics B: Atomic, Molecular and Optical Physics*, 40(11):S259–S272, June 2007.
- [208] I. V. Kudryashova. Structural and functional characteristics of potassium channels and their role in neuroplasticity. *Neurochemical Journal*, 4(3):159–169, September 2010.
- [209] Sandra J Kuhlman and Z Josh Huang. High-resolution labeling and functional manipulation of specific neuron types in mouse brain by Cre-activated viral gene expression. *PloS one*, 3(4):e2005, January 2008.
- [210] Sergei Kühn, Ulf Håkanson, Lavinia Rogobete, and Vahid Sandoghdar. Enhancement of single-molecule fluorescence using a gold nanoparticle as an optical nanoantenna. *Physical review letters*, 97(1):017402, July 2006.
- [211] Harold Kwart and Thomas J George. No Title. pages 5215–5217, 1976.
- [212] Helen C Lai and Lily Y Jan. The distribution and targeting of neuronal voltage-gated ion channels. *Nature reviews. Neuroscience*, 7(7):548–62, July 2006.

- [213] Melike Lakadamyali, Michael J Rust, Hazen P Babcock, and Xiaowei Zhuang. Visualizing infection of individual influenza viruses. *Proceedings of the National Academy of Sciences of the United States of America*, 100(16):9280–5, August 2003.
- [214] J R Lakowicz. Radiative decay engineering: biophysical and biomedical applications. *Analytical biochemistry*, 298(1):1–24, November 2001.
- [215] Leslie Lamport. *TEX: A Document Preparation System. User's Guide and Reference Manual*. Addison-Wesley, Reading, Massachusetts, 1986.
- [216] K. M. Lang, D. A. Hite, R. W. Simmonds, R. McDermott, D. P. Pappas, and John M. Martinis. Conducting atomic force microscopy for nanoscale tunnel barrier characterization. *Review of Scientific Instruments*, 75(8):2726, August 2004.
- [217] Eric C Le Ru and Pablo G Etchegoin. Single-molecule surface-enhanced Raman spectroscopy. *Annual review of physical chemistry*, 63:65–87, January 2012.
- [218] H a Lechner, D a Baxter, and J H Byrne. Classical conditioning of feeding in Aplysia: I. Behavioral analysis. *The Journal of neuroscience : the official journal of the Society for Neuroscience*, 20(9):3369–76, May 2000.
- [219] Hye Young Lee, Woo-ping Ge, Wendy Huang, Ye He, Gordon X Wang, Stephen J Smith, Yuh Nung Jan, and Lily Yeh Jan. Bidirectional Regulation of Dendritic Voltage-gated Potassium Channels by the Fragile X Mental Retardation Protein. *Neuron*, 72(4):630–642, 2012.
- [220] R. Legenstein and W. Maass. Branch-Specific Plasticity Enables Self-Organization of Nonlinear Computation in Single Neurons. *Journal of Neuroscience*, 31(30):10787–10802, July 2011.
- [221] Z Lei, P Deng, Y Li, and Z C Xu. Downregulation of Kv4.2 channels mediated by NR2B-containing NMDA receptors in cultured hippocampal neurons. *Neuroscience*, 165(2):350–62, January 2010.
- [222] Zhigang Lei, Ping Deng, and Zao C Xu. Regulation of Kv4.2 channels by glutamate in cultured hippocampal neurons. *Journal of neurochemistry*, 106(1):182–92, July 2008.
- [223] M J Levene, J Korlach, S W Turner, M Foquet, H G Craighead, and W W Webb. Zero-mode waveguides for single-molecule analysis at high concentrations. *Science (New York, N. Y.)*, 299(5607):682–6, January 2003.
- [224] A. Lewis, M. Isaacson, A. Harootunian, and A. Muray. Development of a 500 Åspatial resolution light microscope. *Ultramicroscopy*, 13(3):227–231, January 1984.
- [225] Cheng-yu Li, Jiang-teng Lu, Chien-ping Wu, Shu-min Duan, and Mu-ming Poo. Bidirectional modification of presynaptic neuronal excitability accompanying spike timing-dependent synaptic plasticity. *Neuron*, 41(2):257–68, January 2004.

- [226] Jeff W Lichtman, Jean Livet, and Joshua R Sanes. A technicolour approach to the connectome. *Nature reviews. Neuroscience*, 9(6):417–22, June 2008.
- [227] KA Lidke, Bernd Rieger, TM Jovin, and Rainer Heintzmann. Superresolution by localization of quantum dots using blinking statistics. *Opt. Express*, 13(18):1599–1609, 2005.
- [228] Dong-Kwon Lim, Ki-Seok Jeon, Jae-Ho Hwang, Hyoki Kim, Sunghoon Kwon, Yung Doug Suh, and Jwa-Min Nam. Highly uniform and reproducible surface-enhanced Raman scattering from DNA-tailorable nanoparticles with 1-nm interior gap. *Nature nanotechnology*, 6(7):452–60, July 2011.
- [229] Dong-Kwon Lim, Ki-Seok Jeon, Hyung Min Kim, Jwa-Min Nam, and Yung Doug Suh. Nanogap-engineerable Raman-active nanodumbbells for single-molecule detection. *Nature materials*, 9(1):60–7, January 2010.
- [230] Susana Q Lima, Tomás Hromádka, Petr Znamenskiy, and Anthony M Zador. PINP: a new method of tagging neuronal populations for identification during in vivo electrophysiological recording. *PloS one*, 4(7):e6099, January 2009.
- [231] John Y Lin, Michael Z Lin, Paul Steinbach, and Roger Y Tsien. Characterization of engineered channelrhodopsin variants with improved properties and kinetics. *Biophysical journal*, 96(5):1803–14, March 2009.
- [232] Lin Lin, Wei Sun, Faith Kung, Mark L Dell’Acqua, and Dax a Hoffman. AKAP79/150 impacts intrinsic excitability of hippocampal neurons through phospho-regulation of A-type K⁺ channel trafficking. *The Journal of neuroscience : the official journal of the Society for Neuroscience*, 31(4):1323–32, January 2011.
- [233] Jennifer Lippincott-Schwartz and Suliana Manley. Putting super-resolution fluorescence microscopy to work. *Nature methods*, 6(1):21–3, January 2009.
- [234] Xu Liu, Steve Ramirez, Petti T Pang, Corey B Puryear, Arvind Govindarajan, Karl Deisseroth, and Susumu Tonegawa. Optogenetic stimulation of a hippocampal engram activates fear memory recall. *Nature*, 484(7394):381–5, April 2012.
- [235] Zhaowei Liu, Hyesog Lee, Yi Xiong, Cheng Sun, and Xiang Zhang. Far-field optical hyperlens magnifying sub-diffraction-limited objects. *Science (New York, N.Y.)*, 315(5819):1686, March 2007.
- [236] T Lohmüller, L Iversen, M Schmidt, C Rhodes, H-L Tu, W-C Lin, and J T Groves. Single molecule tracking on supported membranes with arrays of optical nanoantennas. *Nano letters*, 12(3):1717–21, March 2012.

- [237] Fred D Lorenzetti, Riccardo Mozzachiodi, Douglas a Baxter, and John H Byrne. Classical and operant conditioning differentially modify the intrinsic properties of an identified neuron. *Nature neuroscience*, 9(1):17–9, January 2006.
- [238] Attila Losonczy, Judit K Makara, and Jeffrey C Magee. Compartmentalized dendritic plasticity and input feature storage in neurons. *Nature*, 452(7186):436–41, March 2008.
- [239] Bert Hecht Lukas Novotny. *Principles of Nano-Optics*. Cambridge University Press, 2011.
- [240] Bert Hecht Lukas Novotny. *Principles of Nano-Optics*. Cambridge University Press, 2011.
- [241] J. C; Magee and Daniel Johnston. A Synaptically Controlled, Associative Signal for Hebbian Plasticity in Hippocampal Neurons. *Science*, 275(5297):209–213, January 1997.
- [242] Jeffrey C Magee and Daniel Johnston. Plasticity of dendritic function. *Current opinion in neurobiology*, 15(3):334–42, June 2005.
- [243] Guillaume Maire, Filip Drsek, Jules Girard, Hugues Giovannini, Anne Talneau, Denis Konan, Kamal Belkebir, Patrick Chaumet, and Anne Sentenac. Experimental Demonstration of Quantitative Imaging beyond Abbes Limit with Optical Diffraction Tomography. *Physical Review Letters*, 102(21):213905, May 2009.
- [244] Judit K Makara, Attila Losonczy, Quan Wen, and Jeffrey C Magee. Experience-dependent compartmentalized dendritic plasticity in rat hippocampal CA1 pyramidal neurons. *Nature neuroscience*, 12(12):1485–7, December 2009.
- [245] Robert C Malenka and Mark F Bear. LTP and LTD: an embarrassment of riches. *Neuron*, 44(1):5–21, September 2004.
- [246] M Maletic-Savatic, NJ Lenn, and JS Trimmer. Differential spatiotemporal expression of K⁺ channel polypeptides in rat hippocampal neurons developing in situ and in vitro. *J. Neurosci.*, 15(5):3840–3851, May 1995.
- [247] M Maletic-Savatic, R Malinow, and K Svoboda. Rapid dendritic morphogenesis in CA1 hippocampal dendrites induced by synaptic activity. *Science (New York, N. Y.)*, 283(5409):1923–7, March 1999.
- [248] Suliana Manley, Jennifer M Gillette, George H Patterson, Hari Shroff, Harald F Hess, Eric Betzig, and Jennifer Lippincott-Schwartz. High-density mapping of single-molecule trajectories with photoactivated localization microscopy. *Nature methods*, 5(2):155–7, February 2008.

- [249] H. Markram. Regulation of Synaptic Efficacy by Coincidence of Postsynaptic APs and EPSPs. *Science*, 275(5297):213–215, January 1997.
- [250] S J Martin and R G M Morris. New life in an old idea: the synaptic plasticity and memory hypothesis revisited. *Hippocampus*, 12(5):609–36, January 2002.
- [251] Masanori Matsuzaki, Naoki Honkura, Graham C R Ellis-Davies, and Haruo Kasai. Structural basis of long-term potentiation in single dendritic spines. *Nature*, 429(6993):761–6, June 2004.
- [252] Erwen Mei, Feng Gao, and Robin M Hochstrasser. Controlled bimolecular collisions allow sub-diffraction limited microscopy of lipid vesicles. *Physical chemistry chemical physics : PCCP*, 8(17):2077–82, May 2006.
- [253] Rhiannon M Meredith and Huibert D Mansvelder. STDP and Mental Retardation: Dysregulation of Dendritic Excitability in Fragile X Syndrome. *Frontiers in synaptic neuroscience*, 2:10, January 2010.
- [254] Amy M Michaels, M Nirmal, and L E Brus. Surface Enhanced Raman Spectroscopy of Individual Rhodamine 6G Molecules on Large Ag Nanocrystals. (16):9932–9939, 1999.
- [255] SC Minne, SR Manalis, and CF Quate. Parallel atomic force microscopy using cantilevers with integrated piezoresistive sensors and integrated piezoelectric actuators. *Applied physics letters*, 67(September):3918–3920, 1995.
- [256] Hiroaki Misonou, Durga P Mohapatra, Eunice W Park, Victor Leung, Dongkai Zhen, Kaori Misonou, Anne E Anderson, and James S Trimmer. Regulation of ion channel localization and phosphorylation by neuronal activity. *Nature neuroscience*, 7(7):711–8, July 2004.
- [257] Hiroaki Misonou and James S Trimmer. Determinants of voltage-gated potassium channel surface expression and localization in Mammalian neurons. *Critical reviews in biochemistry and molecular biology*, 39(3):125–45, 2004.
- [258] Shannon J Moore, Donald C Cooper, and Nelson Spruston. Plasticity of burst firing induced by synergistic activation of metabotropic glutamate and acetylcholine receptors. *Neuron*, 61(2):287–300, January 2009.
- [259] H Morawitz and TR Koehler. A model for Raman-active librational modes on a metal surface: Pyridine and CN- on silver. *Chemical Physics Letters*, (1), 1980.
- [260] Kim I Mortensen, L Stirling Churchman, James a Spudich, and Henrik Flyvbjerg. Optimized localization analysis for single-molecule tracking and super-resolution microscopy. *Nature methods*, 7(5):377–81, May 2010.

- [261] M Moskovits. Surface roughness and the enhanced intensity of Raman scattering by molecules adsorbed on metals. (June):4159–4161, 1978.
- [262] Disterhoft Moyer Jr., J.R. Thompson, L.T. Trace eyeblink conditioning increases CA1 excitability in a transient and learning-specific manner. *Journal of Neuroscience*, 16(17):5536–5546, 1996.
- [263] Riccardo Mozzachiodi and John H Byrne. More than synaptic plasticity: role of nonsynaptic plasticity in learning and memory. *Trends in neurosciences*, 33(1):17–26, January 2010.
- [264] Riccardo Mozzachiodi, Fred D Lorenzetti, Douglas a Baxter, and John H Byrne. Changes in neuronal excitability serve as a mechanism of long-term memory for operant conditioning. *Nature neuroscience*, 11(10):1146–8, October 2008.
- [265] P Mühlshlegel, H-J Eisler, O J F Martin, B Hecht, and D W Pohl. Resonant optical antennas. *Science (New York, N. Y.)*, 308(5728):1607–9, June 2005.
- [266] S. Mukamel. *Principles of Nonlinear Optical Spectroscopy*. Oxford Series on Optical and Imaging Sciences, 1995.
- [267] Koton Murase, Takahiro Fujiwara, Yasuhiro Umemura, Kenichi Suzuki, Ryota Iino, Hidetoshi Yamashita, Mihoko Saito, Hideji Murakoshi, Ken Ritchie, and Akihiro Kusumi. Ultrafine membrane compartments for molecular diffusion as revealed by single molecule techniques. *Biophysical journal*, 86(6):4075–93, June 2004.
- [268] Venkatesh N Murthy, Thomas Schikorski, Charles F Stevens, Yongling Zhu, and La Jolla. in Neurotransmitter Release and Synapse Size. 32:673–682, 2001.
- [269] M. S Nadal, Y. Amarillo, E. V.-S. de Miera, and B. Rudy. Evidence for the presence of a novel Kv4-mediated A-type K⁺ channel-modifying factor. *The Journal of Physiology*, 537(3):801–809, November 2001.
- [270] Georg Nagel, Martin Brauner, Jana F Liewald, Nona Adeishvili, Ernst Bamberg, and Alexander Gottschalk. Light activation of channelrhodopsin-2 in excitable cells of *Caenorhabditis elegans* triggers rapid behavioral responses. *Current biology : CB*, 15(24):2279–84, December 2005.
- [271] Georg Nagel, Tanjef Szellas, Wolfram Huhn, Suneel Kateriya, Nona Adeishvili, Peter Berthold, Doris Ollig, Peter Hegemann, and Ernst Bamberg. Channelrhodopsin-2, a directly light-gated cation-selective membrane channel. *Proceedings of the National Academy of Sciences of the United States of America*, 100(24):13940–5, November 2003.

- [272] U Valentin Nägerl, Nicola Eberhorn, Sidney B Cambridge, and Tobias Bonhoeffer. Bidirectional activity-dependent morphological plasticity in hippocampal neurons. *Neuron*, 44(5):759–67, December 2004.
- [273] Jaysen Nelayah, Mathieu Kociak, Odile Stéphan, F. Javier García de Abajo, Marcel Tencé, Luc Henrard, Dario Taverna, Isabel Pastoriza-Santos, Luis M. Liz-Marzán, and Christian Colliex. Mapping surface plasmons on a single metallic nanoparticle. *Nature Physics*, 3(5):348–353, April 2007.
- [274] Michael W Nestor and Dax a Hoffman. Differential cycling rates of Kv4.2 channels in proximal and distal dendrites of hippocampal CA1 pyramidal neurons. *Hippocampus*, 000, April 2011.
- [275] S. Nie. Probing Single Molecules and Single Nanoparticles by Surface-Enhanced Raman Scattering. *Science*, 275(5303):1102–1106, February 1997.
- [276] S. Nie. Probing Single Molecules and Single Nanoparticles by Surface-Enhanced Raman Scattering. *Science*, 275(5303):1102–1106, February 1997.
- [277] Lukas Novotny. *Principles of Nano-Optics*. Cambridge University Press, 2006.
- [278] Lindsay H. Oakley, Stephen A. Dinehart, Shelley A. Svoboda, and Kristin L. Wustholz. Identification of Organic Materials in Historic Oil Paintings Using Correlated Extractionless Surface-Enhanced Raman Scattering and Fluorescence Microscopy. *Analytical Chemistry*, 83(11):3986–3989, June 2011.
- [279] AM Van Oijen, J Köhler, and J Schmidt. Far-field fluorescence microscopy beyond the diffraction limit. *JOSA A*, 16(4):909–915, 1999.
- [280] Takayuki Okamoto. Near-Field Spectral Analysis of Metallic Beads Dielectric Function of Metals. *Near-Field Optics and Surface Plasmon Polaritons, Topics Appl. Phys.*, 123:97–123, 2001.
- [281] Nobuyuki Otsu. A threshold selection method from gray-level histograms. *IEEE Trans. Sys., Man., Cyber.*, 20(1):62–66, 1979.
- [282] Adam M Packer, Darcy S Peterka, Jan J Hirtz, Rohit Prakash, Karl Deisseroth, and Rafael Yuste. Two-photon optogenetics of dendritic spines and neural circuits. *Nature methods*, 9(12):1202–5, December 2012.
- [283] Oren Patashnik. *BibTeXing*. Computer Science Department, Stanford University, Stanford, California, January 1988. Available in the BibTeX release.
- [284] Oren Patashnik. *Designing BibTeX Styles*. Computer Science Department, Stanford University, January 1988.

- [285] George Patterson, Michael Davidson, Suliana Manley, and Jennifer Lippincott-Schwartz. Superresolution imaging using single-molecule localization. *Annual review of physical chemistry*, 61:345–67, January 2010.
- [286] Christy R.W. P.B Johnson. Optical Constants of the Noble Metals. *Physical Review B*, 1318(1970), 1972.
- [287] J. B. Pendry. Negative Refraction Makes a Perfect Lens. *Physical Review Letters*, 85(18):3966–3969, October 2000.
- [288] BNJ Persson and R Ryberg. Brownian motion and vibrational phase relaxation at surfaces: CO on Ni (111). *Physical Review B*, 32(6):3586–3596, 1985.
- [289] K Petrecca, D M Miller, and A Shrier. Localization and enhanced current density of the Kv4.2 potassium channel by interaction with the actin-binding protein filamin. *The Journal of neuroscience : the official journal of the Society for Neuroscience*, 20(23):8736–44, December 2000.
- [290] Anatoliy Pinchuk, Gero Von Plessen, and Uwe Kreibig. Influence of interband electronic transitions on the optical absorption in metallic nanoparticles. *Journal of Physics D: Applied Physics*, 37(22):3133–3139, November 2004.
- [291] D. W. Pohl, W. Denk, and M. Lanz. Optical stethoscopy: Image recording with resolution $\lambda/20$. *Applied Physics Letters*, 44(7):651, April 1984.
- [292] Lucas Pozzo-miller. neurons. 1104(1):45–54, 2010.
- [293] Paras N. Prasad. *Introduction to Biophotonics*. Wiley-Interscience, 2003.
- [294] Paras N. Prasad. *Nanophotonics*. Wiley-Interscience, 2004.
- [295] D C Prieve and J Y Walz. Scattering of an evanescent surface wave by a microscopic dielectric sphere. *Applied optics*, 32(9):1629–41, March 1993.
- [296] Xiaohui Qu, David Wu, Laurens Mets, and Norbert F Scherer. Nanometer-localized multiple single-molecule fluorescence microscopy. *PNAS*, (January), 2007.
- [297] H. Raether. *Surface Plasmons*. Springer, 1998.
- [298] Lord Rayleigh. On the theory of optical images, with special reference to the microscope. *Philos. Mag*, XLII:167–195, 1896.
- [299] W. Rechberger, a. Hohenau, a. Leitner, J.R. Krenn, B. Lamprecht, and F.R. Aussenegg. Optical properties of two interacting gold nanoparticles. *Optics Communications*, 220(1-3):137–141, May 2003.

- [300] Leon G Reijmers, Brian L Perkins, Naoki Matsuo, and Mark Mayford. Localization of a stable neural correlate of associative memory. *Science (New York, N.Y.)*, 317(5842):1230–3, August 2007.
- [301] Junsuk Rho, Ziliang Ye, Yi Xiong, Xiaobo Yin, Zhaowei Liu, Hyeunseok Choi, Guy Bartal, and Xiang Zhang. Spherical hyperlens for two-dimensional sub-diffractive imaging at visible frequencies. *Nature communications*, 1:143, January 2010.
- [302] Maarten B. J. Roelfaers, Gert De Cremer, Julien Libeert, Rob Ameloot, Peter Dedecker, Anton-Jan Bons, Matthias Bäckens, Johan A. Martens, Bert F. Sels, Dirk E. De Vos, and Johan Hofkens. Super-Resolution Reactivity Mapping of Nanostructured Catalyst Particles. *Angewandte Chemie*, 121(49):9449–9453, November 2009.
- [303] J Amiel Rosenkranz, Andreas Frick, and Daniel Johnston. Kinase-dependent modification of dendritic excitability after long-term potentiation. *The Journal of physiology*, 587(Pt 1):115–25, January 2009.
- [304] J Amiel Rosenkranz and Anthony a Grace. Dopamine-mediated modulation of odour-evoked amygdala potentials during pavlovian conditioning. *Nature*, 417(6886):282–7, May 2002.
- [305] S T Ross and I Soltesz. Long-term plasticity in interneurons of the dentate gyrus. *Proceedings of the National Academy of Sciences of the United States of America*, 98(15):8874–9, July 2001.
- [306] Ana Ruiz-Gomez, Britt Mellström, Daniel Tornero, Esperanza Morato, Magali Savignac, Helena Holguín, Koldo Aurrekoetxea, Paz González, Carmen González-García, Valentín Ceña, Federico Mayor, and Jose R Naranjo. G protein-coupled receptor kinase 2-mediated phosphorylation of downstream regulatory element antagonist modulator regulates membrane trafficking of Kv4.2 potassium channel. *The Journal of biological chemistry*, 282(2):1205–15, January 2007.
- [307] Michael J Rust, Mark Bates, and Xiaowei Zhuang. imaging by stochastic optical reconstruction microscopy (STORM). 3(10):793–795, 2006.
- [308] Drorit Saar and Edi Barkai. Long-term modifications in intrinsic neuronal properties and rule learning in rats. *European Journal of Neuroscience*, 17(12):2727–2734, June 2003.
- [309] Arthur L. Samuel. First grade T_EX: A beginner’s T_EX manual. Technical Report SATN-CS-83-985, Computer Science Department, Stanford University, Stanford, California, November 1983.
- [310] Andrey Sarychev, V. Shubin, and Vladimir Shalaev. Anderson localization of surface plasmons and nonlinear optics of metal-dielectric composites. *Physical Review B*, 60(24):16389–16408, December 1999.

- [311] Daisuke Saya and Kimitake Fukushima. Fabrication of single-crystal Si cantilever array. *Sensors and actuators A ...*, 95(2-3):281–287, January 2002.
- [312] Andreas T Schaefer, Matthew E Larkum, Bert Sakmann, and Arnd Roth. Coincidence detection in pyramidal neurons is tuned by their dendritic branching pattern. *Journal of neurophysiology*, 89(6):3143–54, June 2003.
- [313] Roman Schmidt, Christian A Wurm, Stefan Jakobs, Johann Engelhardt, Alexander Egner, and Stefan W Hell. Spherical nanosized focal spot unravels the interior of cells. *Nature methods*, 5(6):539–44, June 2008.
- [314] Philipp Schoenenberger, Yan-Ping Zhang Schäerer, and Thomas G Oertner. Channel-rhodopsin as a tool to investigate synaptic transmission and plasticity. *Experimental physiology*, 96(1):34–9, January 2011.
- [315] M Schrader, K Bahlmann, G Giese, and S W Hell. 4Pi-confocal imaging in fixed biological specimens. *Biophysical journal*, 75(4):1659–68, October 1998.
- [316] P J Schuck, D P Fromm, A Sundaramurthy, G S Kino, and W E Moerner. Improving the mismatch between light and nanoscale objects with gold bowtie nanoantennas. *Physical review letters*, 94(1):017402, January 2005.
- [317] M. Schunack, T. Linderoth, F. Rosei, E. Læ gsgaard, I. Stensgaard, and F. Besenbacher. Long Jumps in the Surface Diffusion of Large Molecules. *Physical Review Letters*, 88(15):156102, March 2002.
- [318] Rossana Scuri, Riccardo Mozzachiodi, and Marcello Brunelli. Activity-dependent increase of the AHP amplitude in T sensory neurons of the leech. *Journal of neurophysiology*, 88(5):2490–500, November 2002.
- [319] K. Seal, D. Genov, a. Sarychev, H. Noh, V. Shalaev, Z. Ying, X. Zhang, and H. Cao. Coexistence of Localized and Delocalized Surface Plasmon Modes in Percolating Metal Films. *Physical Review Letters*, 97(20):206103, November 2006.
- [320] JB Segur and HE Oberstar. Viscosity of glycerol and its aqueous solutions. *Industrial & Engineering Chemistry*, (September):5–8, 1951.
- [321] M. I Shalaev, V. M. & Stockman. Fractals: optical susceptibility and giant Raman scattering. *Z. Phys. D*, 10:71–79, 1988.
- [322] Lin Shao, Berith Isaac, Satoru Uzawa, David A Agard, John W Sedat, and Mats G L Gustafsson. I5S: wide-field light microscopy with 100-nm-scale resolution in three dimensions. *Biophysical journal*, 94(12):4971–83, June 2008.
- [323] Bhavya Sharma, Renee R. Frontiera, Anne-Isabelle Henry, Emilie Ringe, and Richard P. Van Duyne. SERS: Materials, applications, and the future. *Materials Today*, 15(1-2):16–25, January 2012.

- [324] Alexey Sharonov and Robin M Hochstrasser. Wide-field subdiffraction imaging by accumulated binding of diffusing probes. 2006(7), 2006.
- [325] Bin Shen, Kechun Zhou, Shenglian Yang, Tianle Xu, and Yizheng Wang. The Kv4.2 mediates excitatory activity-dependent regulation of neuronal excitability in rat cortical neurons. *Journal of neurochemistry*, 105(3):773–83, May 2008.
- [326] M Sheng, M L Tsaur, Y N Jan, and L Y Jan. Subcellular segregation of two A-type K⁺ channel proteins in rat central neurons. *Neuron*, 9(2):271–84, August 1992.
- [327] Riichi Shibata, Hiroaki Misonou, Claire R Campomanes, Anne E Anderson, Laura a Schrader, Lisa C Doliveira, Karen I Carroll, J David Sweatt, Kenneth J Rhodes, and James S Trimmer. A fundamental role for KChIPs in determining the molecular properties and trafficking of Kv4.2 potassium channels. *The Journal of biological chemistry*, 278(38):36445–54, September 2003.
- [328] Hari Shroff, Catherine G Galbraith, James A Galbraith, and Eric Betzig. Live-cell photoactivated localization microscopy of nanoscale adhesion dynamics. *Nature methods*, 5(5):417–23, May 2008.
- [329] Hari Shroff, Catherine G Galbraith, James A Galbraith, Helen White, Jennifer Gillette, Scott Olenych, Michael W Davidson, and Eric Betzig. Dual-Color Superresolution Imaging of Genetically Expressed Probes within Individual Adhesion Complexes. *Proceedings of the National Academy of Sciences of the United States of America*, (34):12099–12100, 2007.
- [330] G. Shvets, S. Trendafilov, J. Pendry, and A. Sarychev. Guiding, Focusing, and Sensing on the Subwavelength Scale Using Metallic Wire Arrays. *Physical Review Letters*, 99(5):053903, August 2007.
- [331] Ralph M Siegel and Edward M Callaway. Francis Crick’s legacy for neuroscience: between the alpha and the Omega. *PLoS biology*, 2(12):e419, December 2004.
- [332] V Silin, H Weetall, and Dj Vanderah. SPR Studies of the Nonspecific Adsorption Kinetics of Human IgG and BSA on Gold Surfaces Modified by Self-Assembled Monolayers (SAMs). *Journal of colloid and interface science*, 185(1):94–103, January 1997.
- [333] Alcino J Silva, Yu Zhou, Thomas Rogerson, Justin Shobe, and J Balaji. Molecular and cellular approaches to memory allocation in neural circuits. *Science (New York, N. Y.)*, 326(5951):391–5, October 2009.
- [334] P. Jesper Sjostrom, Ede Rancz, Arnd Roth, and Michael Hausser. Dendritic Excitability and Synaptic Plasticity. *Biomedical Research*, pages 769 – 840, 2008.

- [335] Carlas S Smith, Nikolai Joseph, Bernd Rieger, and Keith a Lidke. Fast, single-molecule localization that achieves theoretically minimum uncertainty. *Nature methods*, 7(5):373–5, May 2010.
- [336] Igor I Smolyaninov, Christopher C Davis, Jill Elliott, and Anatoly V Zayats. Resolution enhancement of a surface immersion microscope near the plasmon resonance. *Optics letters*, 30(4):382–4, February 2005.
- [337] Igor I Smolyaninov, Yu-Ju Hung, and Christopher C Davis. Magnifying superlens in the visible frequency range. *Science (New York, N.Y.)*, 315(5819):1699–701, March 2007.
- [338] Manuel P. Soriaga and Arthur T. Hubbard. Determination of the orientation of adsorbed molecules at solid-liquid interfaces by thin-layer electrochemistry: aromatic compounds at platinum electrodes. *Journal of the American Chemical Society*, 104(10):2735–2742, May 1982.
- [339] MP Soriaga and AT Hubbard. Determination of the Orientation of Aromatic Molecules Adsorbed on Platinum Electrodes. The Effect of Solute Concentration. *Journal of the American Chemical . . .*, pages 3937–3945, 1982.
- [340] Michael D. Spivak. *The Joy of T_EX*. American Mathematical Society, 1985.
- [341] Nelson Spruston. Pyramidal neurons: dendritic structure and synaptic integration. *Nature reviews. Neuroscience*, 9(3):206–21, March 2008.
- [342] Pradeep Srinivasan, Fred R Beyette, and Ian Papautsky. Micromachined arrays of cantilevered glass probes. *Applied optics*, 43(4):776–82, February 2004.
- [343] Thorsten Staudt, Marion C Lang, Rebecca Medda, Johann Engelhardt, and Stefan W Hell. 2, 2 0 -Thiodiethanol : A New Water Soluble Mounting Medium for High Resolution Optical Microscopy. *Microscopy Research and Technique*, 9(October 2006):1–9, 2007.
- [344] S. W. Staudt, T., Lang, M. C., Medda, R., Engelhardt, J., & Hell. 2,2 -Thiodiethanol : A New Water Soluble Mounting Medium for High Resolution Optical Microscopy. *Microscopy Research and Technique*, 9, 2006.
- [345] Katja Stehfest, Eglof Ritter, André Berndt, Franz Bartl, and Peter Hegemann. The branched photocycle of the slow-cycling channelrhodopsin-2 mutant C128T. *Journal of molecular biology*, 398(5):690–702, May 2010.
- [346] VA Sterligov, P Cheyssac, SI Lysenko, and R Kofman. Relationship between the scattering of homogeneous and evanescent electromagnetic waves by metallic nanoparticles. *Optics communications*, i(December):27–33, 2000.

- [347] Molly M Stevens, Michael Mayer, Daniel G Anderson, Douglas B Weibel, George M Whitesides, and Robert Langer. Direct patterning of mammalian cells onto porous tissue engineering substrates using agarose stamps. *Biomaterials*, 26(36):7636–41, December 2005.
- [348] Mark Stockman, Sergey Faleev, and David Bergman. Localization versus Delocalization of Surface Plasmons in Nanosystems: Can One State Have Both Characteristics? *Physical Review Letters*, 87(16):167401, September 2001.
- [349] Douglas A Stuart, Kevin B Biggs, and Richard P Van Duyne. Surface-enhanced Raman spectroscopy of half-mustard agent. *The Analyst*, 131(4):568–72, April 2006.
- [350] G Stuart, N Spruston, B Sakmann, and M Häusser. Action potential initiation and backpropagation in neurons of the mammalian CNS. *Trends in neurosciences*, 20(3):125–31, March 1997.
- [351] T Sugiura, T Okada, Y Inouye, O Nakamura, and S Kawata. Gold-bead scanning near-field optical microscope with laser-force position control. *Optics letters*, 22(22):1663–5, November 1997.
- [352] T. H. Taminiau, F. D. Stefani, F. B. Segerink, and N. F. van Hulst. Optical antennas direct single-molecule emission. *Nature Photonics*, 2(4):234–237, March 2008.
- [353] Tim H Taminiau, Robert J Moerland, Frans B Segerink, Laurens Kuipers, and Niek F van Hulst. $\lambda/4$ resonance of an optical monopole antenna probed by single molecule fluorescence. *Nano letters*, 7(1):28–33, January 2007.
- [354] Gareth M Thomas and Richard L Huganir. MAPK cascade signalling and synaptic plasticity. *Nature reviews. Neuroscience*, 5(3):173–83, March 2004.
- [355] Russell E Thompson, Daniel R Larson, and Watt W Webb. Precise nanometer localization analysis for individual fluorescent probes. *Biophysical journal*, 82(5):2775–83, May 2002.
- [356] Russell E Thompson, Daniel R Larson, and Watt W Webb. Precise nanometer localization analysis for individual fluorescent probes. *Biophysical journal*, 82(5):2775–83, May 2002.
- [357] J Thompson, L.T. , Moyer Jr., J.R., Disterhoft. Transient changes in excitability of rabbit CA3 neurons with a time course appropriate to support memory consolidation. *Journal of neurophysiology*, 76(3):1836–1849, 1996.
- [358] N Toni, P A Buchs, I Nikonenko, C R Bron, and D Muller. LTP promotes formation of multiple spine synapses between a single axon terminal and a dendrite. *Nature*, 402(6760):421–5, November 1999.

- [359] Jochen Triesch. Synergies between intrinsic and synaptic plasticity mechanisms. *Neural computation*, 19(4):885–909, April 2007.
- [360] Bruno Truchet, Christine Manrique, Leam Sreng, Franck a Chaillan, François S Roman, and Christiane Mourre. Kv4 potassium channels modulate hippocampal EPSP-spike potentiation and spatial memory in rats. *Learning & memory (Cold Spring Harbor, N.Y.)*, 19(7):282–93, January 2012.
- [361] Hsing-Chen Tsai, Feng Zhang, Antoine Adamantidis, Garret D Stuber, Antonello Bonci, Luis de Lecea, and Karl Deisseroth. Phasic firing in dopaminergic neurons is sufficient for behavioral conditioning. *Science (New York, N.Y.)*, 324(5930):1080–4, May 2009.
- [362] M L Tsaur, C C Chou, Y H Shih, and H L Wang. Cloning, expression and CNS distribution of Kv4.3, an A-type K⁺ channel alpha subunit. *FEBS letters*, 400(2):215–20, January 1997.
- [363] M L Tsaur, M Sheng, D H Lowenstein, Y N Jan, and L Y Jan. Differential expression of K⁺ channel mRNAs in the rat brain and down-regulation in the hippocampus following seizures. *Neuron*, 8(6):1055–67, June 1992.
- [364] Gina Turrigiano. Too Many Cooks? Intrinsic and Synaptic Homeostatic Mechanisms in Cortical Circuit Refinement. *Annual review of neuroscience*, 34:89–103, January 2011.
- [365] Kay M Tye, Julie J Mirzabekov, Melissa R Warden, Emily A Ferenczi, Hsing-Chen Tsai, Joel Finkelstein, Sung-Yon Kim, Avishek Adhikari, Kimberly R Thompson, Aaron S Andalman, Lisa A Gunaydin, Ilana B Witten, and Karl Deisseroth. Dopamine neurons modulate neural encoding and expression of depression-related behaviour. *Nature*, 493(7433):537–41, January 2013.
- [366] Thomas S van Zanten, Alessandra Cambi, and Maria F Garcia-Parajo. A nanometer scale optical view on the compartmentalization of cell membranes. *Biochimica et biophysica acta*, 1798(4):777–87, April 2010.
- [367] Thomas S van Zanten, Maria J Lopez-Bosque, and Maria F Garcia-Parajo. Imaging individual proteins and nanodomains on intact cell membranes with a probe-based optical antenna. *Small (Weinheim an der Bergstrasse, Germany)*, 6(2):270–5, January 2010.
- [368] Andrew W Varga, Li-Lian Yuan, Anne E Anderson, Laura a Schrader, Gang-Yi Wu, Jennifer R Gatchel, Daniel Johnston, and J David Sweatt. Calcium-calmodulin-dependent kinase II modulates Kv4.2 channel expression and upregulates neuronal A-type potassium currents. *The Journal of neuroscience : the official journal of the Society for Neuroscience*, 24(14):3643–54, April 2004.

- [369] Ernst Jan R Vesseur, René de Waele, Martin Kuttge, and Albert Polman. Direct observation of plasmonic modes in au nanowires using high-resolution cathodoluminescence spectroscopy. *Nano letters*, 7(9):2843–6, September 2007.
- [370] Ernst Jan R Vesseur, René de Waele, Martin Kuttge, and Albert Polman. Direct observation of plasmonic modes in au nanowires using high-resolution cathodoluminescence spectroscopy. *Nano letters*, 7(9):2843–6, September 2007.
- [371] Gorden Videen, Mustafa M. Aslan, and M. Pinar Mengüç. Characterization of metallic nano-particles via surface wave scattering: A. Theoretical framework and formulation. *Journal of Quantitative Spectroscopy and Radiative Transfer*, 93(1-3):195–206, June 2005.
- [372] G. Villanueva and J.a. Plaza. Deep reactive ion etching and focused ion beam combination for nanotip fabrication. *Materials Science and ...*, 26(2-3):164–168, March 2006.
- [373] G. Villanueva, J.a. Plaza, a. Sánchez-Amores, J. Bausells, E. Martínez, J. Samitier, a. Errachid, Pradeep Srinivasan, Fred R Beyette, Ian Papautsky, Daisuke Saya, Kimitake Fukushima, Hiroshi Toshiyoshi, Gen Hashiguchi, Hiroyuki Fujita, Hideki Kawakatsu, S C Minne, S R Manalis, C F Quate, J H Hafner, C L Cheung, a T Woolley, C M Lieber, Mélanie Favre, Jérôme Polesel-Maris, Thomas Overstolz, Philippe Niedermann, Stephan Dasen, Gabriel Gruener, Réal Ischer, Peter Vettiger, Martha Liley, Harry Heinzelmann, André Meister, Ami Chand, Mario B Viani, Tilman E Schäffer, Paul K Hansma, J. Brugger, R.a. Buser, N.F. de Rooij, Anja Boisen, Ole Hansen, Siebe Bouwstra, Yoomin Ahn, Takahito Ono, and Masayoshi Esashi. No Title.
- [374] W. Stocker, G. Bar, M. Kunz, M. Moller, S. N. Magonov TM and H.-J. Cantow. Atomic force microscopy on polymers and polymer related compounds. *Polymer Bulletin*, 222(26):215–222, 1991.
- [375] E.R. Walters, E.T., Byrne, J.H., Carew, T.J., Kandel. Mechanoafferent neurons innervating tail of Aplysia. II. Modulation by sensitizing stimulation. *Journal of neurophysiology*, 50(6):1543–1559, 1983.
- [376] Chun-Chieh Wang, Chia-Wei Lee, Chia-Yun Huang, Jiunn-Yuan Lin, Pei-Kuen Wei, and Chau-Hwang Lee. Observation of nanoparticle internalization on cellular membranes by using noninterferometric widefield optical profilometry. *Applied optics*, 47(13):2458–64, May 2008.
- [377] Hongxia Wang, Yuka Sugiyama, Takuya Hikima, Eriko Sugano, Hiroshi Tomita, Tetsuo Takahashi, Toru Ishizuka, and Hiromu Yawo. Molecular determinants differentiating photocurrent properties of two channelrhodopsins from chlamydomonas. *The Journal of biological chemistry*, 284(9):5685–96, February 2009.

- [378] Jing Wang, David A Borton, Jiayi Zhang, Rebecca D Burwell, and Arto V Nurmikko. A neurophotonic device for stimulation and recording of neural microcircuits. *Conference proceedings : ... Annual International Conference of the IEEE Engineering in Medicine and Biology Society. IEEE Engineering in Medicine and Biology Society. Conference*, 2010:2935–8, January 2010.
- [379] Sheng Wang, Stephanie Szobota, Yuan Wang, Matthew Volgraf, Zhaowei Liu, Cheng Sun, Dirk Trauner, Ehud Y Isacoff, and Xiang Zhang. All optical interface for parallel, remote, and spatiotemporal control of neuronal activity. *Nano letters*, 7(12):3859–63, December 2007.
- [380] Yuling Wang and Joseph Irudayaraj. Surface-enhanced Raman spectroscopy at single-molecule scale and its implications in biology. *Philosophical transactions of the Royal Society of London. Series B, Biological sciences*, 368(1611):20120026, February 2013.
- [381] Zhuren Wang, Jodene R Eldstrom, Joshua Jantzi, Edwin D Moore, and David Fedida. Increased focal Kv4.2 channel expression at the plasma membrane is the result of actin depolymerization. *American journal of physiology. Heart and circulatory physiology*, 286(2):H749–59, February 2004.
- [382] Warren S. Warren. *The physical basis of chemistry*. Academic Press, 2 edition, 2000.
- [383] Shigeo Watanabe, Dax a Hoffman, Michele Migliore, and Daniel Johnston. Dendritic K⁺ channels contribute to spike-timing dependent long-term potentiation in hippocampal pyramidal neurons. *Proceedings of the National Academy of Sciences of the United States of America*, 99(12):8366–71, June 2002.
- [384] Volker Westphal, Silvio O Rizzoli, Marcel A Lauterbach, Dirk Kamin, Reinhard Jahn, and Stefan W Hell. Video-rate far-field optical nanoscopy dissects synaptic vesicle movement. *Science (New York, N. Y.)*, 320(5873):246–9, April 2008.
- [385] Ian R Wickersham, David C Lyon, Richard J O Barnard, Takuma Mori, Stefan Finke, Karl-Klaus Conzelmann, John A T Young, and Edward M Callaway. Monosynaptic restriction of transsynaptic tracing from single, genetically targeted neurons. *Neuron*, 53(5):639–47, March 2007.
- [386] Katrin I Willig, Silvio O Rizzoli, Volker Westphal, Reinhard Jahn, and Stefan W Hell. STED microscopy reveals that synaptotagmin remains clustered after synaptic vesicle exocytosis. *Nature*, 440(7086):935–9, April 2006.
- [387] Denis Wirtz. Particle-tracking microrheology of living cells: principles and applications. *Annual review of biophysics*, 38:301–26, January 2009.
- [388] A Wokaun, H Lutz, A P King, U P Wild, and R R Ernst. Energy transfer in surface enhanced luminescence. 79(February), 1983.

- [389] Wei Wong, Evan W Newell, Denis G M Jugloff, Owen T Jones, and Lyanne C Schlichter. Cell surface targeting and clustering interactions between heterologously expressed PSD-95 and the Shal voltage-gated potassium channel, Kv4.2. *The Journal of biological chemistry*, 277(23):20423–30, June 2002.
- [390] C D Woody and Patricia Black-Cleworth. Differences in excitability of cortical neurons as a function of motor projection in conditioned cats. *Journal of neurophysiology*, 36:1104–1116, 1973.
- [391] P Woody, C.D., Black Cleworth. Differences in excitability of cortical neurons as a function of motor projection in conditioned cats. *Journal of Neurophysiology*, 36(6):1104–1116, 1973.
- [392] Soap Works. Glycerol Viscosity Tables 1 1 . 4 ~ 1 ~ . 9(9), 1931.
- [393] Dongmin Wu, Zhaowei Liu, Cheng Sun, and Xiang Zhang. Super-resolution imaging by random adsorbed molecule probes. *Nano letters*, 8(4):1159–62, April 2008.
- [394] Jun Xu, Ning Kang, Li Jiang, Maiken Nedergaard, and Jian Kang. Activity-dependent long-term potentiation of intrinsic excitability in hippocampal CA1 pyramidal neurons. *The Journal of neuroscience : the official journal of the Society for Neuroscience*, 25(7):1750–60, February 2005.
- [395] Ahmet Yildiz, Joseph N Forkey, Sean a McKinney, Taekjip Ha, Yale E Goldman, and Paul R Selvin. Myosin V walks hand-over-hand: single fluorophore imaging with 1.5-nm localization. *Science (New York, N.Y.)*, 300(5628):2061–5, June 2003.
- [396] Ofer Yizhar, Lief E Fenno, Matthias Prigge, Franziska Schneider, Thomas J Davidson, Daniel J O’Shea, Vikaas S Sohal, Inbal Goshen, Joel Finkelstein, Jeanne T Paz, Katja Stehfest, Roman Fudim, Charu Ramakrishnan, John R Huguenard, Peter Hege-
mann, and Karl Deisseroth. Neocortical excitation/inhibition balance in information processing and social dysfunction. *Nature*, 477(7363):171–8, September 2011.
- [397] Li-Lian Yuan, J Paige Adams, Michael Swank, J David Sweatt, and Daniel Johnston. Protein kinase modulation of dendritic K⁺ channels in hippocampus involves a mitogen-activated protein kinase pathway. *The Journal of neuroscience : the official journal of the Society for Neuroscience*, 22(12):4860–8, June 2002.
- [398] Li-Lian Yuan and Xixi Chen. Diversity of potassium channels in neuronal dendrites. *Progress in neurobiology*, 78(6):374–89, April 2006.
- [399] Edward Zagher, Andres Ozaita, Su Ying Chang, Marcela S Nadal, Udele Lin, Michael J Saganich, Tom McCormack, Karen O Akinsanya, Shu Y Qi, and Bernardo Rudy. DPP10 modulates Kv4-mediated A-type potassium channels. *The Journal of biological chemistry*, 280(19):18853–61, May 2005.

- [400] Vladislav V Zarayskiy, Ganesh Balasubramanian, Vladimir E Bondarenko, and Michael J Morales. Heteropoda toxin 2 is a gating modifier toxin specific for voltage-gated K⁺ channels of the Kv4 family. *Toxicon : official journal of the International Society on Toxinology*, 45(4):431–42, March 2005.
- [401] Feng Zhang, Viviana Gradinaru, Antoine R Adamantidis, Remy Durand, Raag D Airan, Luis de Lecea, and Karl Deisseroth. Optogenetic interrogation of neural circuits: technology for probing mammalian brain structures. *Nature protocols*, 5(3):439–56, March 2010.
- [402] Feng Zhang, Matthias Prigge, Florent Beyrière, Satoshi P Tsunoda, Joanna Mattis, Ofer Yizhar, Peter Hegemann, and Karl Deisseroth. Red-shifted optogenetic excitation: a tool for fast neural control derived from *Volvox carteri*. *Nature neuroscience*, 11(6):631–3, June 2008.
- [403] Feng Zhang, Li-Ping Wang, Martin Brauner, Jana F Liewald, Kenneth Kay, Natalie Watzke, Phillip G Wood, Ernst Bamberg, Georg Nagel, Alexander Gottschalk, and Karl Deisseroth. Multimodal fast optical interrogation of neural circuitry. *Nature*, 446(7136):633–9, April 2007.
- [404] Cuiping Zhao, Lang Wang, Theoden Netoff, and Li-Lian Yuan. Dendritic mechanisms controlling the threshold and timing requirement of synaptic plasticity. *Hippocampus*, 21(3):288–97, March 2011.
- [405] Shengli Zhao, Catarina Cunha, Feng Zhang, Qun Liu, Bernd Gloss, Karl Deisseroth, George J Augustine, and Guoping Feng. Improved expression of halorhodopsin for light-induced silencing of neuronal activity. *Brain cell biology*, 36(1-4):141–54, August 2008.
- [406] Yu Zhou, Jaejoon Won, Mikael Guzman Karlsson, Miou Zhou, Thomas Rogerson, Jayaprakash Balaji, Rachael Neve, Panayiota Poirazi, and Alcino J Silva. CREB regulates excitability and the allocation of memory to subsets of neurons in the amygdala. *Nature neuroscience*, 12(11):1438–43, November 2009.
- [407] Bende Zou, Yan Li, Ping Deng, and Zao C Xu. Alterations of potassium currents in ischemia-vulnerable and ischemia-resistant neurons in the hippocampus after ischemia. *Brain research*, 1033(1):78–89, February 2005.
- [408] R S Zucker. Short-term synaptic plasticity. *Annual review of neuroscience*, 12:13–31, January 1989.